Ligamentum arteriosum:

Structure, innervation, neurochemistry and function

INAUGURATION DISSERTATION

to obtain the Degree of a

Doctor of Human Biology

of the Faculty of Medicine

of the Justus-Liebig-University, Giessen

by

Benedicta Mensah

from

Accra, Ghana

Giessen 2021

From the Institute of Anatomy and Cell Biology

Visceral Neurobiology

Head: Prof. Dr. Wolfgang Kummer

of the Faculty Of Medicine

of the Justus-Liebig-University, Giessen

Supervisor and committee member: Prof. Dr. Wolfgang Kummer

Second reviewer and committee member: PD Dr. Bernd Niemann

Day of disputation: 30.11.2021

Dedicated to

Family & friends

Esp Michael, Jaden & Noel

I INTRODUCTION

1.1 History and anatomy of ductus arteriosus

1.1.1. Ductus arteriosus

The ductus arteriosus is the embryonic connection between the pulmonary trunk and the aortic arch which allows oxygenated fetal blood to be shunted from the right ventricle into systemic circulation by-passing pulmonary circulation. Although the ductus arteriosus directly connects two elastic arteries, it is a muscular artery (Chuaqui et al. 1977, Toda et al. 1980). The first report of a structure allowing for the passage of blood from the left to the right side of the heart was by Galen in his De Usu Partium in the second century when he wrote: "*This is the explanation of the communication of the vena cava with the vein-like artery [i.e., our pulmonary veins and left atrium] during foetal life. In as much as this latter vessel was then acting as the venous supply of the lung, its companion [i.e., the artery-like vein, or our pulmonary trunk and its branches] had to act as the arterial supply of that organ, and nature therefore made a communication between it and the great artery [i.e., the aorta]. As, however, the two vessels were separated by a short distance, a small third vessel [i.e., the ductus] was created by nature to unite them"* (Reese 2018). Though accepted, this was not given a lot of consideration and simply remained a curiosity. Leonardo Botallo, an Italian surgeon in 1564, whose name appears in several dictionaries for the three major anatomical shunts in foetal circulation, refuted the earlier reports of Galen and gave the name canalis to the ductus arteriosus (Dorland 1974, Feneis 1976). In 1561, both Fallopio and Vesalius also mentioned the ductus arteriosus and the foramen ovale in a report (Franklin 1941, Gatzsche 1952). Then in 1564, another Italian physician, Julio Cesare Aranzio, pupil of Vesalius at Padua who later became a professor of anatomy at Bologna, acknowledged the earlier descriptions of Galen before publishing a more detailed description of the fetal foramen ovale and the ductus arteriosus (Fransson 1999).

In 1660, Van Home also acknowledged the earlier works of Galen and Botallo by inserting a short version of Botallo and also briefly mentioning Galen's description. He then gave a description of some cardiovascular structures in his edition of the Opera Omnia and gave a footnote and illustration of the heart. A persistent ductus arteriosus after birth was described much later in 1757 by the German Reinmann.

In 1786, the Swedish surgeon Hagströmer presents a correct knowledge of physiology of the ductus arteriosus in fetal circulation (Franklin 1941, Gillispie 1970). All these great men of science in one way or another added a bit of enlightenment to this structure, however, none gave a known complete and concrete description of the ligamentum arteriosum (LA) or what becomes of the layers of the ductus arteriosus after birth.

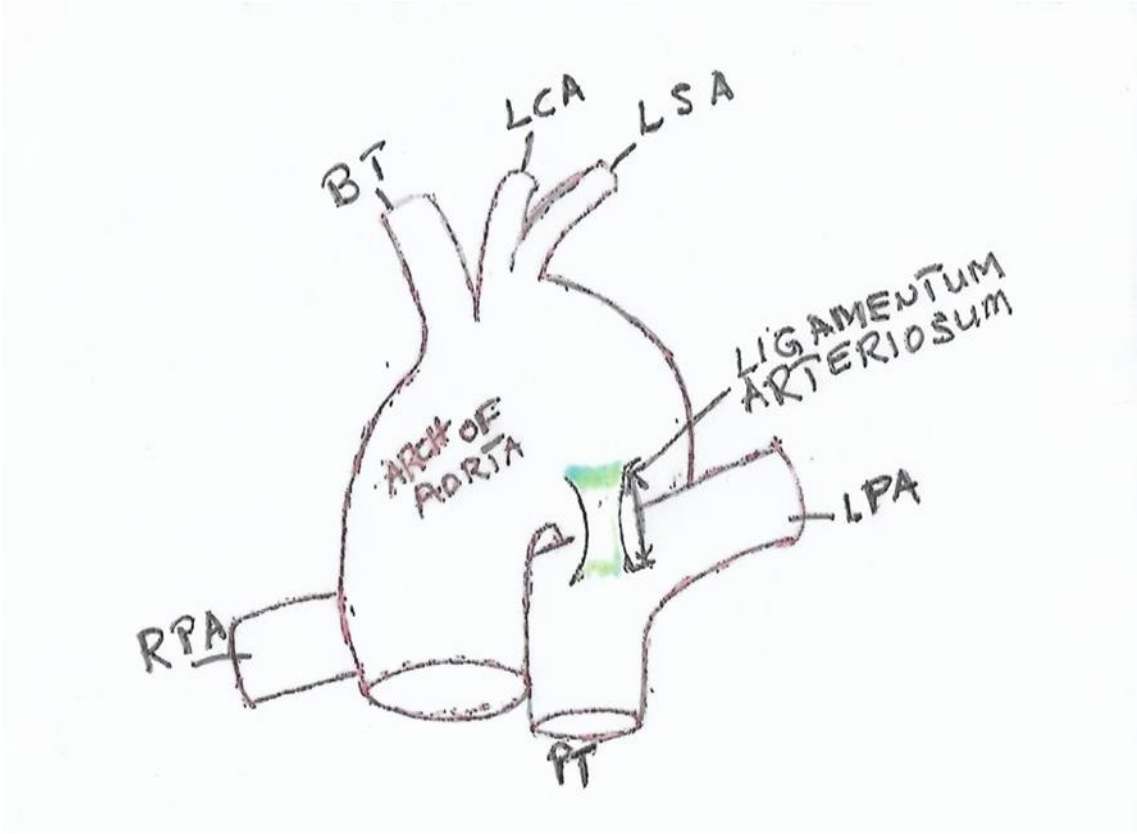

Figure 1. LA and its attachment to the pulmonary trunk (PT) and the aortic arch. The PT giving off the left pulmonary artery (LPA) and right pulmonary artery (RPA). The aortic arch also giving off the first 3 branches brachiocephalic trunk (BT), left carotid (LCA) and left subclavian artery (LSA). Green, blue and yellow colour within LA indicates areas of intense innervation in the structure.

1.1.2. Fetal circulation

In the normal adult, oxygenation of de-oxygenated blood and its distribution to the entire body is achieved be two main types of circulation. These are pulmonary circulation (with major organs being the pulmonary vessels, lungs and its accessory structures, found within and around the heart, and responsible for oxygenating the oxygen deficient blood returning

from the right side of the heart) and systemic circulation (blood vessels and other accessory structures found outside and further away from the heart responsible for sending the oxygenated blood to all the cells and tissues in the body and even the heart itself).

This kind of arrangement is completely different in the foetus. Pulmonary circulation is not functioning at its normal capacity (Benirschke 2006). During the first trimester, when circulation has been established, low oxygen in blood is replenished by a completely different structure, i.e. the placenta. This absence of pulmonary circulation in the intrauterine environment, however, makes fetal circulation fundamentally different in both morphology and physiology. The transport, supply and oxygenation of blood are predominantly performed through 2 umbilical arteries and 1 umbilical vein which are together referred to as the umbilical cord. The umbilical arteries carry de-oxygenated blood from foetus beck to placenta for oxygenation and the umbilical vein carries oxygenated and nutrient rich blood back to the foetus (Benirschke 2006).

The presence of specific shunts has been designed to facilitate these needs (Table 1) to enable establishment and ensure maintenance of this type of circulation. These contralateral and ipsilateral directional vascular shunts are crucial for fetal survival and nourishment as well as metabolic and CO_2 waste clearance because they allow bypass of the blood mainly of the lungs and the liver. These shunts close immediately or a few weeks after birth.

SHUNT	ORGAN BYPASSED	TYPE OF BLOOD CARRIED
Ductus arteriosus	Lungs	Oxygenated blood
Foramen ovale	Lungs	Oxygenated blood
Ductus venosus	Liver	Oxygenated blood

Table 1 Vascular shunts found in fetal circulation

In the prenatal heart, the ductus arteriosus and foramen ovale allow blood to be routed around the lungs by diverting blood from pulmonary artery directly to the aorta and from the right to left atrium, respectively.

The uninflated lungs of the foetus are filled with amniotic fluid (Marty and Lui 2019), thus protected from blood perfusion by the creation of high pressure within it. Blood entering

the right atrium through the two main pathways (inferior and superior vena cava) courses through either one of the two shunts. The foramen ovale, found within the atrial septal wall of the right atrium, directs blood from this location directly to the left atrium, then to the left ventricle and to the ascending aorta and finally to systemic circulation. The ductus arteriosus, seen as the second course can be viewed as a backup of the initial lung by-pass because it is responsible for shunting the blood that misses the foramen ovale route and enters the right ventricle due to flow pattern (Wang and Zhao 2010).

1.1.3. Morphology and innervation of ductus arteriosus

Gross anatomically, all blood vessels except capillaries are made up of 3 distinct layers, namely, the outer layer (tunica adventitia) providing structural support and shape to the vessels, the middle layer (tunica media) regulating the internal diameter of the vessel, and finally the inner layer (tunica intima) lining the whole vascular lumen and providing a frictionless pathway for blood flow.

Histologically, these layers from within outward are also described. The tunica intima is made up of endothelial cells (simple squamous epithelium) and a thin subendothelial made up of loose connective tissue layer. Smooth muscle cells also referred to as vascular smooth muscle cells, collagen and elastin fibers are the major elements found within the tunica media. The last layer, tunica adventitia is a fairly wide collagenous layer with interspersed bundles of elastin. Nerves bundles, fibroblasts as well as progenitor cells are also present in this layer. Embryonically, the ductus arteriosus develops as a continuation of the pulmonary trunk from the distal part of the 6th left aortic arch and it terminates in the dorsal aorta. This makes the point of attachment of the ductus arteriosus to the pulmonary trunk the origin of the structure. During the development of the pulmonary artery (embryogenesis) there is a field of cells expressing the undifferentiated mesenchyme marker platelet-derived growth factor receptor (PDGFR)-β.

However, shortly thereafter PDGFR-β+ cells adjacent to the nascent endothelial cell tube downregulate PDGFR-β and upregulate smooth muscle actin (SMA). This may lead one to postulate that, αSMA may be an abundant marker found within the smooth muscle cells of this structure (Mazurek et al. 2016). Depending on the type, size, function and location of a blood vessel, the amount of muscle, connective tissue, collagen or elastic fibers may vary (Szyszka-Mroz and Wozniak 2003). Anatomically, human muscular arteries are very similar to that in mouse, though the latter is considerably smaller in size. Histologically,

mouse muscular arteries have lesser muscle layers. Though present, the subendothelial layer is rarely seen (Laflamme et al. 2012). Porcine arteries are far more elastic in both circumferential and axial direction compared with the human arteries. Consequently, the porcine arteries could be safely stretched by 60% to 70% compared with about 20% for the human arteries before reaching their maximum circumferential strain (Van Andel et al. 2003).

The anatomical structure of the ductus arteriosus has been reported by numerous studies (Boudreau and Rabinovitch 1991, Gittenberger et al. 1980, 1985, Silver et al. 1981). These morphological studies were performed in order to better understand the process of its obliteration (Boudreau et al. 1991, Gittenberger et al. 1980, Mato and Aikawa 1968).

Studies describe the ductus arteriosus as a small muscular artery (Garcia 1975, Toda et al. 1980). Histologically, its layers almost follow the classical layers found in muscular arteries. An intima made up of a monolayer of endothelial cells sits on an avascular subendothelial structure. The internal elastic lamina (IEL), which is usually incomplete and convoluted, is found between the intima and the media. This is then followed by a fairly thick layer of vascular smooth muscle cells with collagen and elastin fibers dispersed amongst these cells. The adventitia, which mostly contains collagen, elastin, blood vessels and nerve fibers, is not separated from the outer borders of the media by an external elastic lamina (O'Rahilly and Müller F 2001). So is this small artery innervated at all and if it is, how is it innervated?

The ductus arteriosus is generally regarded as being derived from the sixth branchial arch arteries of the embryo (Fransson 1999). The adventitia, which mostly contains collagen, elastin, blood vessels and nerve fibers, is not separated from the outer borders of the media by an external elastic lamina (O'Rahilly and Müller F 2001). So is this small artery innervated at all and if it is, how is it innervated?

Earlier studies into the innervation of the ductus arteriosus reported innervation from the left aortic and vagus nerves. Boyd in 1941 speculated that the vagus contributed chiefly to the innervation of the antero-inferior aspect of the vessel while the aortic nerve was concerned mainly with the innervation of its postero-superior surface though in a few specimens, the inferior aspect of the ductus arteriosus received some fibers from the recurrent laryngeal nerve as this nerve hooks under it. These fibers may be presumed to be vagal fibers which are leaving the nerve at a lower level than is usual and which accompany

the recurrent nerve for a short distance. In the younger embryos, however, the fibers tend to penetrate further into the wall of the ductus, approaching, and sometimes reaching, the intima. The fibers which reach the intima usually bend back into the muscular coat of the ductus. In the older embryos and new-born foetuses, the fibers are for the most part restricted to the outer third of the media and to the adventitia, but a few fibers can always be traced more deeply into the wall of the ductus. Additionally, fibers of sympathetic origin are closely related to the terminal ramifications of the aortic nerve and, in some specimens, it has been possible to trace distinct bundles from the sympathetic trunk into the vagus nerve and, more rarely, to the ductus itself (Boyd 1941). Further studies report and support the contribution of sympathetic nerves in ductus arteriosus innervation (Aronson et al. 1970, Boreus et al. 1969, Cassels and Moore 1973, Ikeda 1970), though there have been contrary reports (Barcroft et al. 1938). Furthermore, some fibers appear to reach the ductus arteriosus from the lower cervical and upper thoracic sympathetic chain of the left side.

There is substantial and significant histological evidence supporting the presence of a baroceptive apparatus by the ductus arteriosus in foetal life. This baroceptive apparatus is similar to what is present in the carotid sinus or the aortic arch (Boyd 1941, Muratori 1937, Takino and Watanabe 1937). The published work of Boyd supported prior theoretically reports of the presence of baroceptors with specialized nerve endings on mammalian arteries. The baroceptors were believed to be remnants of the embryonic branchial arch arterial system in (Boyd 1934). Furthermore, Boyd reported a sensory innervation of the mammalian ductus, very similar to that possessed by the aorta and carotid sinus (Boyd 1941). In addition, he reported that it was impossible to separate innervation from the left aortic nerve origin and the left vagus origin once the fibers have entered the adventitia of the ductus.

Furthermore, Takino and Watanabe (1937) also described slowing of the heart and a marked fall in blood pressure following mechanical or electrical stimulation of the pulmonary artery in the region of attachment of the LA of adult rabbits. The bradycardia and fall in blood pressure were not obtained when the stimulation had been preceded by sectioning of the left aortic (depressor) and left vagus nerves.

Though the functional significance of the presence of all these nerve fibers and even pressor receptors have not been fully and completely assessed, it does not change the narrative that

they are present. Boyd (Boyd 1941) speculated their role as being concerned in reflexes which aid in fetal blood pressure control.

Conclusive experiments about what happens to the innervation at birth when the circulation of blood through the ductus ceases are inconsistent and very scanty.

One study reports the persistence of a few of the nerve endings (Takino and Watanabe 1937), another report (Nonidez 1935) did not explicitly state that he found such endings in the LA of the adult rabbit but his statements suggest that he did for he writes *'the possible function of nerve-endings in the wall of the obliterated duct (LA of the adult) can only be surmised'*. Another study also reported the nerves of the ductus arteriosus as having a depressor function which is lost with age. The depressive function of this nerve is meant to serve during the first period of postembryonic development when the depressive function of Ludwig and Cyon nerve is absent the report concluded (Gavrilov 1958). The Ludwig and Cyon nerve is a depressor nerve which lowers blood pressure when stimulated.

1.1.4. Closure of ductus arteriosus

Postnatally, foetal circulation must swiftly make some adjustments to enable its transition into extra uterine life without any complications. This often requires closure of foetal shunts. This closure is both anatomical and physiological in nature and its relevance cannot be downplayed as failure to close is abnormal and leads to diverse disorders within the cardiopulmonary vascular system and increased mortality in babies (Friedman and Fahey 1993, Morton and Brodsky 2016, Poeppelman and Tobias 2018).

Anatomically, this closure is characterized by formation of cushions by the intima cells, followed by infiltration of the subendothelial space with collagen, fibronectin and laminin, then the fragmentation of the internal elastic lamina and finally smooth muscle cell migration from the tunica media layer into the subendothelial space. From this point, permanent closure is achieved through structural remodeling and fibrosis of the tunica intima and media (De Reeder et al. 1989, Ho and Anderson 1979, Yoder et al. 1978).

Physiologically, the ductus arteriosus is no longer needed for lung by-pass after the newborn takes its first breath.

This requires then that the lumen of the structure obliterates and a cascade of processes is initiated to facilitate this obliteration which is determined by two overlapping processes,

i.e. increase in the level of arterial oxygen after first breath of baby and significant decrease in prostaglandin E2 leading to inability to sustain prenatal patency. Initial physiological changes together with initiation and maintenance of cascade of the earlier described anatomical occurrence are what ultimately lead to permanent ductus arteriosus closure (Coceani and Baragatti 2012). Though the ductus arteriosus normally closes after birth, occasionally the ductus arteriosus fails to close, resulting in a patent ductus arteriosus, which is clinically diagnosed when the ductus arteriosus is still open in term infants older than three months of age (Borow et al. 1981, Forsey et al. 2009). Such patients are treated for patent ductus arteriosus.

1.1.5. Ligamentum arteriosum

Also called the arterial ligament is a structure which connects to the superior surface of the proximal aortic arch and the pulmonary trunk. It usually develops about 3 weeks after birth and is considered as a remnant of the ductus arteriosus. Numerous earlier reports of the prenatal ductus arteriosus described this structure as undergoing complete obliteration and fibrosis shortly after birth and the remnant of this by-pass forms the LA (Chiruvolu and Jaleel 2009, Clyman 2006, Clyman et al. 1999, Heymann and Rudolph 1975). There have been few reports, however, reporting the persistence of smooth muscle in the structure (Dohr et al. 1986, Garcia 1975). Postnatal anatomical changes in the LA are also known to occur, and include calcification and bone formation. Calcification of the LA has been observed in both children and adults during computed tomography (CT) imaging (Beluffi et al. 1998, Currarino and Jackson 1970, Wimpfheimer 1996). Comparatively, there have been published reports on the morphology of the ductus arteriosus in several species (Boudreau et al. 1991, Gittenberger et al. 1980, 1985, Silver et al. 1981).

The generally accepted description of the LA is it being a band of connective tissue representing the remnant of the ductus arteriosus. No known studies reports what happens to the innervation of the ductus arteriosus in extra uterine life and (or) after its supposed obliteration.

1.2 Vascular innervation

1.2.1 Structural organization

Regulation of blood flow is under extensive control by the nervous system. Yet, vascular innervation is not uniform. Each organ and even each specific segment of the vascular bed within a given organ receives a characteristic supply of nerve fibers with distinct connectivities and distinct content of transmitters (Kummer 2011, Morris and Gibbins 1986). As the LA originates from the ductus arteriosus connecting the pulmonary arteries with the aorta, the innervation of arteries rather than of veins will be outlined here. Functional divisions of the peripheral nervous system contributing to arterial innervation include postganglionic sympathetic, postganglionic parasympathetic and sensory neurons.

1.2.2 Sympathetic innervation and noradrenergic signaling

Practically all arteries receive postganglionic sympathetic fibers. Their dominating transmitter is noradrenalin (NA), a catecholamine which is synthesized by neurons in a 3-step reaction from the amino acid tyrosine. Catecholamines are catechols, which are chemicals that have adjacent hydroxyl groups on a benzene ring (Westfall and Westfall (2006). Others also define catecholamines as they contain a catechol moiety, an amine side-chain and they are all derived from the amino acid tyrosine (Ahlquist 1948, Rang et al. 2007). Phenylalanine is the precursor for biosynthesis of catecholamines by being hydroxylated into the amino acid tyrosine by phenylalanine hydroxylase (PH). Tyrosine is then hydroxylated to 3, 4-dihydroxyphenylalanin (L-DOPA) by the action of tyrosine hydroxylase (TH) using molecular oxygen, iron and tetrahydrobiopterin as co-factors. This is the rate limiting step in catecholamine synthesis. Dopamine is synthesized from L-DOPA by decarboxylation through aromatic L-amino acid decarboxylase (AADC) with pyridoxal phosphate as a co-factor. Dopamine is then converted to NA by the dopamine-beta-hydroxylase (DβH) and finally by adding a methyl group NA is converted to adrenaline by the phenylethanolamine-N-methyltransferase (PNMT) enzyme (Nagatsu et al. 1964). Conclusively, a cell that uses adrenaline as its transmitter contains five enzymes (PH, TH, AADC, DβH, PNMT), where for NA it will be three enzymes lacking PNMT and in dopamine only PH, TH and AADC (Fig. 2). TH is a marker for neuron and endocrine cells containing dopamine, NA and epinephrine (Weihe et al. 2006). It is present in the central nervous system (CNS), peripheral sympathetic neurons and the adrenal medulla and is encoded by the TH gene in humans (Nagatsu 1995). TH-immunoreactivity is indicative of

cells synthesizing adrenaline, noradrenaline or dopamine (Olsson 2016) and TH-immunolabeling is a suitable tool to visualize perivascular sympathetic nerve fibers (Wassall et al. 2009).

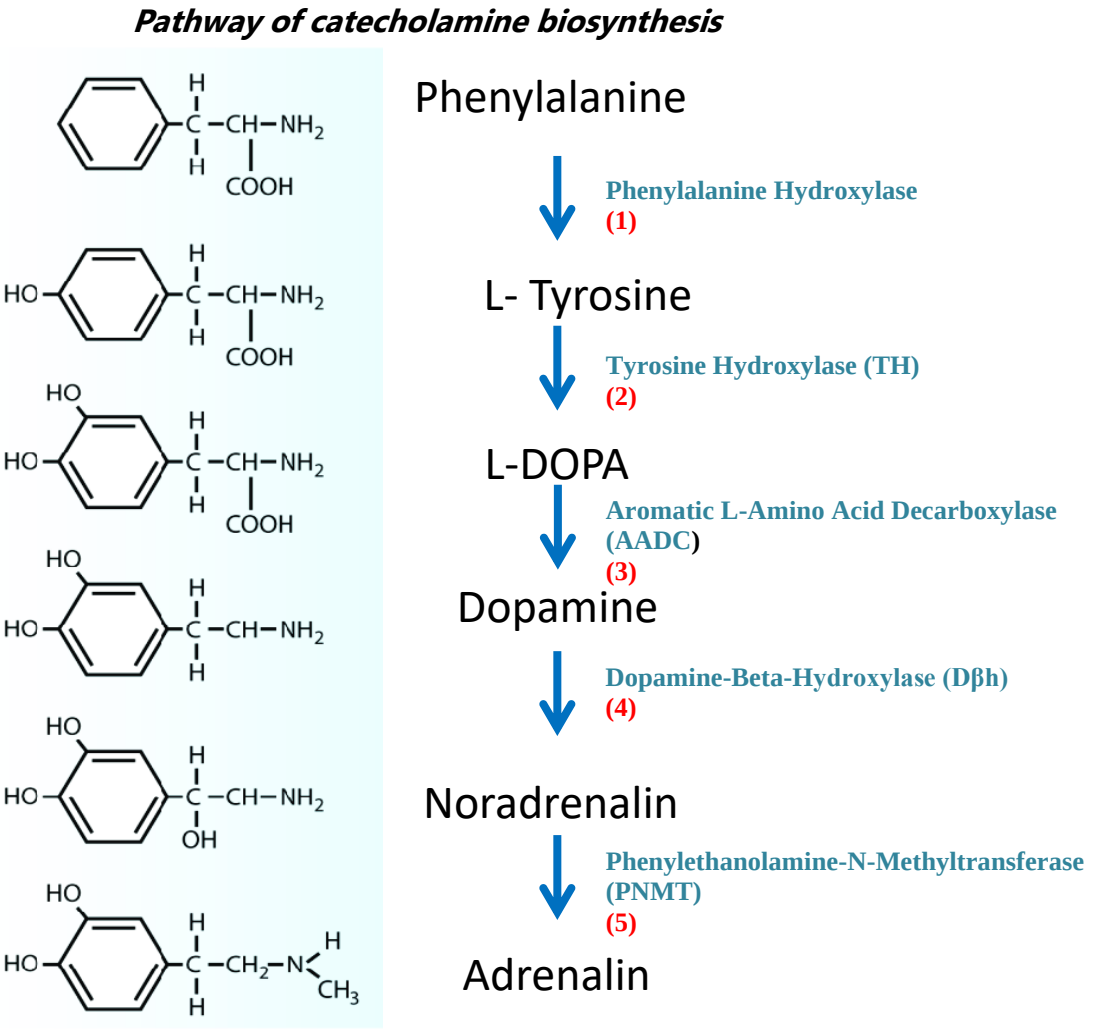

Figure 2. Schematic diagram of catecholamines biosynthesis pathway and its enzymatic.

steps.

Once released from sympathetic terminals, NA acts upon adrenergic receptors on target cells. Ahlquist in 1948 classified the adrenergic receptors as alpha or beta (α or β), based on their response to epinephrine, norepinephrine, and isoproterenol. They all a G-protein coupled receptors (GPCR). Alpha receptors are further divided into alpha 1&2 (α1 & α2). These are currently further grouped into 3 subtypes each (α1A, α1B, α1D, α2A/D, α2B, α2C). Beta adrenoceptors also have 3 subtypes (β1, β2, and β3) (Guimarães and Moura 2001, Strosberg 1993). The β-adrenoceptors respond to much lower concentrations of epinephrine or norepinephrine than α-receptors. All of the β-adrenoceptors are linked to

the G-protein Gs; α1 receptors are linked to Gq, and α2 receptors are linked to Gi (Guimarães and Moura 2001, Insel 1993, Strosberg 1993). Alpha 1A (α1) is present in the eye, urethra and prostate, and α1B and α1D are present in blood vessels playing a role in vasoconstriction and blood pressure maintenance. Alpha 2 receptors are present in both pre and post-synaptic nerve terminals and act as a brake by inhibiting the release of noradrenaline (Schwartz 1997). Some other actions of α2 receptors, on the other hand, include, but are not limited to, increasing the blood's clotting tendency, decreasing the release of insulin, and decreasing vascular resistance in the periphery (Fagerholm et al. 2011).

Beta adrenergic receptors are responsible for stimulating different physiological functions. β2-receptors promote smooth muscle relaxation in organs such as blood vessels, bronchus, uterus, and gastrointestinal tract, skeletal muscle metabolism, and insulin secretion (Rang et al. 2007, Westfall and Westfall (2006), and increased perfusion and vasodilation in blood vessels (Rang 2003). Beta 3-adrenoreeceptors facilitate lipolysis, detrusor smooth muscle relaxation, increase bladder capacity, and promote thermogenesis in skeletal muscle (Ferrer-Lorente et al. 2005, Rang 2003).

The vascular endothelium possesses at least five different adrenoceptor subtypes (α2A/D, α2C, β1, β2, and β3), which has an effect on basal vascular tone regulation directly or indirectly by stimulating the release and metabolism of nitric oxide release. (Altman et al. 1999, Jin and Loscalzo 2010).

1.2.3 Co-transmission in sympathetic innervation

Vascular control by sympathetic fibers is not limited to noradrenergic signaling acting upon adrenergic receptors, but commonly there are co-transmitters also being released upon stimulation of sympathetic terminals. One of these is adenosinetriphosphate (ATP) that acts on various purinergic receptors in the arterial wall (Blanco-Rivero et al. 2021, Ralevic 2000, Zhang et al. 2006). Besides these small molecule transmitters (NA, ATP), several neuropeptides can be produced by and released from sympathetic neurons. The most common peptide found within perivascular sympathetic nerve fibers is neuropeptide Y (NPY, Lundberg et al. 1982, Morris et al. 1986a, Uddman et al. 1985). In axon terminals, it is not stored in the small synaptic vesicles containing NA, but in large dense core vesicles (Paquet et al. 1996, Marx et al. 1999). Thus, its release is not necessarily coupled to NA release. In general, NA release is higher at low firing frequencies of the neuron, and release

of NPY (as that of neuropeptides in general) occurs predominantly at higher firing frequencies (Morris et al. 1995, Morris 1995). NPY is a 36 amino acid long tyrosine-rich peptide acting upon 6 different specific G protein-coupled receptors (GPCRs) termed Y1R to Y6R (Tan et al. 2018). Amongst its many roles such as being a potent vasoconstrictor, there is also an opposing effect between NA and NPY like in the control of lipolysis or even regulation of NA release. It has also been implicated in vasculature and metabolism pathology (Everitt et al. 1984, Hokfelt et al. 1983, Hunt et al. 1981, Tan et al. 2018). It needs to be emphasized that expression of NPY is not restricted to noradrenergic sympathetic neurons. It is also sometimes co-localized with the neuropeptide vasoactive intestinal peptide (VIP) in non-noradrenergic sympathetic neurons (Kummer and Heym 1991) and, even more frequently, in cholinergic parasympathetic neurons (Kawashima et al. 2021, Leblanc et al. 1987). Thus, identification of perivascular axons as noradrenergic sympathetic fibers utilizing NPY as co-transmitter required simultaneous demonstration of both, TH and NPY.

1.2.4 Parasympathetic vascular innervation

Parasympathetic innervation of arteries is restricted to certain vascular beds, being particularly prominent around cranial (Baraniuk 1992, Wahl et al. 1985) and pelvic vessels (Anderson 1984, Greiss et al. 1967), but absent at arteries supplying the limbs. In the thorax, the vasculature of heart and lung also receives parasympathetic fibers (Morris and Gibbins 1990). The prototypical transmitter utilized by postganglionic parasympathetic neurons is acetylcholine (ACh). The enzyme choline acetyltransferase (ChAT) synthesizes ACh from choline and acetyl-CoA, and acetylcholinesterase (AChE) can degrade it into the inactive metabolites choline and acetate (de Jonge et al. 2005). Acetylcholine can bind to two types of receptors, These receptors are named based on their responsiveness to the muscarine and nicotine receptors as either muscarinic (mAChR) or nicotinic (nAChR) respectively, and are both widely expressed in neuronal as well as non-neuronal cells (Carlson and Kraus 2019, Purves et al. 2008). Many different nicotinic (α1–α10 and β1–β4) and muscarinic (M1–M5) subunits have been identified, leading to a wide variety of possible receptors with different physiological functions (de Jonge et al. 2005, Kalamida et al. 2007, Wess 1996). Nicotinic receptors are a group of transmembrane ion-channel proteins which open to selectively allow ions to pass. For this reason they are referred as ionotropic or ligand-gated ion channel receptor. On the other hand, muscarinic ACh receptors are GPCR and signal via heterotrimeric GTP binding proteins (G proteins). The

M3 receptors are mainly expressed in vascular endothelium. The predominate effect of M3 receptor activation is dilatation of the vessels, by stimulating nitric oxide (NO) production by vascular endothelial cells (Brodde and Michel 1999).

Like in sympathetic neurons, cotransmission is the rule rather than the exception also in parasympathetic neurons. In terms of vascular actions, NO and the neuropeptide vasoactive intestinal peptide (VIP) are even more relevant than ACh. NO can be synthesized by 3 different isoforms of NO synthases (NOS), and one of them was originally identified in the nervous system and is, therefore, termed neuronal NOS (nNOS, Bredt et al. 1990). NO relaxes smooth muscle by raising intracellular cyclic GMP levels through direct activation of a soluble guanylate cyclase (Waldman and Murad 1988). Parasympathetic vasodilator neurons express nNOS together with VIP (Kummer et al. 1992), a peptide activating specific GPCR coupled to adenylate cyclase, thereby raising intracellular cyclic adenosine monophosphate (cAMP) levels (Groneberg et al. 2006). Not all nitrergic (utilizing NO as transmitter) parasympathetic neurons are also cholinergic, as it has been convincingly shown first for a subset of parasympathetic NOS/VIP-positive neurons innervating tracheal smooth muscle (Fischer et al. 1996). With regard to parasympathetic vascular innervation, it has not been systematically investigated yet, whether the postganglionic express ChAT and NOS simultaneously, so that ACh and NO a true co-transmitters, or whether there are separate subsets of cholinergic and nitrergic neurons. Thus, to visualize parasympathetic perivascular fibers, the occurrence of nNOS and ChAT has to be investigated, since restriction to only one of them might lead to missing a substantial fiber population.

1.2.5 Sensory vascular innervation

All arteries are innervated by at least some sensory nerve fibers. Specialized mechanosensitive fibers ramify in the wall of some particular segments of the vascular bed, such as the carotid sinus and the aortic arch, and monitor distension, which is readout for intravascular blood pressure (Ditting et al. 2005, Park et al. 2003). This information is carried towards the brainstem via fast conducting myelinated fibers and represents the afferent arc of pressure-lowering baroreflexes (Longhurst 1984). Nearly ubiquitous, however, is innervation by C-fiber terminals containing the neuropeptides calcitonin gene-related peptide (CGRP) and/or substance P (SP) (Furness et al. 1982, Gibbins et al. 1985, Papka et al. 1984, Wharton et al. 1981). CGRP is a potent dilator of peripheral blood vessels (Brain et al. 1985, Fischer et al. 1983, Uddmann et al. 1985). Furthermore,

immunocytochemical studies have revealed that CGRP coexists with SP in nerve cell bodies of sensory ganglia (Gibbins et al. 1985, Sundler et al. 1985). Such fibers have the peculiar property that, upon stimulation, they not only convey this information to the CNS, but they also release these neuropeptides into their surrounding (local effector function of sensory neurons: Holzer and Maggi 1998). At postcapillary venules, the combined action of CGRP, a vasodilator, and SP, which induces leakiness by leading to gap formation between endothelial cells, leads to readness (increased blood flow) and swelling (plasma extravasation), the so-called "neurogenic inflammation" (Holzer 1998). Thus, neural regulation of blood vessels is not always mediated by autonomic efferent (sympathetic or parasympathetic) neurons, as it can involve other mechanisms.

1.3 Hypothesis

Though the LA has generally been considered as a fibrosed remnant of the ductus arteriosus, rupture of the aortic arch in certain blunt trauma conditions indicates that it may still has mechanical impact on both the pulmonary bifurcation and the aortic arch. Significant evidence reports autonomic nerve fibers and baroceptive apparatus within the ductus arteriosus in-utero whereas for the LA, reports are anecdotal and contradictory. Based on this premise, we hypothesize that:

1. LA, the remnant of the foetal muscular artery (ductus arteriosus) which connects the main lung (pulmonary trunk) and main body (aorta) arteries during embryological circulation, is not a mere fibrotic remnant resulting from the complete metamorphosis of the ductus arteriosus but may retain some of its contractile muscular elements.

2. Even in post-uterine life, this foetal shunt still receives innervation.

3. This innervation controls contractility of the muscular elements.

1.4 Aim of the study

To test hypothesis 1, LA of human, pig, wild-type and transgenic mice were studied using routine standard and special histological staining methods, immunofluorescence labeling using antibodies directed against smooth muscle cell and transmission electron microscopy (TEM) to elucidate the general histological morphology and ultrastructure of the LA. Furthermore, organ bath experiments were performed to measure isometric contraction in

pigs LA after administration of adrenergic agonists and antagonists. To test hypothesis 2, two different transgenic mice strains expressing green fluorescence protein (GFP) in autonomic postganglionic neurons were used. Also, LA of human, pig, and wild-type mice were studied using single- and double-immunofluorescence labeling using antibodies directed against neurotransmitter synthesizing enzymes (TH, nNOS, ChAT) and neuropeptides (NPY, SP, CGRP, VIP). Additionally, TEM and immunohistochemical studies were performed. Finally, hypothesis 3 was investigated by subjecting pig LA to electrical field stimulation (EFS).

2 Materials and methods

2.1 Samples used

2.1.1 Mice

Chat^{BAC}-eGFP transgenic mice (Tallini et al. 2006) of both genders, aged 6 weeks to 5 months, expressing enhanced green fluorescence protein (eGFP) under the control of the promoter of the acetylcholine synthesizing enzyme, choline acetyltransferase (*Chat*-eGFP, n = 8, aged 6 to 20 weeks, both genders) were obtained from Jackson Laboratory (Bar Habor, ME, USA). Transgenic mice expressing eGFP under the promoter of neuronal nicotinic ACh receptor subunit alpha 3 (nAChRα3-eGFP, Frahm et al. 2011, n = 10, aged 6 to 20 weeks, both genders) served as a tool to visualize the expression of the α3 nicotinic ACh receptor (nAChR) subunit. Wild type mice (C57BL/6J, n = 20 aged between 8 to 30 weeks) from Janvier Laboratories (Le Genest-Saint-Isle, France) were also used. All animals were housed under standard laboratory specific-pathogen-free (SPF) conditions (10 h dark, 14 h light). In this facility, health monitoring of mice takes place quarterly following the FELASA recommendations for health monitoring of rodents. The protocol was registered by the local authorities (Animal Welfare Officer at the University of Giessen and the Committee for Animal Welfare, Dept. V54, Regierungspräsidium Giessen, Germany; reference no. 571_M, 572_M and 714_M. All samples were taken after mice were killed by inhalation of 5% isoflurane (Abbott, Wiesbaden, Germany) followed by cervical dislocation. Sacrificed mice were fixed on a board, and after application of 70% alcohol, were dissected to expose the thoracic cavity and its contents. Mediastinal blocks without the heart, excised within the pericardial sac were harvested and immersed in Zamboni fixative (2% paraformaldehyde and 15% saturated picric acid in 0.1 M phosphate buffer, pH 7.4) for 5–6 h. Specimens were then repeatedly washed in 0.1 M phosphate buffer (0.1 M NaH_2PO_4, 0.1 M Na_2HPO_4) until fluid was clear, incubated overnight in 18 % sucrose (Carl Roth GmbH and Co, Germany) in 0.1 M phosphate buffer, pH 7.4, and then frozen in optimal cutting temperature (OCT) compound (Tissue Tek, Sakura Finetek, Staufen, Germany) by using 2-methylbutane (Carl Roth GmbH and Co, Germany) chilled with liquid nitrogen. The sample blocks were labeled with the type of organ, batch number of mouse, type of mouse and day of sacrifice.

MOUSE

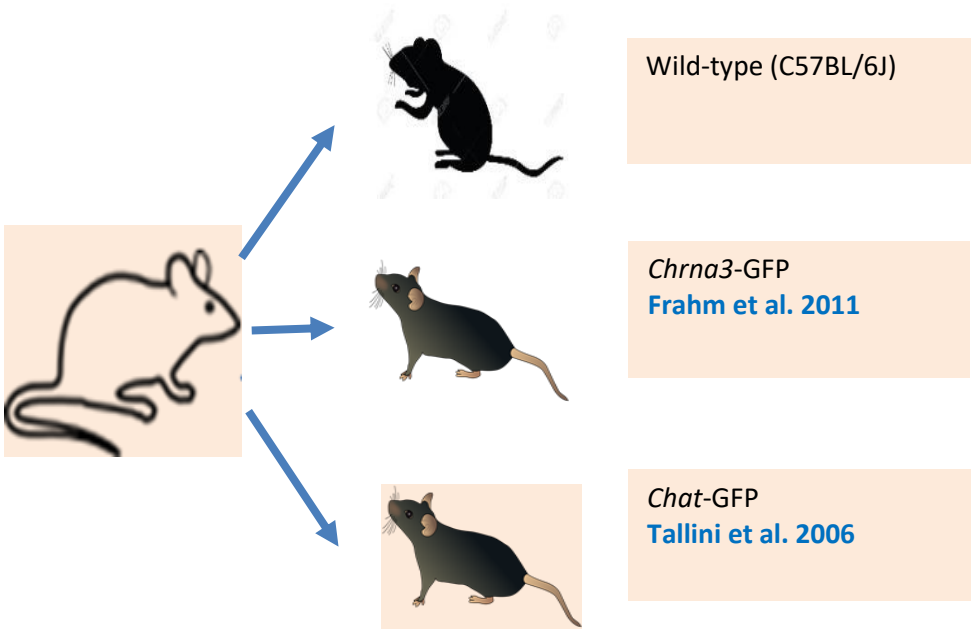

Figure 3. Mouse strains used in this study. nAChRα3-eGFP mice, express fluorescence in all postganglionic autonomic neurons. *Chat*-GFP mice express fluorescence in all cholinergic neurons.

2.1.2 Pig

Mediastinal blocks including the heart and lungs were acquired from a commercial pig abattoir in Hüttenberg. The pigs were females (n = 60) aged between 6 months to one year. The mediastinal blocks were immediately kept on ice and transported to the laboratory in an ice cooler. The LA was dissected and excised from its attachments to the aorta and pulmonary trunk (Figure 4). The samples to be used for organ bath experiments were immediately put in minimum essential medium (MEM, 51200-046, Thermo Fisher, Germany) mixed with 1% penicillin and streptomycin (P4353, Sigma-Aldrich, Germany). Samples for immunofluorescence were immersed in Zamboni fixative (n = 35) for between 5-6 h. Specimens were then repeatedly washed in 0.1 M phosphate buffer until fluid was clear, incubated overnight in 18 % sucrose (Carl Roth GmbH and Co, Germany) in 0.1 M phosphate buffer, and then frozen in tissue tek OCT compound (Sakura Finetek, Staufen, Germany) by using 2-methylbutane chilled with liquid nitrogen. The sample blocks were labeled with the type of organ and day of sample acquisition from the abattoir. The abattoir

has a qualified veterinary doctor who was present at the beginning of slaughter until the end. Pigs were thoroughly examined by the veterinarian.

2.1.3 Human

The LA from body donors of the anatomy dissection course in the Justus Liebig University was dissected and excised with its attachment to the two major vascular segments that it is attached. There were 6 females and 4 males aged between 67-97 years. The ligaments were immersed in Zamboni fixative for one day to refix them even though they had already been fixed with a fixative for the dissection course comprising of 10 l of 90% ethanol (57%), 1.3 l of 37% formalin (3%), 0.8 l of phenoxyethanol (5%) and 0.8 l of glycerin (5%). These were all added to 3 l of water.

2.2 Tissue processing and sectioning for microscopy

2.2.1 Cryoprotection and freezing

In mice, harvested mediastinal blocks containing the LA, and in pigs, the LA dissected and excised from its attachment to the aorta and pulmonary trunk, were placed in Zamboni fixative for about 5-6 h. The solution was then replaced by 0.1 M phosphate buffer and changed every hour until fluid around the sample was clear. The sample was then incubated overnight in 18% sucrose in 0.1 M phosphate buffer and kept at 4ºC. The samples were removed from sample bottles and put in a petri dish on ice. They were then individually put into a cryomold (Sakura, Finetek, Niederland) filled with OCT compound (tissue tek, Sakura Finetek, Staufen, Germany) and brought to a freeze using 2-methylbutane solution (Carl Roth GmbH, Germany) which had been chilled using liquid nitrogen. The frozen samples were carefully removed from the cryomold and attached to a labelled filter paper (Schleicher and Schuell, Germany). The samples were then wrapped in parafilm (Bermis, USA), put in labeled zip lock bags (type of animal, type of tissue, date of sacrifice) and kept at -20 ºC.

Samples from mediastinal blocks of mice, human, and pig LA, subjected to processing protocol described above were used for negative and positive control for all immunofluorescent staining.

The gut of wild-type mice were harvested and processed using earlier described protocol, and used as positive controls in nicotinamide adenine dinucleotide phosphate (NADPH) diaphorase reaction.

For sectioning, tissues were removed as needed and placed in temperature between -15 to -25℃ for 30 min in cryostat (Microm HM560, Thermo Fisher Scientific, Germany). After calibration of cryostat, sample blocks were cut in thickness of 10 µm and collected on precleaned, SuperFrost microscope slides (R. Langenbrinck, Emmendingen, Germany). They were then air dried for at least one hour and put in labelled plastic slide boxes and put back in -20℃. The cryostat was cleaned and disinfected using a brush and Leica cryofect (Leica, Nussloch, Germany).

2.2.2 Paraffin embedding and sectioning

Using an automatic processor (Leica TP 1020, Germany), tissues were dehydrated, cleared and infiltrated using increasing concentrations of ethanol, xylene immersions and paraffin wax (Sigma-Aldrich GmbH, Germany) respectively. The whole process was set up to run overnight using the underlisted protocol

Clearing

1. Xylene (VWR Chemicals, France)	20 min
2. Xylene (VWR Chemicals, France)	20 min
3. Xylene (VWR Chemicals, France)	45 min

Dehydration

1. 70% Ethanol (Sigma Aldrich, Germany)	15 min
2. 90% Ethanol (Sigma Aldrich, Germany)	15 min
3. 100% Ethanol (Sigma Aldrich, Germany)	15 min
4. 100% Ethanol (Sigma Aldrich, Germany)	15 min
5. 100% Ethanol (Sigma Aldrich, Germany)	30 min
6. 100% Ethanol (Sigma Aldrich, Germany)	45 min

Wax infiltration

Paraffin wax was infiltrated into tissues at 60°C and then allowed to cool to 20°C where it solidified to a consistency that allowed sections to be consistently cut.

1. Paraffin wax	30 min
2. Paraffin wax	30 min
3. Paraffin wax	45 min

The blocks were sectioned at 10 µm thickness (Leica RM 2255, Germany). Paraffin ribbons or slices were placed in 40-45ºC water bath and swimming paraffin sections were fished out using SuperFrost glass slides. Sections were dried at 37ºC. Every continuous series of 5 were collected and stored in this fashion and the next 25 sections were discarded.

2.2.3 Electron microscopy

LA of wild type mice (n = 8) was fixed overnight in a fixative mixture consisting of 1.5% glutaraldehyde (Merck, Germany) and 1.5% paraformaldehyde (Merck, Germany) in 0.1 M phosphate buffer. After fixation, tissues were washed in 0.15 M HEPES buffer 5 x 10 min, osmicated for 2 h in aqueous 1% osmium tetroxide (Sigma Aldrich, Germany) and washed in distilled water 3 x 10 min each. Specimens were contrasted in aqueous 1% uranyl acetate (Merck, Germany) overnight. Tissues were washed 2 x 15 min in distilled water and dehydrated with increasing concentration of ethanol (30%, 50%, 70%, and 90%) 10 min for each concentration. Tissues were dehydrated 2 x 10 min in 100% ethanol, then 1 x 15 min in 100% ethanol + propylene oxide (Merck, Germany), then for 1 h in propylene oxide (Merck, Germany) + epon (Agar scientific, UK) and embedded in epon overnight. The next day, samples were put in desiccators for 2 h and put in fresh epon and left in 37°C for 48 h. Epon embedded blocks were trimmed after 48 h using sample trimmer (C. Reichert TM 60, Austria). Using an ultra-microtome (Leica Ultracut E, Wetzlar, Germany), semi-thin sections of 750 nm thickness were cut and stained with ready to use methylene blue solution (Carl Roth GmbH and Co, Germany) in 1% tri-potassium phosphate (Merck, Germany) in 1:1 ratio, respectively. This was followed by cutting ultra-thin sections between 70 to 90 nm thicknesses, which were collected on 150 mesh copper grids (Firma Plano, Wetzlar, Germany). The ultrathin sections were viewed using an transmission electron microscope (EM 902 N, Zeiss, Germany) equipped with a slow scan 2 K CCD

camera (TRS, Tröndle, Moorenweis, Germany) connected to Image SP software version 1.2.8.57 (Unitary enterprise “SYSPROG”).

All measurements for LA were conducted using the automatic scale bars obtained with micrographs. For counting the number of dense core and small clear vesicles, measurement of vesicle size, length and width of dense bands and nerve terminals, the ImageJ 1.X software (Schneider et al. 2012) was used.

2.3 Staining techniques

2.3.1 Immunofluorescence

Frozen tissues sections were allowed to air-dry for 1 h at room temperature. Then they were covered for 1 h with blocking medium (Table 2) and subsequently incubated with primary antibodies (Table 3). The primary antibodies were dissolved in phosphate buffered saline (PBS) with addition of NaN_3+S (0.01% NaN_3 and 0.05 M NaCl) in the working dilution. For transgenic mice expressing eGFP, single-immunolabelling was performed by applying primary antibodies overnight at room temperature, followed by washing steps (2 × 10 min in PBS) and subsequent 1 h incubation with secondary antibodies all conjugated to cyanine 3 (Cy3, Table 4). In 12 wild-type mice, double-immunolabelling was performed by applying primary antibody against αSMA conjugated to fluorescein isothiocyanate (FITC) overnight at room temperature, followed by washing steps (2 × 10 min in PBS) and subsequent 1 h incubation with secondary antibodies all conjugated to cyanine 3 (Cy3, Table 4) targeted at primary antibodies against antigens other than αSMA. Additionally, in the remaining 8 wild-type mice, when primary antibody directed against αSMA was not used, double-immunolabelling was performed using a cocktail of primary antibodies against two different antigens applied overnight at room temperature, followed by washing steps (2 × 10 min in PBS) and subsequent 1 h incubation with secondary antibodies conjugated to Cy3 and FITC (Table 4). This was followed by PBS washes (2 × 10 min). The sections were fixed in 4% paraformaldehyde (PFA) for 10 min, followed by a final washing in PBS (2 x 10 min). Finally, sections were covered in carbonate-buffered glycerol (Carl Roth GmbH and Co, Karlsruhe, Germany) at pH 8.6. Evaluation and measurements were done using an epifluorescence microscope (BX 60, Olympus, Hamburg, Germany or Axioplan 2 imaging, Zeiss, Jena, Germany) equipped with cameras (Olympus DP73 and AxioCam MRm, Germany) connected to Cell Sens Dimension 2.1 and AxioVision Rel

4.8.2 SPZ softwares, respectively. The microscope was equipped with the appropriate filter combinations (Table 5).

Measurements for LA were obtained using scale bars obtained from objective micrometer (Ax0003 OB-M, Japan). Images of interest were printed and imaginary longitudinal and cross-sectional lines intersecting at the center of LA was used as a point of reference to measure the size of the structure. Using a measuring ruler with reference to scale bar obtained from the micrometer, measurements were taken from its longest axis.

Zamboni solution	2% paraformaldehyde, 15% saturated picric acid in 0.1 M phosphate buffer, pH 7.4
0.1 M phosphate buffer	0.1 M NaH_2PO_4 x $2H_2O$ 31.2 g/l, 0.1 M Na_2HPO_4 x $2H_2O$ 35.6 g/l, pH 7.4
18% sucrose	99.5% saccharose + 0.1 M phosphate buffer
blocking solution	10% normal pork serum, 0.1% bovine serum albumin (BSA), 0.5% Tween 20 in PBS
buffered glycerol	solution A: 1.5 M Na_2CO_3, solution B: 1.5 M Na_2CO_3 pH 8.6, solution C: 100% glycerol
phosphate buffered salt solution (PBS)	solution A: NaH_2PO_4 x $2H_2O$ 28.75 ml, solution B: Na_2HPO_4 x $2H_2O$ 96.2 ml, pH 7.4, 22.4 g NaCl
PBS+S	solution A: NaH_2PO_4 x $2H_2O$ 28.75 ml, solution B: Na_2HPO_4 x $2H_2O$ 96.2 ml, pH 7.4, 44.8 g NaCl
4% paraformaldehyde	paraformaldehyde, 0.1 M phosphate buffer
citric acid	9.62 g/l citric acid, 13 pellets NaOH, 2 M NaOH, pH 6.0

Table 2 Buffers and solutions used

Antigen	Host species	Dilution	Source	Code
Protein gene product 9.5 (PGP 9.5)	Rabbit (P)	1:8000	BioTreno, Germany	BT-78-63050
Calcitonin gene-related peptide (CGRP)	Goat (P)	1:40 000	Peninsula Laboratories International, Inc, U.S.A.	A-16947
Substance P (SP)	Rat (M)	1:400	Santa Cruz Biotechnology, U.S.A.	SC 21715
Tyrosine hydroxylase (TH)	Sheep (P)	1:800	Merck, Millipore, Germany	AB 1542
Neuropeptide Y (NPY)	Rabbit (P)	1:20000	Sigma-Aldrich, Germany	N-95528
Vasoactive intestinal peptide (VIP)	Sheep (P)	1:3000	Chemicon international, Germany	AB 1581
Nitric oxide synthase (NOS)	Rabbit (P)	1:800	Thermo Fisher Scientific, Germany	AB 6170
Choline acetyltransferase (ChAT)	Goat (P)	1:8000	Merck, Millipore, Germany	AB 144P
Alpha smooth muscle actin (αSMA)	Mouse (M)	1:1000	Sigma-Aldrich, Germany	F3777
Enhanced green fluorescent protein (eGFP)	Chicken (P)	1:2000	Novus Bio, Germany	NB-100-1614

Table 3 List of primary antibodies used. M = monoclonal, P = polyclonal

Antigen	Conjugate	Host species	Dilution	Catalogue number	Source
Rabbit Ig	Cy3	Donkey	1:2000	AP182C	Merck, Germany
Rat Ig	Cy3	Donkey	1:2000	712165150	Dianova, GmbH, Germany
Goat Ig	Cy3	Donkey	1:400	AP180C	Millipore, Germany
Mouse Ig	Cy3	Donkey	1:1000	715165151	Dianova, GmbH, Germany
Sheep Ig	Cy3	Donkey	1:2000	713165003	Dianova, GmbH, Germany
Rabbit Ig	Alexa 488	Donkey	1:500	A21206	Thermo Fisher, Germany
Rat Ig	FITC	Donkey	1:800	712095153	Dianova, GmbH, Germany
Chicken IgY	FITC	Donkey	1:800	713095147	Dianova, GmbH, Germany

Table 4 List of secondary antibodies used

Fluorochrome	Colour	Excitation filter (nm)	Barrier filter (nm)
4′,6-Diamidino-2-phenylindole (DAPI)	blue	360-370	420-460
FITC	green	460-490	515-550
Alexa 488	green	460-490	515-550
Cy3	red-orange	525-560	570-650

Table 5 Fluorochrome filters and excitation wavelengths in fluorescence microscopy

Human sections obtained from paraffin blocks, kept at room temperature in slide boxes, were also subjected to immunostaining.

The slides were put through dewaxing by incubating with xylene (2 x), then graded alcohol (100%, 96%, and 70%) for 5 min each.

All sections were washed 2 x in PBS and sections not selected for an antigen retrieval step through microwave treatment were left in PBS.

A cuvette containing sections for microwave treatment was immersed in 50 mM citric acid (Carl Roth GmbH and Co, Germany) buffer. Cuvette in citric acid was placed in a bowl containing 700 ml of water and put in microwave which had been set at 700 W. The microwave was observed until bubbles started appearing in the water. It was then set at the same wavelength and brought to a boil for 5 min. The sections were taken out and allowed to cool for about 15 min. The sections were removed and washed in PBS for 5 min. Then they were dried and blocking medium was applied. Procedure for immune staining as already described above was followed through after this point.

For controls in direct and indirect immunofluorescence, cryo- or paraffin sections from mediastinal blocks of mice, pig and human LA dissected from its attachment to major vessels from the same samples were processed and used. Negative controls, where the primary antibody were omitted and replaced by PBS and (or) positive controls where samples were stained under the same staining conditions were used for testing the specificity of antibody labeling. Samples for controls were usually a different section on the same slide or the immediate follow-up slide.

2.3.2 Histological staining

2.3.2.1 Hematoxylin and eosin staining

Paraffin embedded sections were deparaffinized using xylene (VWR Chemicals, France) 2 x for 3 to 4 min each, then rehydrated by passing it through the graded alcohol in decreasing order, i.e. absolute alcohol, 96% ethanol, then 70% ethanol (all from the same manufacturer, Sigma-Aldrich, Germany) 1 x for 5 min for each step. Sections were then washed in tap water and rinsed in distilled water. Before staining with dyes, sections were well drained. The slides were dipped in jar containing hematoxylin (Merck, Germany) stain for 3-5 min.

The slides were removed and put in distilled water for 20 s and left under running tap water for 10 min. The slides were dipped in eosin solution (Chroma Gesellschaft GmbH and Co, Germany) for 30 s to 1 min and rinsed with distilled water until water was clear. Slides were then passed through graded alcohol in increasing order, i.e. 70%, 96% then absolute alcohol for 1 x 5 min for each step. The slides were placed in xylene for 3 min, and then

the excess xylene was drained. Slides were mounted with distyrene plasticizer xylene (DPX, Sigma-Aldrich, Germany), cover-slipped and left to dry under the hood overnight.

2.3.2.2 Masson Goldner staining

Paraffin sections were deparaffinized using xylene 2 x for 3 to 4 min each, then rehydrated by passing it through the graded alcohol in decreasing order, i.e. absolute alcohol, 96% ethanol then 70% ethanol 1 x for 5 min for each step. Sections were then washed once in distilled water for 3 min. The slides were dipped in jar containing 'eisenhematoxylin' (Carl Roth GmbH and Co, Germany) stain for 5 min. The slides were removed and washed under running tap water for 15 min. The slides were dipped in Goldner I solution (Ponceau-Säurefuchsin, Carl Roth GmbH and Co, Germany) for 5 min, then in distilled water plus 1% vinegar for 30 s, then Goldner II (light green or differentiation stain, Carl Roth GmbH and Co, Germany) for 5 min and again in distilled water plus 1% vinegar (Merck, Germany) for 30 s. Slides were thereafter dehydrated very quickly through 70%, 90% and absolute alcohol, and cleared in isopropanol (Chem solute, Germany). Finally, slides were mounted with distyrene plasticizer xylene (DPX, Sigma-Aldrich, Germany), cover-slipped and left to dry under the hood overnight.

2.3.2.3 Elastica van Gieson staining

Paraffin sections were deparaffinized using xylene 2 x for 3 to 5 min each and rehydrated by passing it through the graded alcohol in decreasing order, i.e. absolute alcohol, 96% ethanol, then 70% ethanol for 1 x for 5 min for each step. The slides were dipped in jar containing resorcin fuchsin (Morphisto, Germany) stain for 15 min. The slides were removed and washed under running tap water until the water was clear and dye free. The slides were observed under a light microscope (Leica DM750, Germany) to ensure that slide is not over-stained. The slides were dipped in hematoxylin (Carl Roth GmbH and Co, Germany) for 2-3 min, removed and washed under running tap water for 10 min, then in distilled water for 1 min.

The slides were dipped again in Van-Gieson-Pikrofuchsin (Morphisto, Germany) for 2 min. Slides were thereafter dehydrated very quickly through 2 x 90% and 2 x absolute alcohol and cleared in isopropanol (Chem solute, Germany). Finally, slides were mounted with distyrene plasticizer xylene (DPX, Sigma-Aldrich, Germany), cover slipped and left to dry under the hood overnight.

2.3.2.4 Nicotinamide adenine dinucleotide phosphate (NADPH)-diaphorase reaction

I allowed frozen sections to air dry for 1 h at room temperature. A clean cuvette was warmed up at 37°C (B5042, Heraeus, Germany). While waiting, I mixed up 300 µl of Triton-100 (Carl Roth GmbH and Co, Karlsruhe, Germany) 0.1 mg/ml of nitroblue tetrazolium (Biomol, Hamburg, Germany), and 1 mg/ml of nicotinamide adenine dinucleotide phosphate (Biomol, Hamburg, Germany) in 0.1 M phosphate buffer in a flask. I covered the flask with silver foil and stirred it for 15 min until it was uniform. I then air-dried slides and incubated them in a warm cuvette at 37℃ for 45 min to 1 h. I washed 3 x 5 min in 0.1 M phosphate buffer. I dried and applied buffered glycerol and coverslips.

All sections subjected to the various histological staining's observed under a bright field microscope (Leica DM750, Germany) with integrated digital camera (ICC50 HD; Germany) connected to a monitor.

2.4 Organ bath

2.4.1 Tissue preparation

I dissected the LA from pig tissues obtained fresh from the commercial abattoir (Manz, Hüttenberg) and kept on ice immediately. Extra precaution was taken not pull or tug on the ligament as which may damage the tissue. The perivascular adipose tissue, all other extraneous tissue and blood clots were removed until the LA and its point of attachment to both the aorta and pulmonary trunk was visible (Figure 4). I ensured that the surrounding tissue around the ligament was handled gently and avoided direct contact as much as possible. I gently held the ligament at its point of attachment to the aorta and pulmonary trunk with forceps and used a scissors to dissect and detach the ligament between the two great vessels. I immediately placed it into minimum essential medium (MEM, 51200-046, Gibco, United Kingdom) mixed with 1% penicillin-streptomycin antibiotic (P4353, Sigma-Aldrich, Germany).

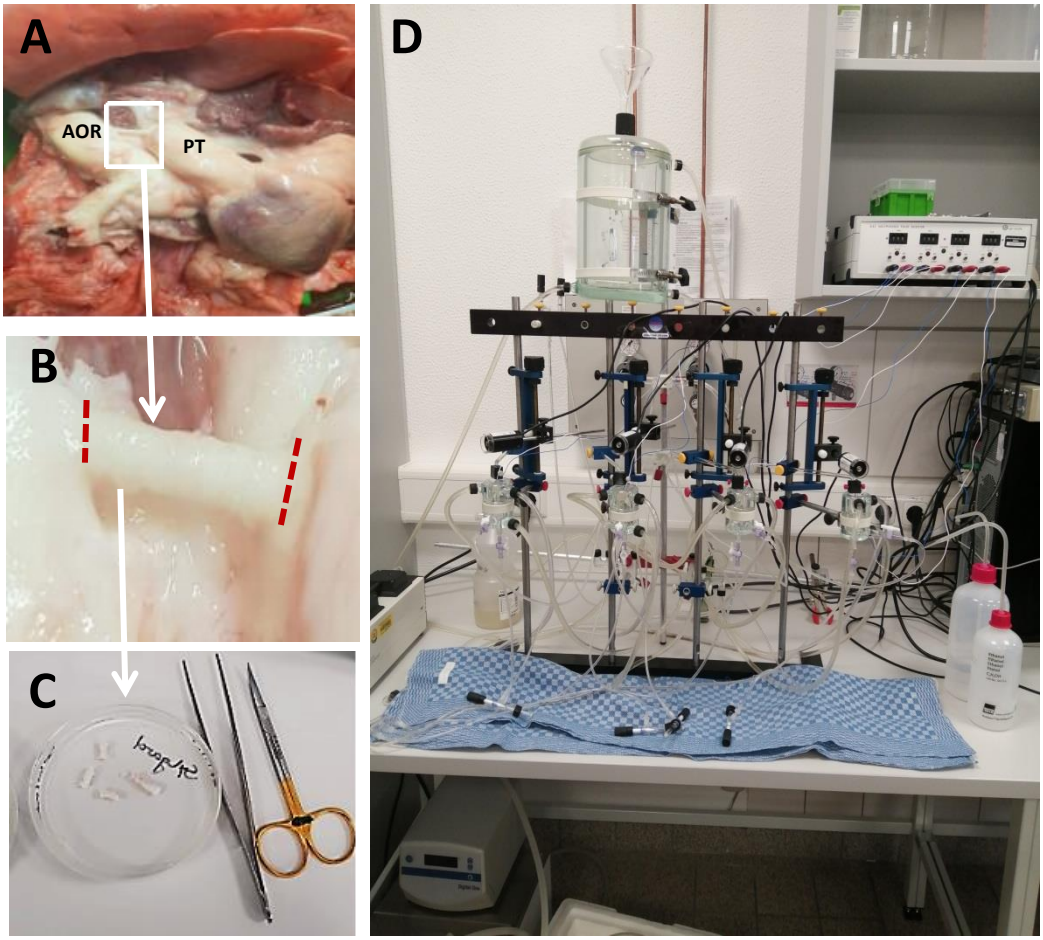

Figure 4 Pig LA preparations. A. Cleaned and dissected LA from pig mediastinal block with attachment to aorta (AOR) and pulmonary trunk (PT) intact. B. Excision of LA from aortic and pulmonary attachments. C. Excised LA in medium for organ bath experiments. D. Organ bath apparatus.

2.4.2 System preparation and setup

I filled the chambers with approximately 15 ml of MEM and primed the system to remove any air bubbles within the aeration tubing. Then I preheated the system to 37 °C by turning on the recirculating heated water bath (AD Instruments GmbH, Heidelberg, Germany) and allowed the solution to reach optimal temperature. I ensured that the launched data acquisition software (AD Instruments, Pty Ltd, Australia) had connection with data acquisition system. I then calibrated the force transducers at a resting tension between 0.3 – 0.5 g before I placed the tissue in bath.

2.4.3 Tissue placement in bath

I placed the LA in a prepared petri dish containing warm MEM. Using tooth-forceps, I gently placed tissue hooks on both edges of the LA.

I placed the end of isometric force transducer connected by cotton thread superiorly, while the opposite was connected to a fixed point at the bottom of the tissue holder. I placed and made sure the tissue was fully immersed in bath chamber and the rod was secure. I also ensured the silk thread hanged freely and the bath chambers were not slanted. These steps were repeated for the remaining chambers.

2.4.4 Experiments

For dose response curve experiments, at the beginning of each experiment, tissues were allowed to maintain a resting tension between 0.3 to 0.6 g for 10 min and thereafter subjected to electrical field stimulation (EFS, Multiplexing Pulse Booster, Ugo Basile, Gemonio, Italy) at 8, 16, and 32 Hz, 2 ms, 150 mA, 10 v for 1 min with 5 min resting time between these stimulations. This was then followed by administration of a cumulative concentration of noradrenalin (NA, A7257, Sigma-Aldrich, Germany), dissolved in 0.5 M HCl (Merck, Darmstadt, Germany) in MEM to reach the final desired concentration (0.1 µM, 1 µM, 10 µM, 100 µM, 500 µM, 1 mM and finally 1.5 mM). Allowing 10 min between each dose, NA doses were administered until the curve plateaued. In control experiments, the same protocol for EFS was followed; however, NA was replaced vehicle in tissue samples. Changes in tension were recorded as force in 30 s interval and evaluated by software (Lab Chart 7 AD Instruments GmbH, Heidelberg, Germany). All analyses were done and the half maximal effective concentration (EC_{50}) in response to NA was calculated using the GraphPad Prism software (asknet, Karlsruhe, Germany).

At the beginning of further experiments to observe effect of adrenergic blockers on a precontracted LA, tissues were allowed to maintain a resting tension between 0.3 to 0.6 g for 10 min and thereafter followed by administration of two successive but cumulative doses of NA (100 µM, 500 µM) allowing 10 min between each dose. This was followed by the cumulative administration of alpha1-adrenergic receptor blockers (tamsulosin, Cat # PHR1524 and prazosin, Cat # P7791), both purchased from Sigma-Aldrich, Germany to observe if these antagonists would relax the precontracted LA to baseline. Analysis of the

half maximal inhibition concentration (IC_{50}) in response to NA was calculated using the GraphPad Prism software Version 7.

2.4.5 Exclusion criteria

When the effect of EFS-induced contraction on the LA was investigated, only samples with more than 15% increase in tension to EFS at 16 Hz, 2 ms, 150 mA, 10 V were used. To study the effect of vasodilators on induced vasoconstriction, samples with more than 50% increase in tension from baseline after first dose (100 µM) of adrenergic agonists (NA) administration were used.

2.5 Data analysis

Data are presented as mean ± SEM (standard error of mean). The resulting data was graphed using GraphPad Prism 7. One way analysis of variance (ANOVA) was used to test for statistical significance of differences in maximal contraction values of EFS. EC_{50} and IC_{50} values of agonist and inhibitor responses respectively were estimated using nonlinear regression sigmoidal curve analysis using GraphPad Prism 7. Two tailed t-Test statistical testing was used to test the differences in length and width of dense bands found in myocytes. Differences were considered statistically significant when $P \leq 0.05$.

3 Results

3.1 General histological morphology of LA

3.1.1 Human

Routine and special histological staining revealed that in cross section, the LA could be divided into three distinct regions, namely from outward within, a tunica adventitia, tunica media and tunica intima (Figure 5A & B). The outermost layer, tunica adventitia is mainly made up of intertwining connective tissue cells, collagen fibers, nerves fiber bundles, and blood vessels. Aortic bodies were observed in 4 out of 10 samples (Figure 6). Numerous adipocytes and nerve fiber bundles were observed in the adventitial region and also within the connective tissue surrounding the adventitia. No clear distinction could be made between the adventitia region and surrounding connective tissue (Figure 7). The middle layer, the tunica media, averagely measuring 950 µm in width, was sharply contrasted from the adventitia. This layer could be further divided into an outer and inner zone. The outer zone was made up of loose connective tissue and sparsely arranged smooth muscle cells (Figure 8). The inner zone was mainly made up of smooth cells and collagen. The smooth muscle cells were compactly arranged and had several layers running in different orientations. In this same zone, there were areas where the collagenous tissue far exceeded the smooth muscle cells and other areas where only traces of collagen were seen between the layers of smooth muscle cells (Figure 9). Additionally, Elastica van Gieson stain confirmed the presence of elastic fibers (Figure 10). The innermost layer, averagely measuring 200 µm in width, had the appearance of the remnant of the tunica intima. There was the presence of an intricate network of collagen making up the core of this layer. In samples obtained from 3 females aged between 90 to 97 years old, this layer showed calcification and fibrosis at the core (Figure 11). In 4 out of ten samples processed for histological staining, there was the presence of a funnel with partial patency from the part of the LA connected to the aorta. This opening was not patent through the whole LA, therefore could not serve as passage way for blood flow from aortic side of the LA to the pulmonary side (Figure 12).

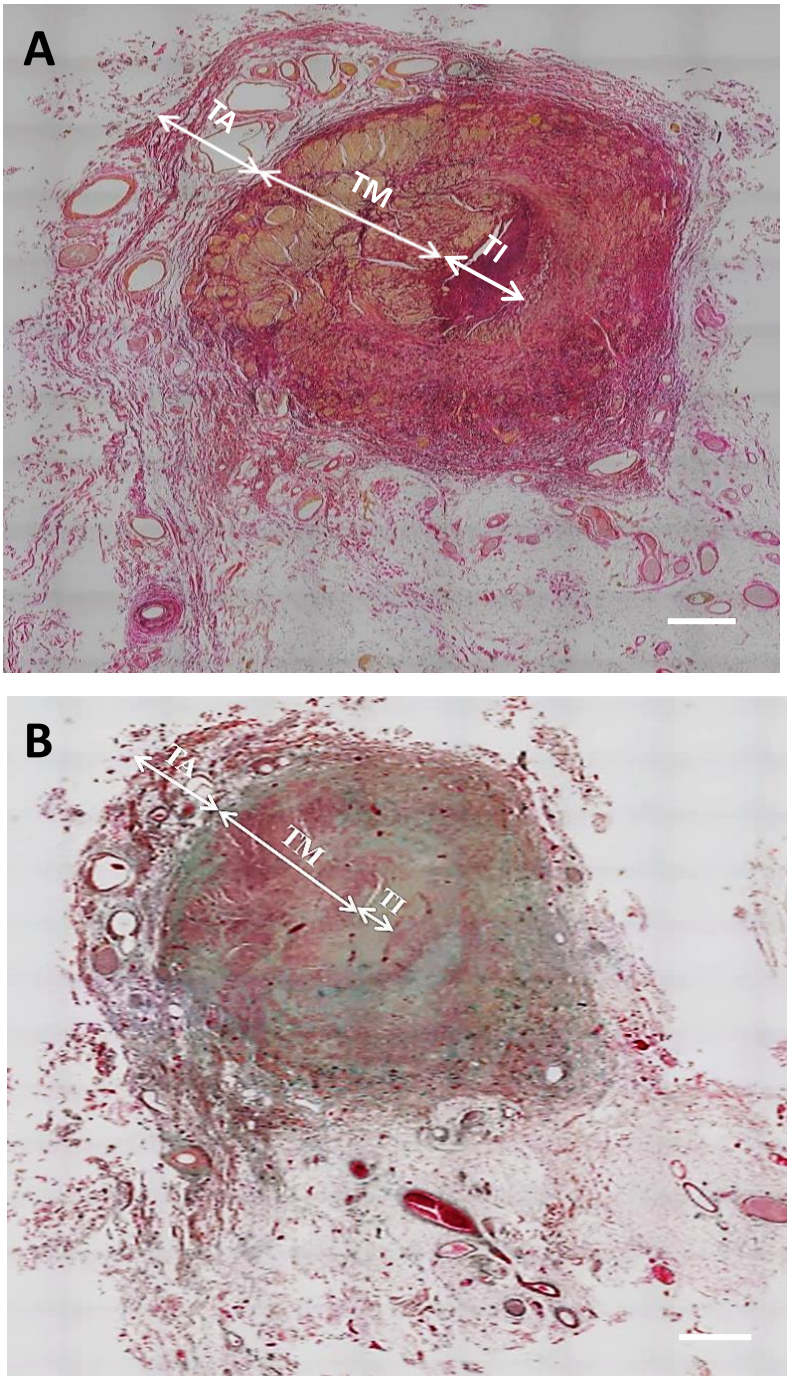

Figure 5. Elastica van Gieson (A) and Masson Goldner stain (B) of paraffin embedded human LA in cross-section showing three regions from outward within tunica adventitia and surrounding connective tissue (TA), tunica media (TM), and tunica intima (TI). Color scheme for (A) Red = collagen, Yellow = muscle, Violet-black = elastic fibers. For (B) Red = muscle/blood cells, Green = collagen, Black-brown = nuclei. Scale bars = 300 µm.

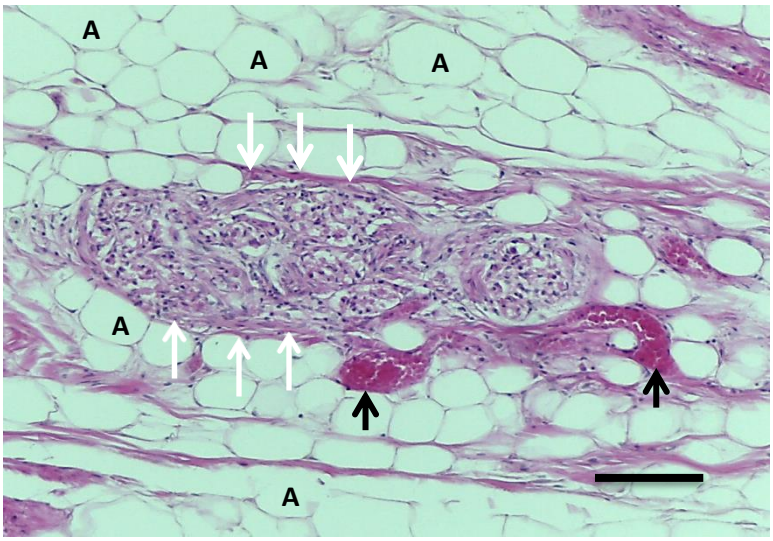

Figure 6. Hematoxylin and eosin staining of paraffin embedded LA showing an aortic body (white arrow) surrounded by various sizes of adipocytes (A) and venules (black arrows), located in the adventitia. Scale bar = 50 µm.

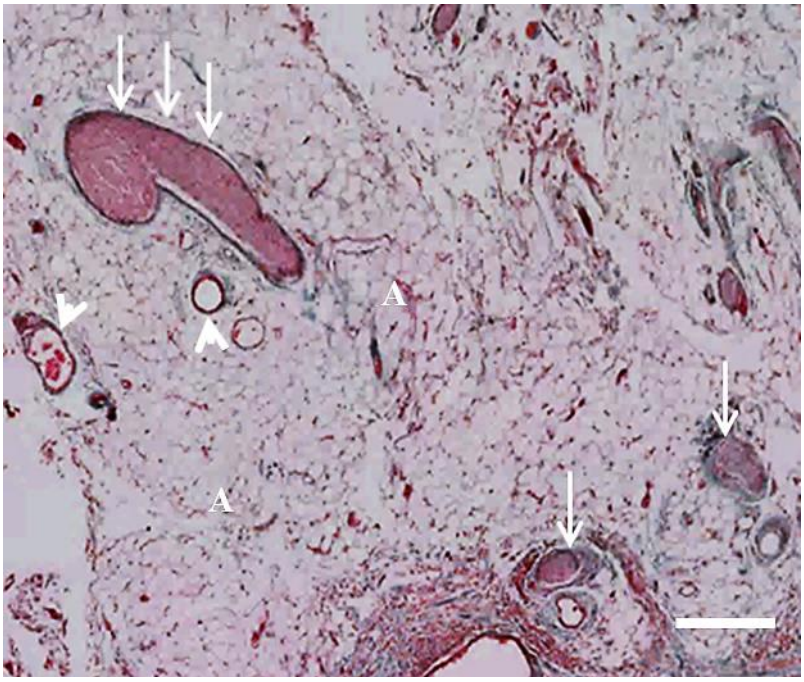

Figure 7. Paraffin embedded human LA stained with Masson Goldner Trichrome showing numerous adipocytes (A), nerves (white arrows), and blood vessels (white arrow heads) within the adventitial layer and the surrounding connective tissue. Scale bar = 50 µm.

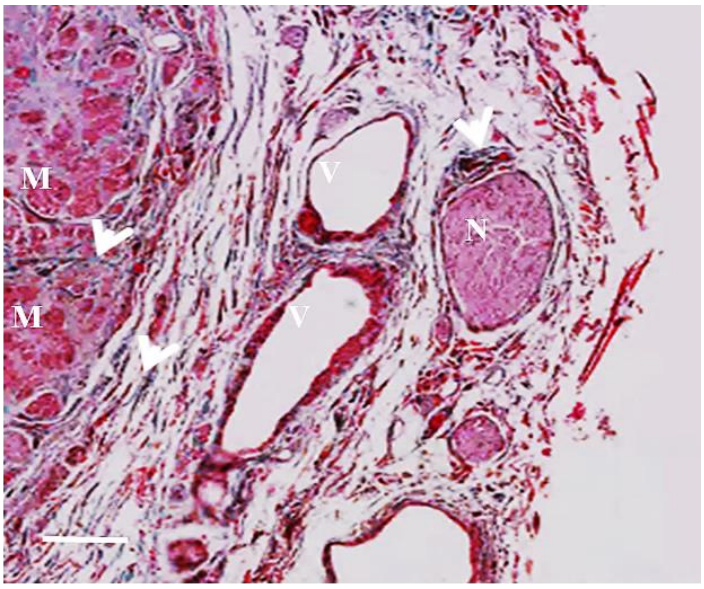

Figure 8. Paraffin embedded human LA stained with Masson Goldner trichrome showing a nerve (N), blood vessels (V), and collagen fibers (white arrow heads) in the adventitial layer. Bundles of myocytes (M) observed in the medial layer. Note the sharp contrast between the medial and the adventitial layer. Scale bar = 50 µm.

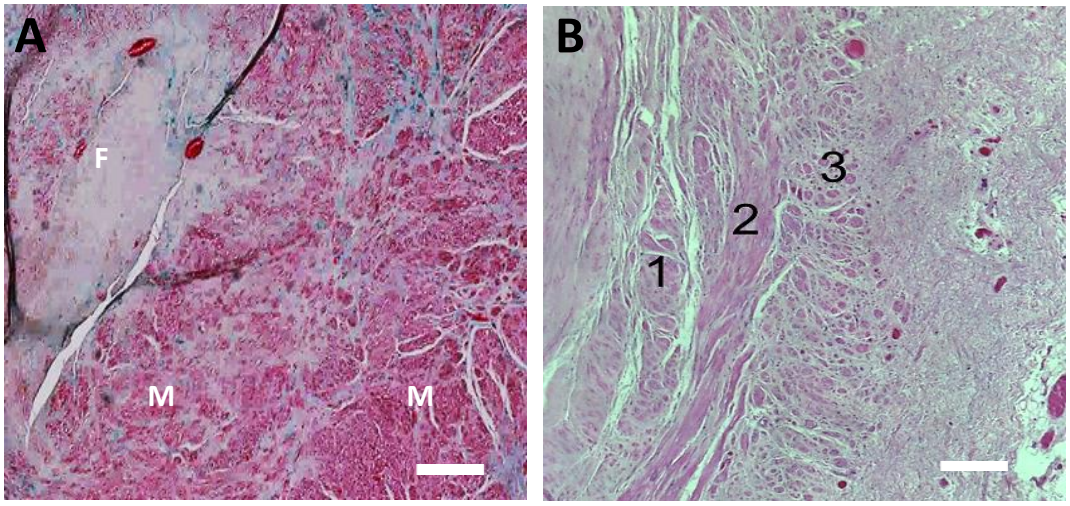

Figure 9. Paraffin embedded human LA stained with Masson Goldner trichrome (A) showing a fibrous core (F) in the intimal layer and narrowing layer of muscle cells (M) in the tunica media layer. Paraffin embedded human LA stained with hematoxylin and eosin (B) showing layers of muscle cells (1-3). Scale bar = 50 µm.

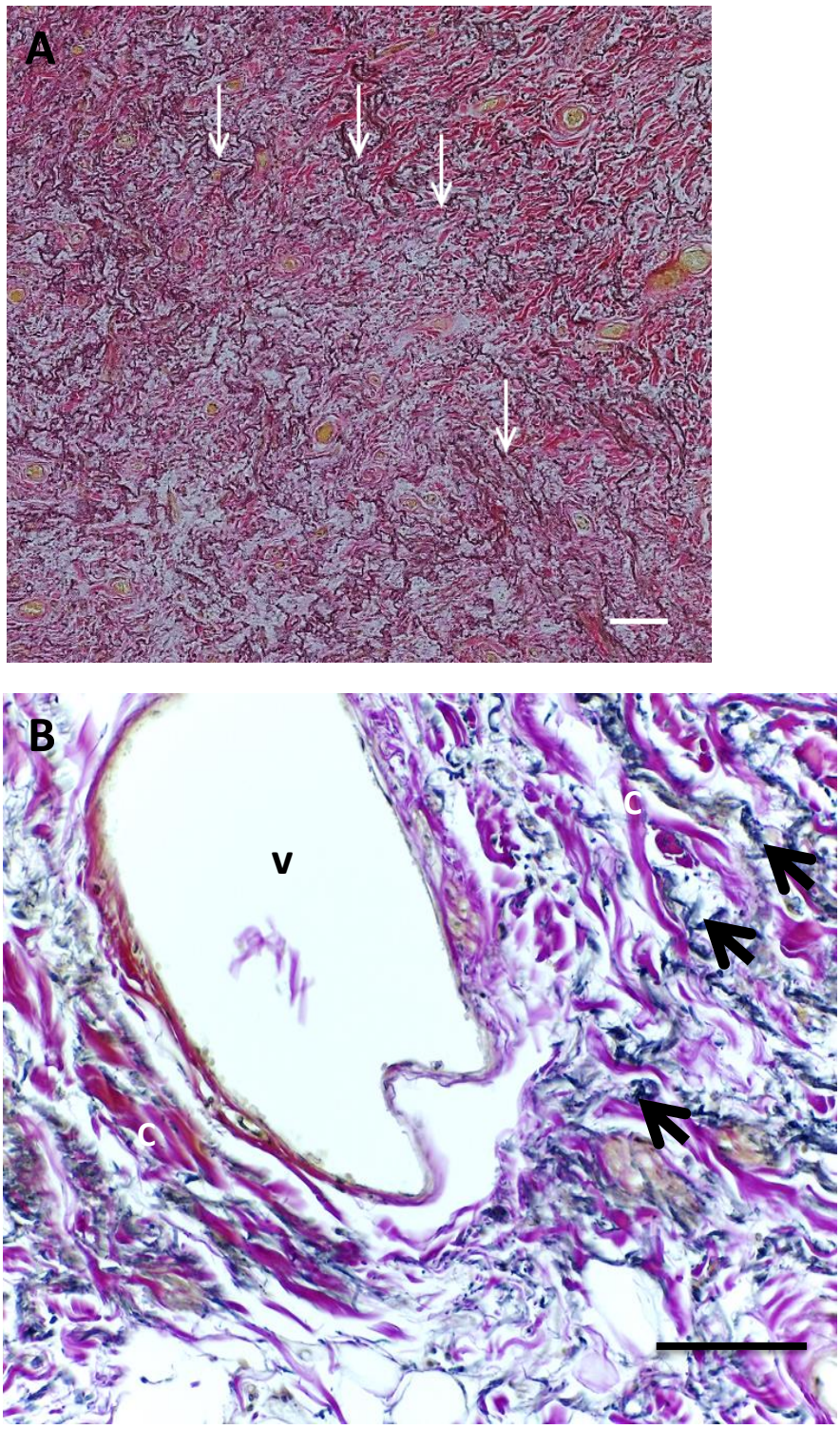

Figure 10. Paraffin embedded human LA showing the tunica media (A) stained with Elastica van Gieson. Elastin fibers (white arrows) were observed in this layer. Same staining (B) of paraffin embedded human LA revealed elastin fibers (black arrow), collagen fibers (C), and a vein (V) within the adventitial layer. Scale bar = 50 µm.

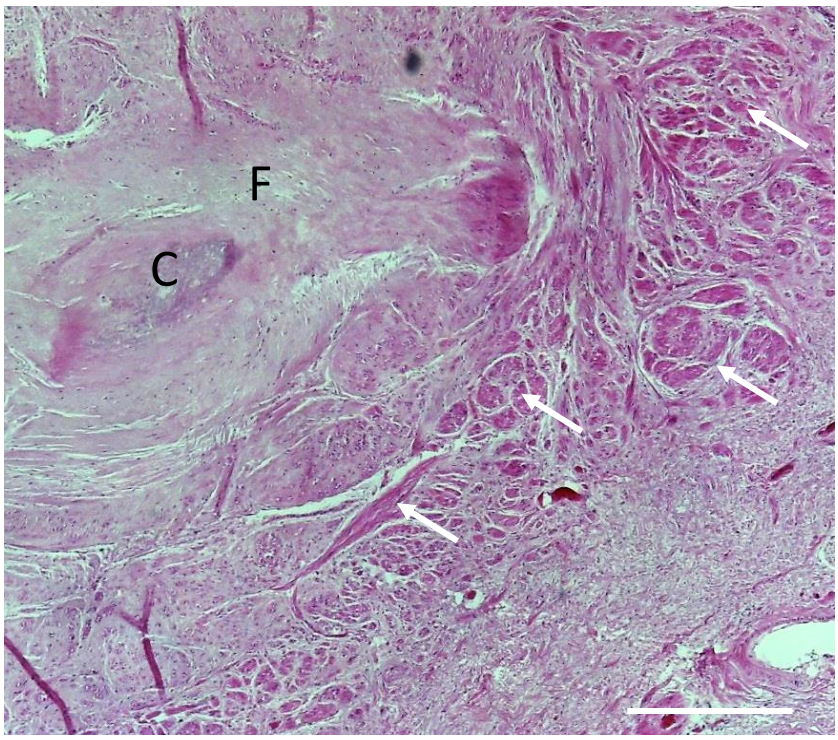

Figure 11. Paraffin embedded human LA stained with hematoxylin and eosin showing a fibrous core (F) with calcification (C). White arrows indicating layers of muscle cells. Scale bar = 100 µm.

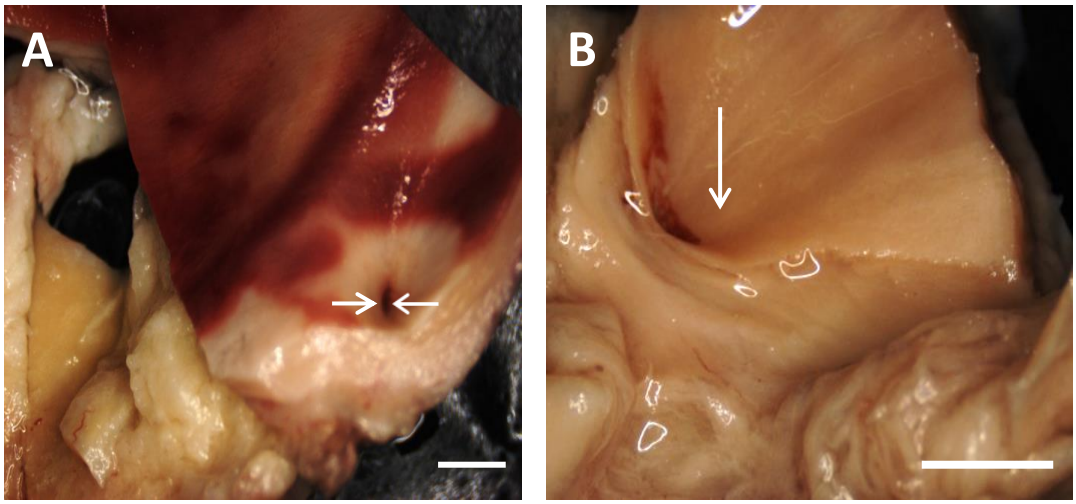

Figure 12. Samples of human LA obtained from dissection course, yet to be subjected to histological processing showing the presence of a funnel (white arrows) with partial patency from the part of the LA connected to the aorta. Scale bars = 50 µm.

3.1.2 Mouse

3.1.2.1 Methylene blue stained semi-thin sections

Semi-thin sections of murine samples processed for TEM were stained with methylene blue to provide more detail on general histological organization of the LA. The LA of mice had the same general morphology like what was previously observed in human samples revealing the presence of the 3 distinct layers namely, from outward within, a tunica adventitia, media and intima. There were the presence of lumen with partial patency from the part of the LA connected to the aorta in 3 mice samples processed for TEM. This lumen was not patent through the whole LA, therefore could not serve as passage way for blood flow from aortic side of the LA to the pulmonary side. The recurrent laryngeal branch of the vagus nerve was observed in the neighborhood of the ligament. The adventitial of the LA was generally surrounded by fat. Adipocytes, distally placed in the surrounding areas beyond the adventitia, were also observed (Figure 13).

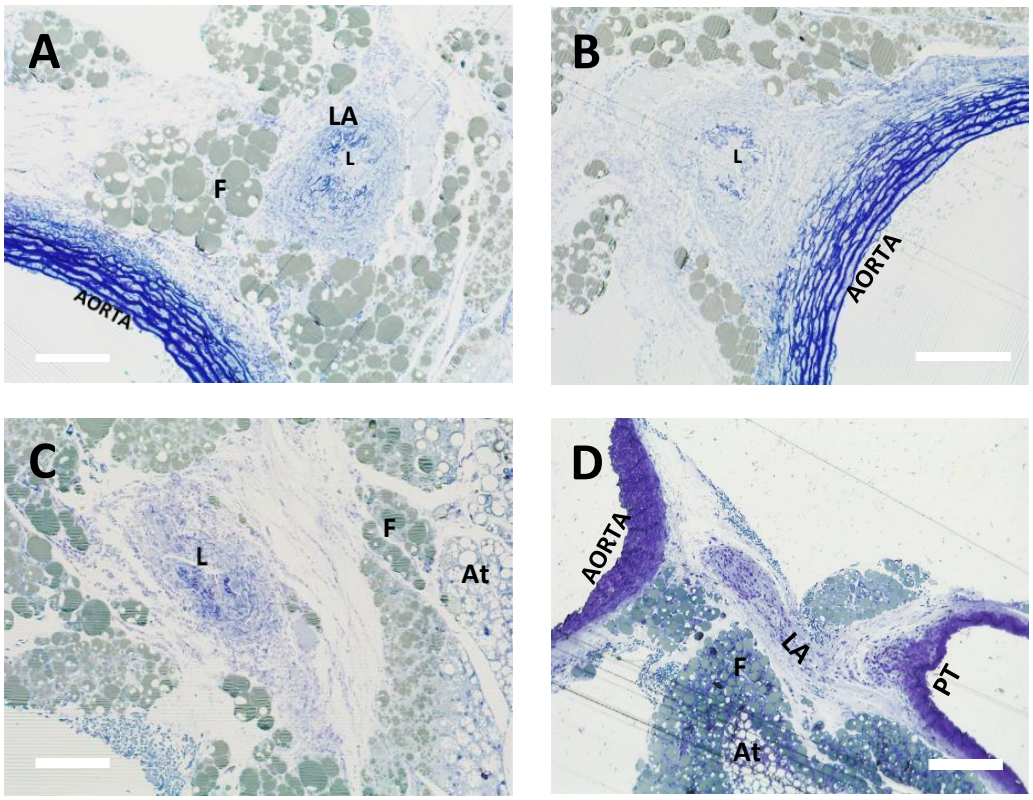

Figure 13. Semi-thin sections of murine LA stained with methylene blue. The LA partially and completely attached to the aorta by connective tissue respectively, (A, B). A lumen (L) was present. In C is a partially obliterated LA with lumen (L). Its attachment to the aorta or pulmonary trunk was not seen.

Figure 13 cont'd. (D) Longitudinal section of the LA with its attachment to the pulmonary trunk (PT) and the aorta. Note the difference in color appearance of the numerous adipocytes present. Adipocytes preserved by osmium appear olive (F) whereas empty fat cells appear as empty spaces or white (At). Scale bar = 50 µm.

3.1.2.2 TEM showing the general structure of LA in mice

The LA could be subdivided into three main regions. A central core, middle muscular and peripheral connective tissue regions, referring to the tunica intima, media and adventitia in that order. The tunica adventitia made up the outermost region. This area had extensive amount of collagen fibers running in various directions. Nerve terminals were present. Internally, the collagenous tissue terminated into the muscular layer composed of numerous myocytes with lesser amount of collagen. Elastin fibers as well as nerve terminals were also present within this muscular part (Figure 14). In 3 mouse samples, the core of the ligament was made up of elastin sheet which had an amorphous appearance with fibrillin microfibrils. There was a scanty amount of collagen fibrils observed (Figure 15). In 5 out of 8 samples, the core of the LA was made up of a scanty number of myocytes and what appeared to be cell debris. The internal elastic lamina though present was fragmented (Figure 16).

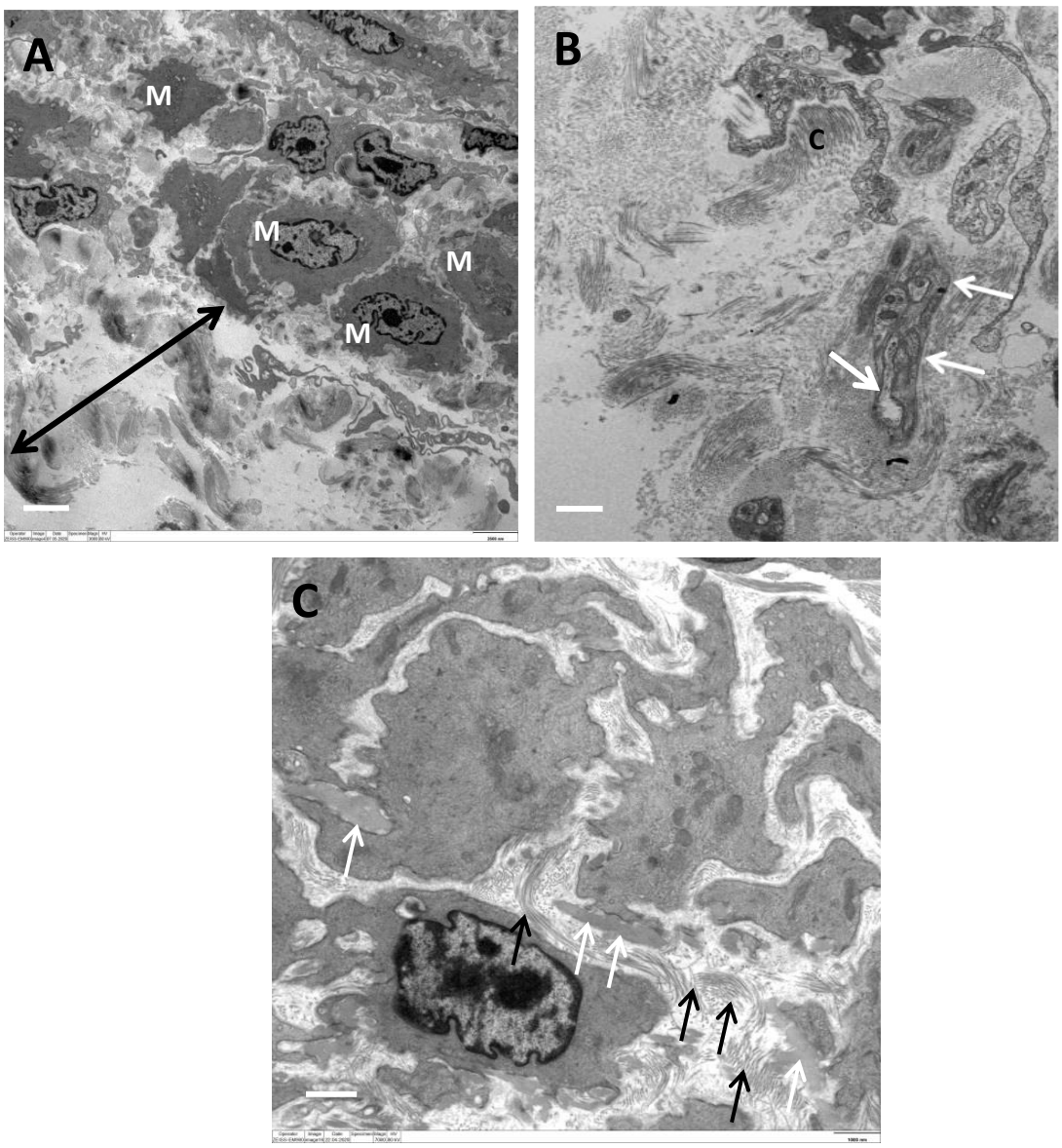

Figure 14. TEM of murine LA. (A) An outer collagenous region (black doubled arrow) and an inner region with myocytes (M). (B) Adventitial layer, with abundant collagen fibers (c). A nerve fiber bundle (white arrows) observed within the collagenous tissue of the adventitial layer. (C) Elastin (white arrows) and collagen (black arrows) located within the muscular region of the LA. Scale bars: A & C = 1 µm, B= 0.5 µm.

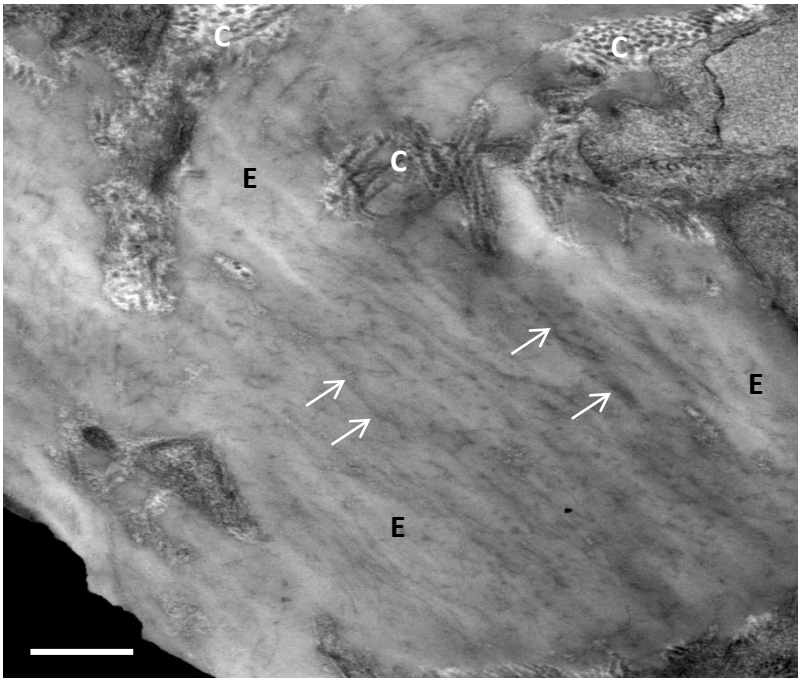

Figure 15. TEM of mouse LA. The presence of extensive elastin (E) as well as fibrillin microfibrils (white arrows) within its substance. Collagen fibrils (C) are also observed. Scale bar = 0.5 µm.

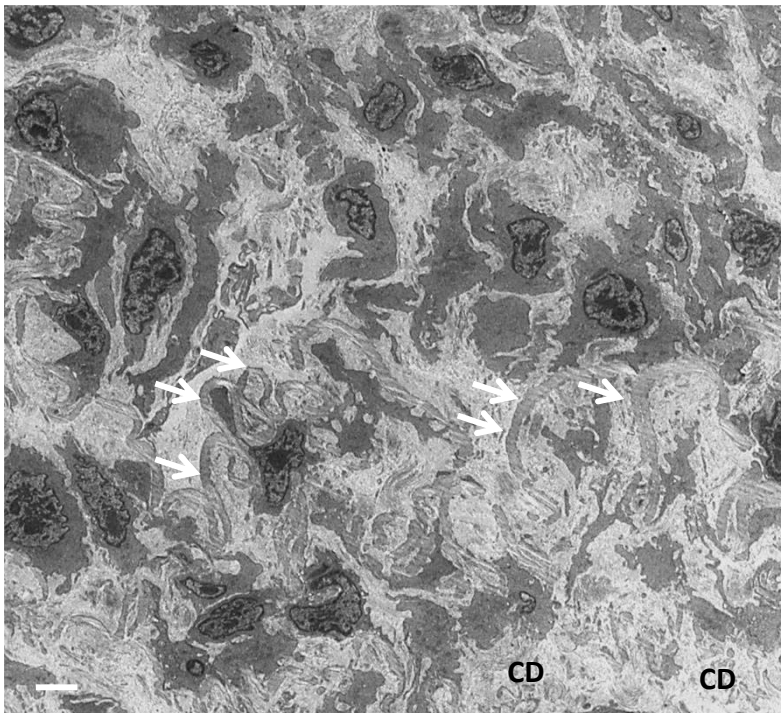

Figure 16. TEM of mouse LA. Note the presence of fragmented elastic lamina (white arrows) as well as cell debris (CD) in the core of the LA. Scale bar = 5 µm.

3.2 Myocyte component of the LA

3.2.1 Mouse

3.2.1.1 Single-labeling immunofluorescence using antibodies against smooth muscle actin

Immunofluorescent labelling using FITC-conjugated monoclonal antibody against αSMA revealed immunoreactive smooth muscle cells in the LA. This was present in LA samples sectioned along both its longitudinal and cross-sectional axis. The width of the LA in cross-section averagely measured 150 ± 12 µm (mean ± SEM, n = 8) There was no fluorescence of the LA when antibody against αSMA was omitted (Figure 17).

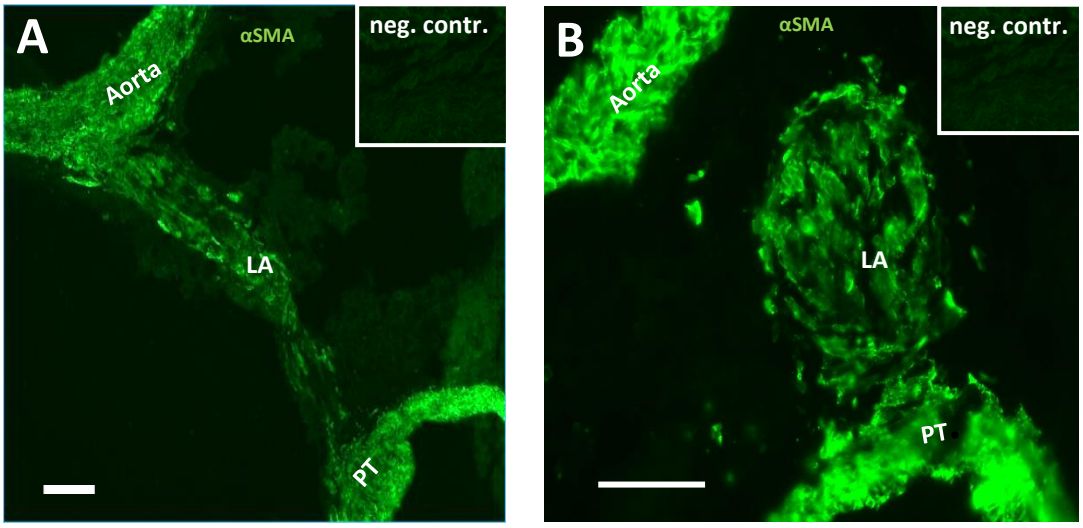

Figure 17. Single-immunolabeling of frozen sections from mouse LA. (A) Longitudinal section of the LA appearing between and attached to the aorta and pulmonary trunk (PT) with immunofluorescent αSMA-positive cells throughout its length (green fluorescence). (B) Cross-section of the LA with attachment to the pulmonary trunk (PT) but not the aorta (A). Note the immunofluorescent αSMA-positive cells. Controls run without antibody against αSMA (neg. contr.) are shown in the inserts. Scale bars = 100 µm.

3.2.1.2 Transmission Electron Microscopy

Generally, the myocytes observed within the LA, though numerous, lacked a consistent orientation and also did not have the typical spindle shape of smooth muscle cells. I observed the presence of mononucleated muscle cells with a prominent nucleolus. Observed also were plasma membrane indentations called the caveoli. There was also the presence of cell organelles such as mitochondria and rough endoplasmic reticulum, in the cytoplasm. Additionally, dense bodies were observed within the cytoplasm. There was also the presence of a basal lamina as well as collagen fibrils around the external periphery of these cells. Actin filaments anchored to attachment zones (also called dense bands) on the plasma membrane were present. The dense bands of adjacent myocytes were sometimes found in close apposition with each other forming coupling cell mechanical junction a.k.a. attachment plaques (Hammers & Lee Sweeney 2018). In some myocytes observed, elastin sheets were seen attaching to the extracellular border of dense bands. Dense bands with extracellular elastin attachment usually appeared more pronounced in comparism to dense bands without extracellular elastic attachment (Figure 18).

In the LA, the average length of dense bands, parallel to the plasma membrane measured in 60 myocytes from 4 different samples was 0.4 ± 0.20 µm with a width of 0.049 ± 0.007 µm (mean ± SEM, n = 60) respectively. Comparatively, I observed the dense bands in the pulmonary trunk were lengthier 0.9 ± 0.09 µm and also thicker (0.078 ± 0.022 µm, mean ± SEM, n = 60) than what I observed in the LA (Figure 19). The difference in length and width between dense bands observed within the LA and pulmonary trunk subjected to a two-tailed t-test were statistically significant ($P \leq 0.0001$). Additionally, areas with extracellular elastin abutting the dense bands in usually appeared more pronounced (Figure 18-19).

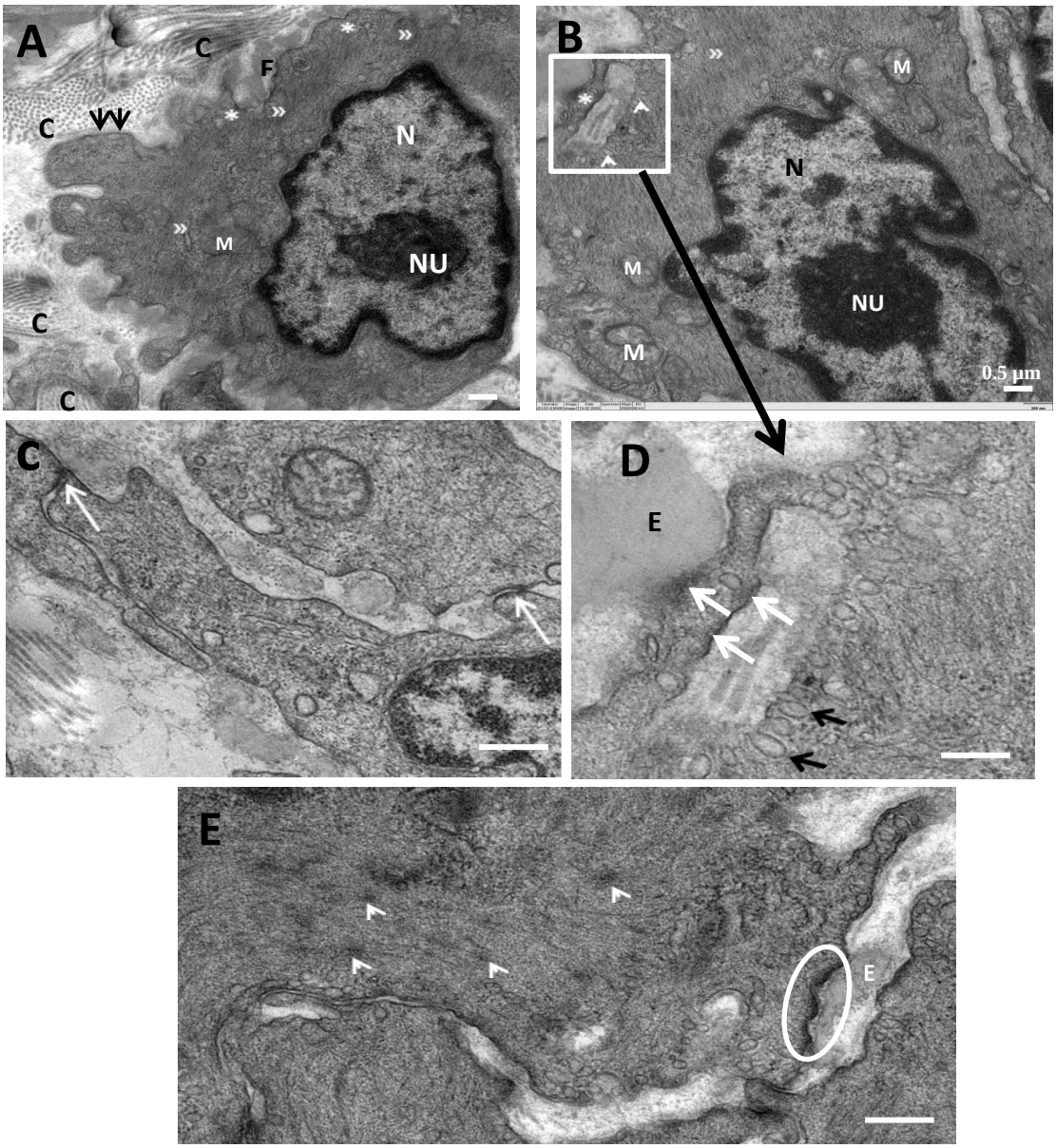

Figure 18. TEM of murine LA. (A) Smooth muscle cell with heart shaped nucleus (N) and its nucleolus (NU) in it. The actin filaments (double arrowheads) and attachment zones (white asterisk) are seen. Elastin sheet fragment (E) is attached to the plasma membrane. Collagen fibrils (C) surrounding the myocyte are present. (B) Nucleus (N) and its nucleolus (NU) as well as caveoli (white arrowhead) are present. Attachment zone (white asterisk) and mitochondria (M) are also observed. (C) Region of interaction between two dense bands (white arrows) of two myocytes.

(D) Magnification of white insert in panel B displaying caveolae (black arrows) and dense bands (white arrows) attached to the plasma membrane. On the opposite, elastin (E) seen abutting a dense band (white arrow). (E) Dense bodies (white arrowhead) within cytoplasm of myocyte. Note a region with elastin (E) anchored to a pronounced dense band (white oval). Scale bars: A = 1 µm, B = 0.5 µm, C-E = 0.25 µm.

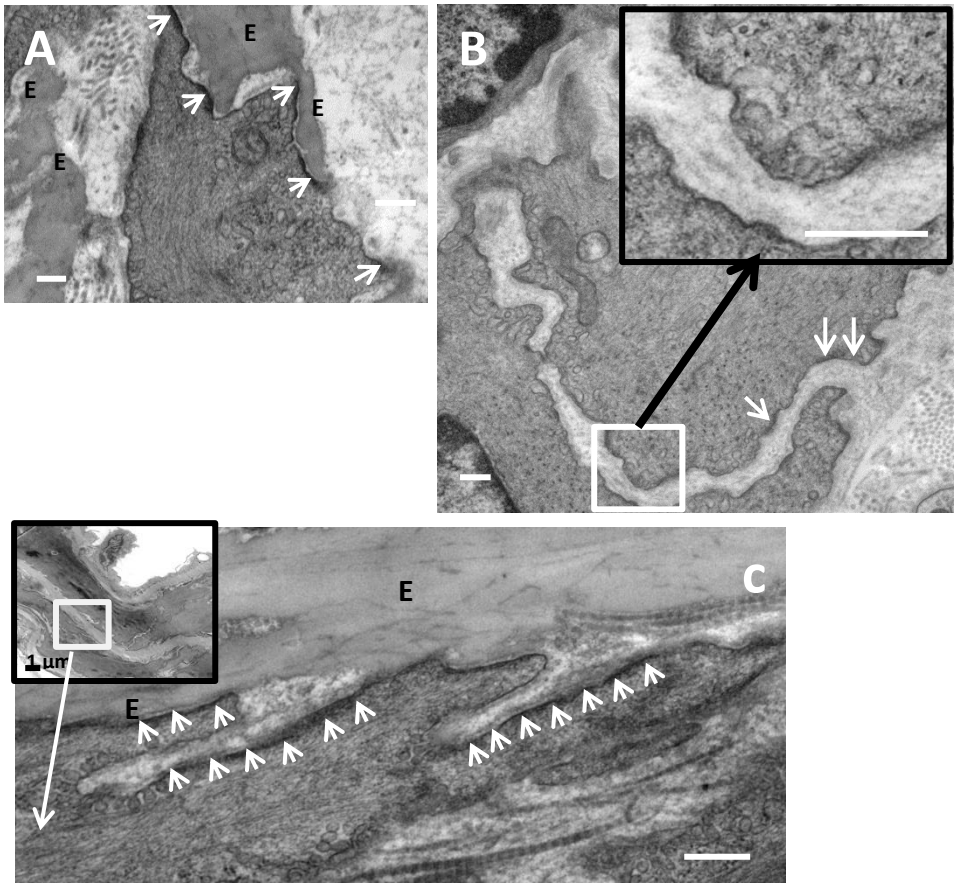

Figure 19. TEM of comparism of dense bands in mice LA and pulmonary trunk. (A) Myocyte within LA medial layer with numerous elastin (E) attachments and well pronounced dense bands (white arrow). (B) Myocytes within LA with comparatively less pronounced dense bands (white arrows). White insert region in higher magnification in black insert. (C) Magnification of region of insert (white square) showing dense bands in pulmonary trunk myocyte. Note that not all dense bands are in contact with the elastin lamella (E) present (white arrows). Scale bars = 0.25 µm.

3.2.2 TEM of arterioles in the vicinity of mouse LA

Small arterioles were observed in the vicinity of the LA in mice. It walls were built up by the three layers, tunica intima, media and adventitia from within outward. The tunica intima was made up of a single layer of endothelial cells. Blood cells were also observed in the lumen of the arteriole. A single circular layer of smooth muscle cells made up the media layer. The myocytes found here had the typical features of vascular smooth muscle such as caveoli, myofilaments, and mitochondria. Using the plasma membrane as a point of reference, I categorized dense bands present into 2 populations,

namely dense bands that appeared pyramidaly shaped and those extending parallel to the plasma membrane (Figure 20). Measurements taken from 35 myocytes with pyramidaly shaped dense bands revealed an average length of 0.4 ± 0.008 µm (mean ± SEM). The average width at the shortest distance was 0.028 ± 0.003 µm (mean ± SEM) and 0.058 ± 0.006 µm (mean ± SEM) at the region where it was thickest. In the other population, dense bands averagely measured 0.7 ± 0.042 µm in length and 0.017 ± 0.002 µm (mean ± SEM, n = 35), in width. The difference in width between the regularly and pyramidaly shaped dense bands was statistically significant ($P \leq 0.0020$). The differences in width between regular and pyramidally shaped dense bands, as well as between the shortest and longest distance in the pyramidally shaped bands were all statistically significant ($P \leq 0.0001$). Though the myocytes present had similar characteristics in comparism to the ones found within the LA, the caveolae present were very pronounced and the mitochondria were numerous with a more elongated shape (Figure 20).

The adventitia revealed the presence of telocytes and fibroblasts identified by plenty rough endoplasmic reticulum within their cytoplasm. Numerous collagen fibrils running in different profiles were also observed. A basal lamina was also present surrounding the plasma membrane. Nerve terminals with and without vesicles were also present. They were partially covered by the respective Schwann cell and the vesicles were either large dense core or small clear core (Figure 20).

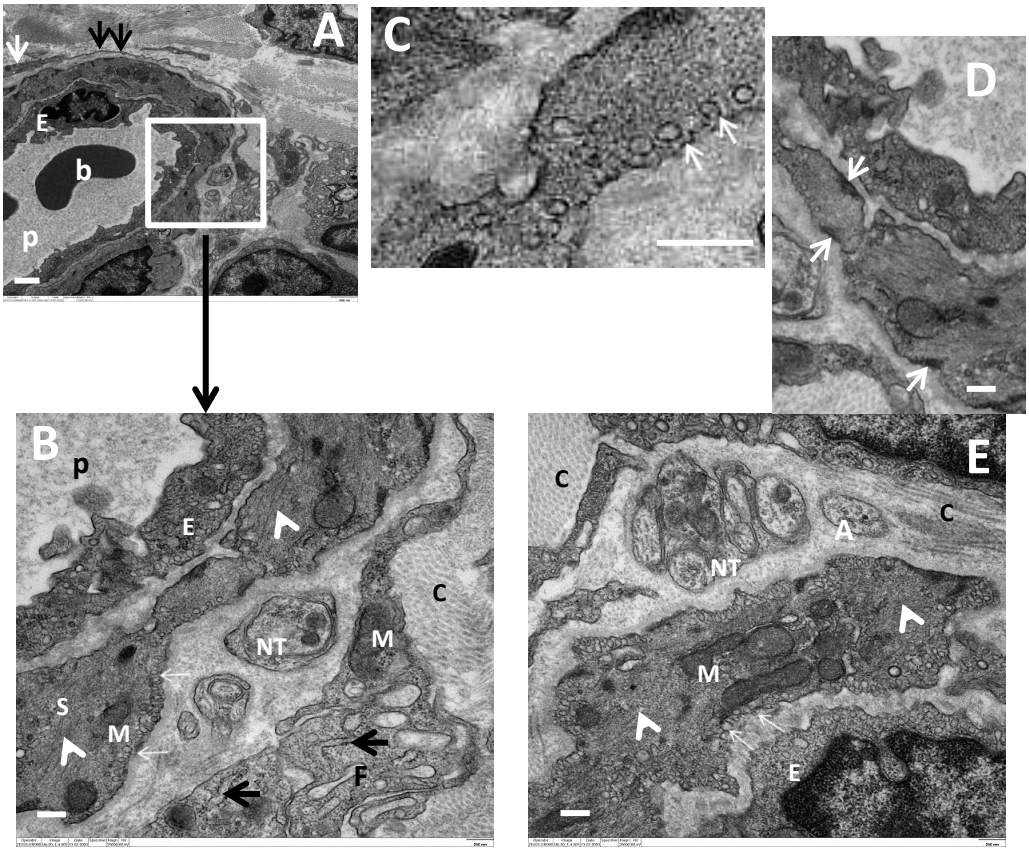

Figure 20. TEM of arteriole in the vicinity of mice LA. A) An arteriole with a telocyte (white arrow) and telopodes (black arrows). Note the presence of the single endothelial cell (E) facing the lumen and its plasma (P). A red blood cell (b) also revealed.

B) A higher magnification showing endothelial cell (E) and a single layered smooth muscle cell (S) with numerous mitochondria within its cytoplasm (M). Myofilaments (white arrowheads) are also shown. Note how prominent the caveoli (white arrows) appear. A higher magnification of caveoli in picture C Extracellularly, a nerve terminal (NT) is seen between smooth muscle and fibroblasts (F). Mitochondria (M), as well as rough endoplasmic reticulum (black arrows) seen within the cytoplasm of the fibroblast. Collagen fibrils (C) are also present. D) Pyramidaly shaped dense bands (white arrow) in smooth muscle cell. E) Showing arteriole revealing the presence of a nerve terminal (NT) within the adventitia. A naked nerve axon without a Schwann cell (A) is also observed. Note the presence of mitochondria (M) and myofilaments (white arrowheads) within the cytoplasm of the smooth muscle cell. The distance between the nerve terminal and the smooth muscle was 0.25 µm. Scale bars: A= 1 µm, B, C, D, E = 0.25 µm.

3.2.3 Pig

3.2.3.1 Single-labeling immunofluorescence using antibodies against smooth muscle actin

Immunofluorescence using FITC-conjugated monoclonal antibody against αSMA revealed extensive amount of immunoreactive smooth muscle cells in pig LA (Figure 21). There was no fluorescence when antibody against αSMA was omitted.

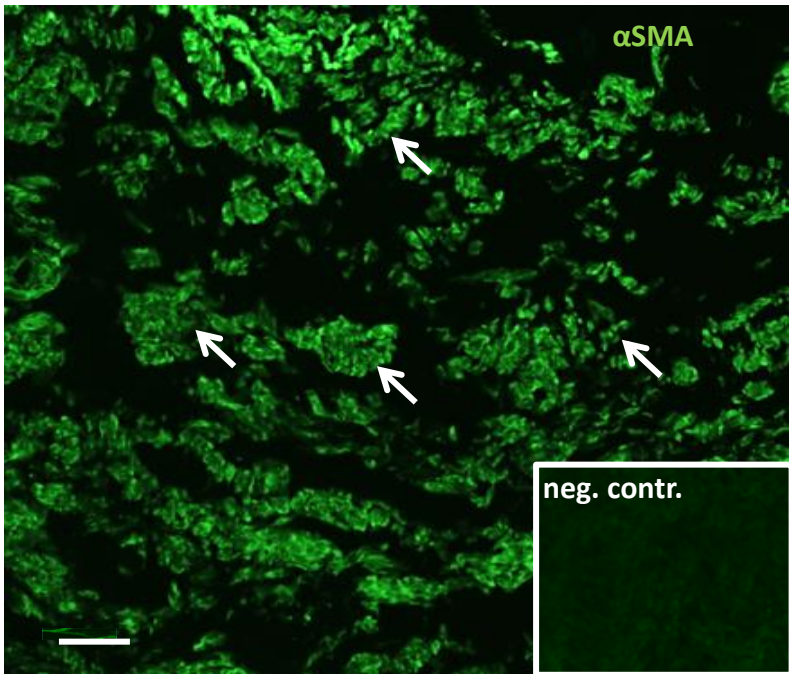

Figure 21. Immunolabeling of pig LA with αSMA-positive cells (white arrows). Control run without antibody against αSMA (neg. contr.) shown in the insert. Scale bar = 50 µm

3.2.3.2 TEM of myocyte in pig

The myocytes I observed with TEM revealed the typical appearance of myocytes with pronounced caveoli, dense bands as well as myofilaments. Mitochondria were present. Some myocytes found here revealed gap junctions indicating intercellular communication. Myocytes were surrounded by a basal lamina (Figure 22).

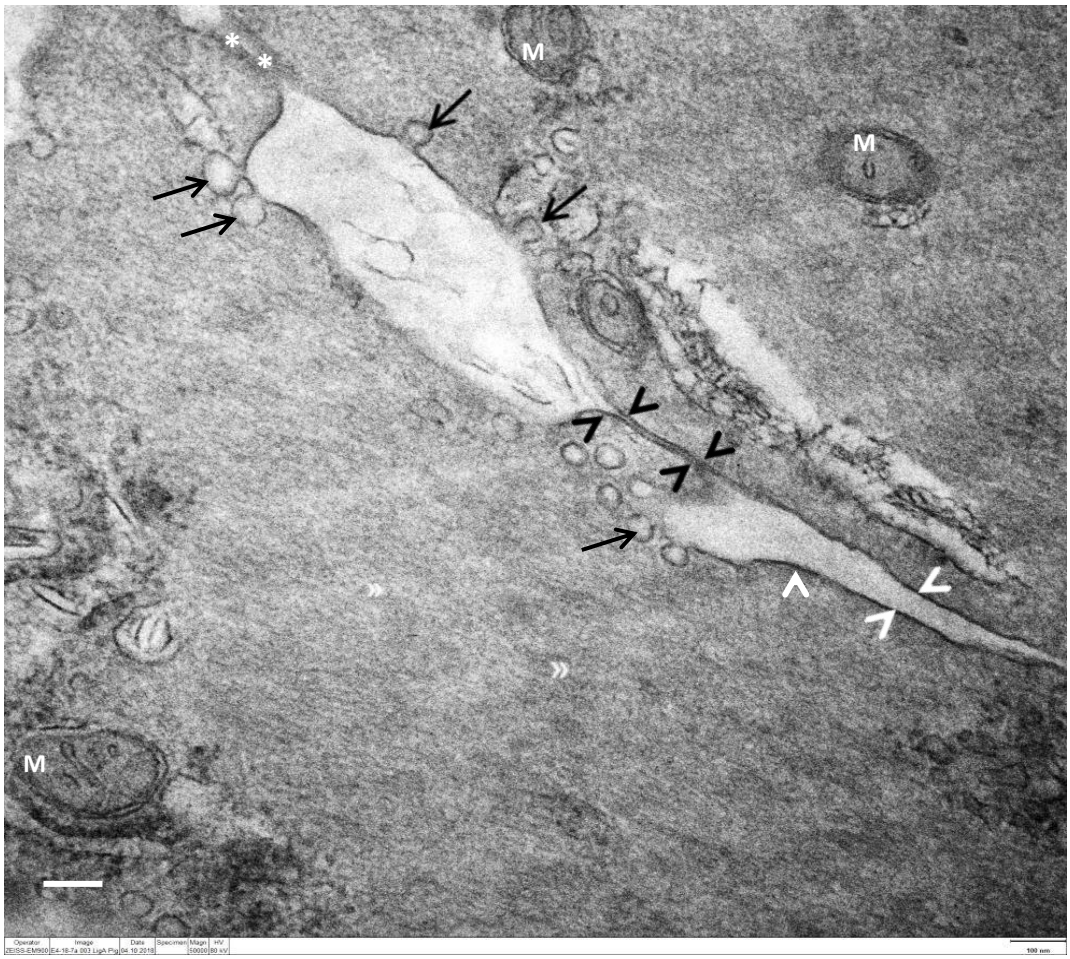

Figure 22. TEM of mice LA. Smooth muscle cell, with actin filaments (double arrowheads) and dense bands (white arrowheads). Note the presence of caveoli in the plasma membrane (black arrows) and mitochondria (M). A gap junction (black arrowheads) is connecting two myocytes. A basal lamina (white asterisk) is also present. Scale bar = 0.1 µm.

3.2.4 Human

3.2.4.1 Single-labeling immunofluorescence using antibodies against smooth muscle actin

Immunofluorescence using FITC-conjugated monoclonal antibody against αSMA revealed immunoreactivity to αSMA in the smooth muscle cells of the LA and this was present extensively throughout the whole structure. There was no fluorescence when antibody against αSMA was omitted (Figure 23).

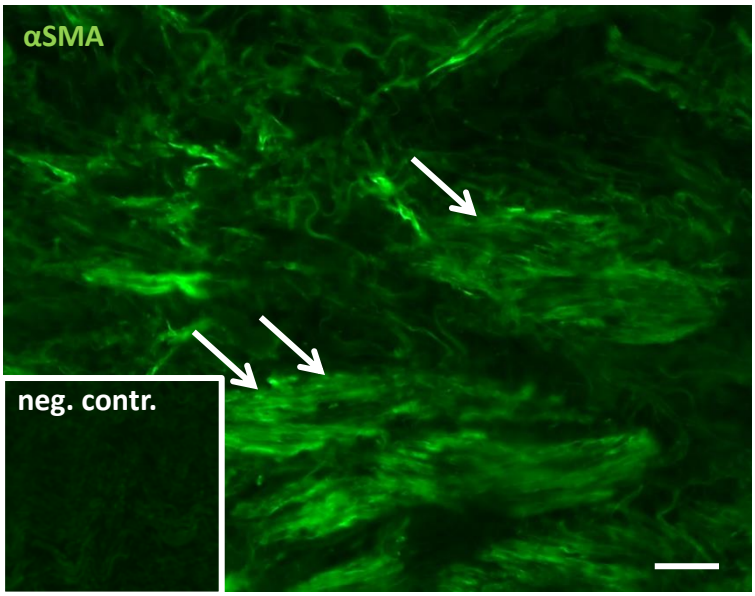

Figure 23. Immunolabeling of human LA with immunoreactivity to αSMA (white arrows). Control run without antibody against αSMA (neg. contr.) shown in the insert. Scale bar = 50 µm.

3.3 Connective tissue component of the LA

3.3.1 Cells

3.3.2 TEM of connective tissue cells in mouse

In TEM, I observed the presence of mononucleated fibroblasts with elongated spindle or stellate shape cytoplasmic projections. Within the cytoplasm were plenty of rough endoplasmic reticulum. Nucleoli were also present within the nuclei. Fibroblasts were surrounded by elastin, collagen fibers in close proximity and running in different orientations (Figure 24 & 25). Myofibroblasts, exhibiting some features of both fibroblasts (rough endoplasmic reticulum) and smooth muscle cell (actin filament and dense bodies within the cytoplasm) were also present (Figure 26). There were the presence of telocytes with cell bodies and nuclei surrounded by minimal cytoplasm. Extending from the cell bodies were elongated projections referred to as telopodes with a moniliform aspect, representing segments with dilations or 'bead on a string' appearance due to the formation of podoms and podomers, which are described as the dilated, cistern-like regions and thin fibrillar segments respectively (Hanan et al. 2020). There were also dichotomous branching of podomers which ultimately terminated into long convoluted podomer. Telopodes were usually in contact with other telopodes or

heterogeneous surrounding cell types such as muscle cells, nerve fibers or immune cells (Figure 27-28).

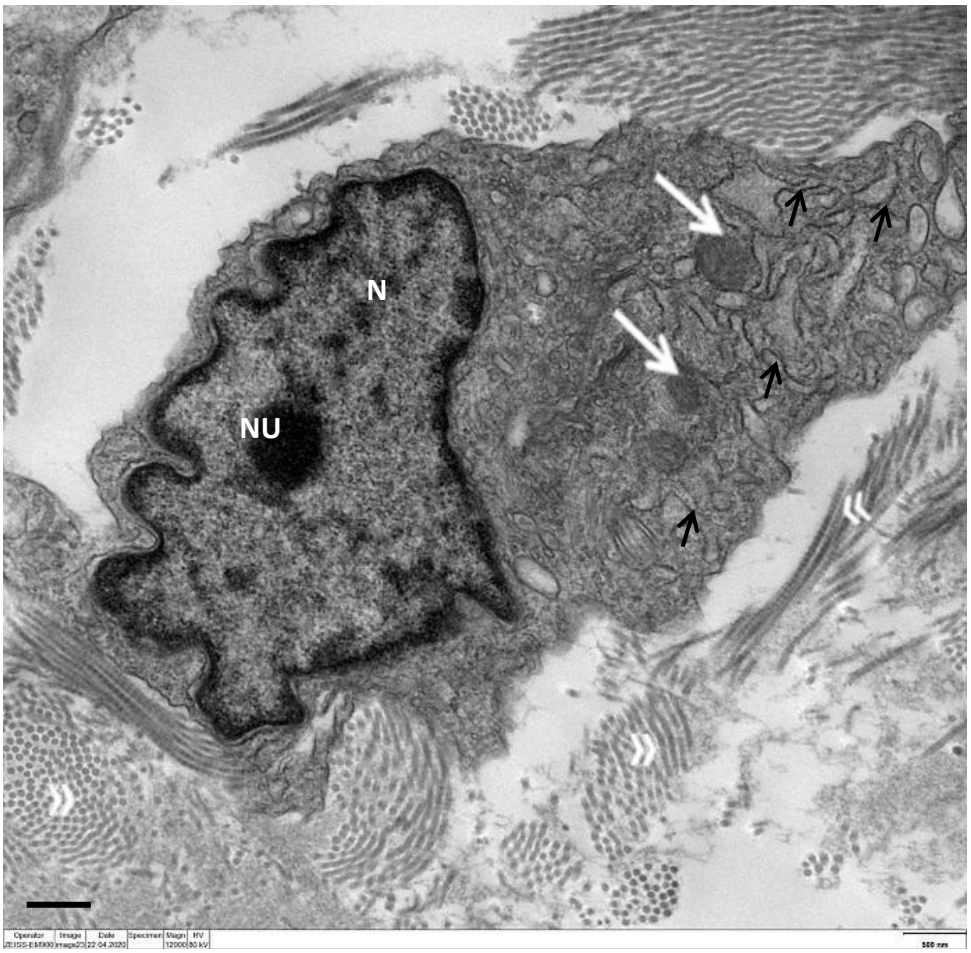

Figure 24. TEM of murine LA. Fibroblast with nucleus (N), nucleolus (NU), rough endoplasmic reticulum (black arrows) and mitochondria (white arrows) within its cytoplasm. There was also the presence of peripherally placed collagen fibers running in different orientations (double white arrowhead). Scale bar = 0.5 µm

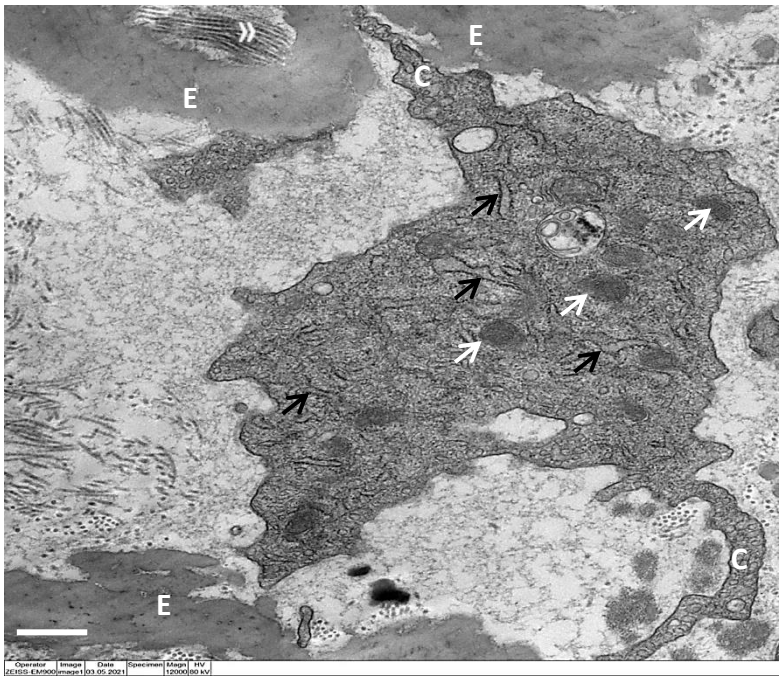

Figure 25. TEM of murine LA. Fibroblast with cytoplasmic extensions (C), rough endoplasmic reticulum (black arrows) and mitochondria (white arrows) within its cytoplasm. There was also the presence of peripherally placed elastic (E) and collagen fibers running in different orientations (double white arrowhead). Scale bar = 0.5 µm.

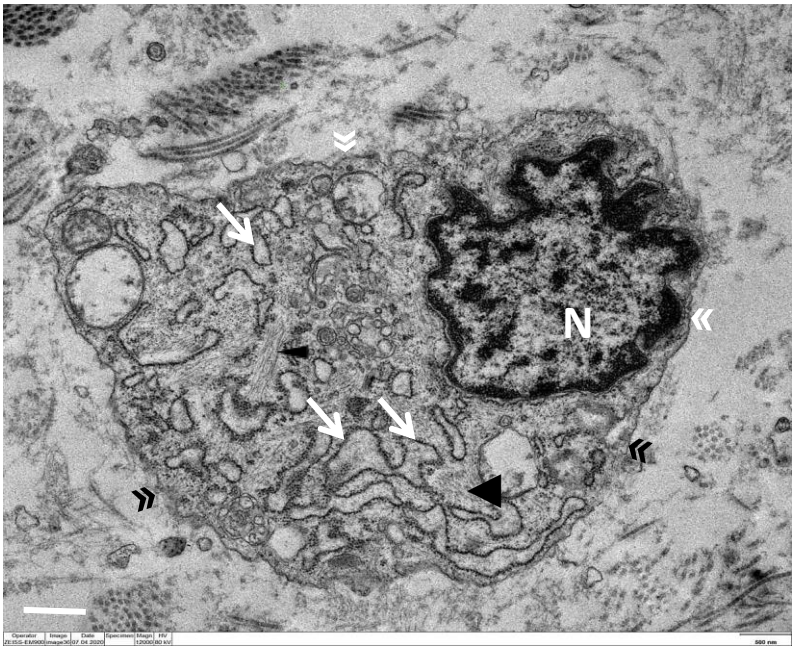

Figure 26. TEM of murine LA. Myofibroblast with plenty rough endoplasmic reticulum in the cytoplasm (white arrows) and a peripherally placed nucleus (N). There is also the presence of actin filaments within the cytoplasm (black arrow head). Note the discontinuous basal lamina present (double white and black arrowheads). Scale bar = 0.5 µm.

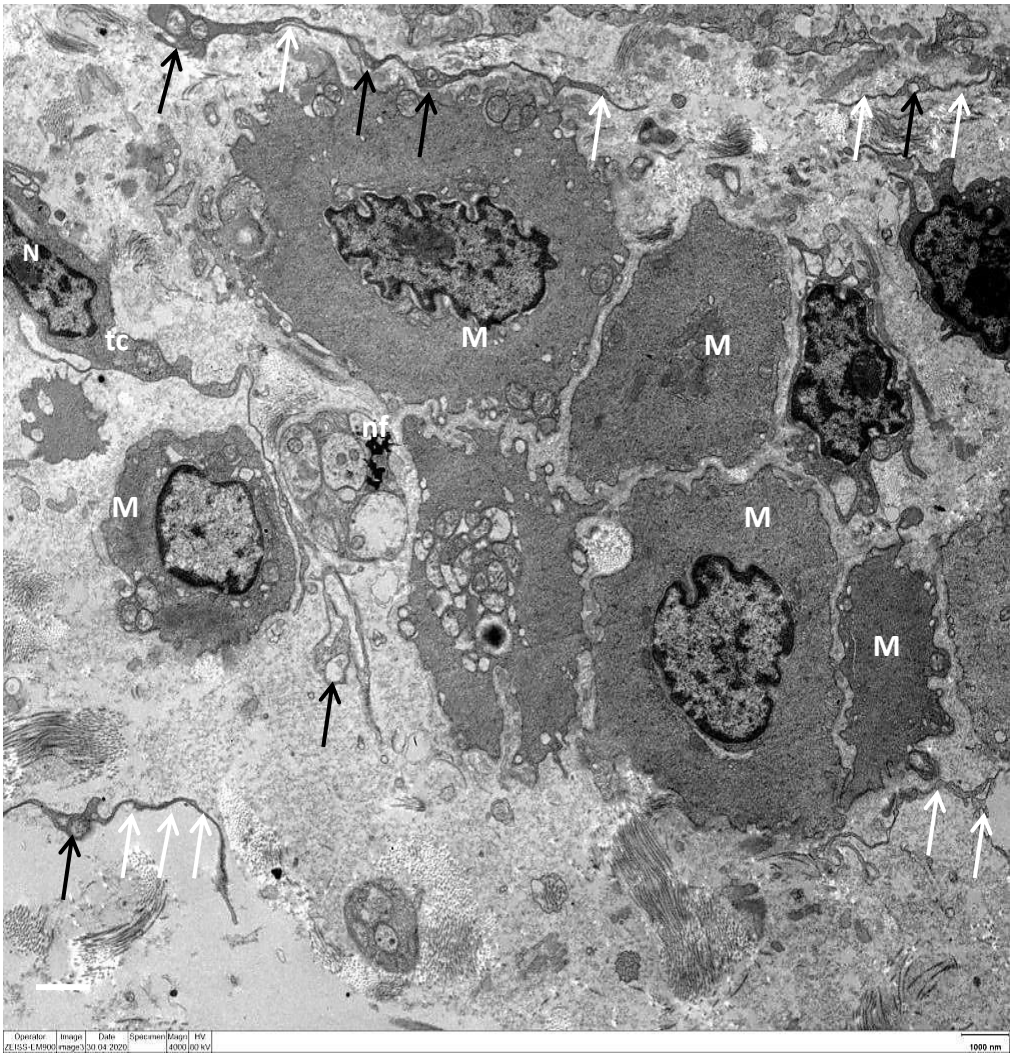

Figure 27. TEM of murine LA showing mono-nucleated (N) telocyte cell body (tc) and telopodes (white arrows) as well as podoms (black arrows). A region with podom and podomer appeared sandwiched between a nerve fiber bundle (nf) and a myocyte (M). Additionally, the presence of other telopodes (white arrows) and podoms (black arrows) were seen in close proximity to myocytes (M). Scale bar = 1 µm.

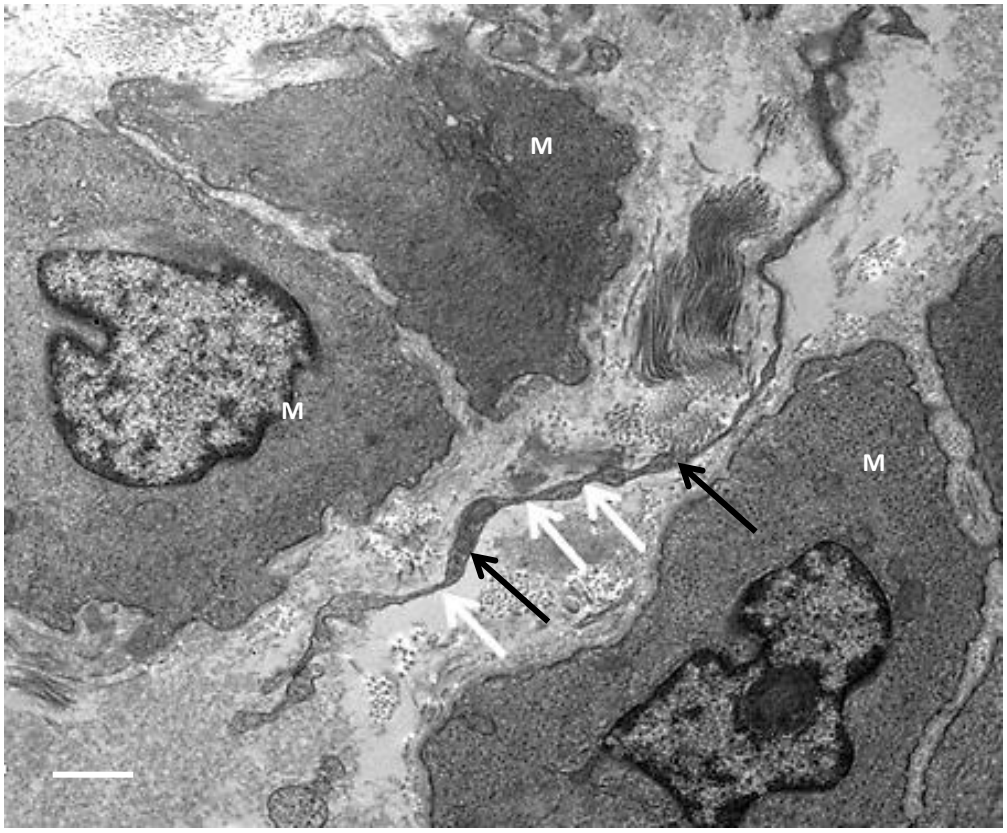

Figure 28. TEM of murine LA showing a telopode with podomers (white arrows) and podoms (black arrows) sandwiched between myocytes (M). Scale bar = 1 µm

3.3.3 TEM of connective tissue cells in pig

I observed the presence of fibroblasts, irregular shaped mono-nucleated cells with numerous mitochondria, cytoplasmic projections and vesicles of varied sizes (Figure 29 & 30). The presence of telocytes in the LA of pig (Figure 30) with cell body, surrounded by minimal cytoplasm was observed. Extending from the cell body were elongated projections with a moniliform aspect representing segments with dilations or 'bead on a string' appearance. The elongated projections were sometimes spotted 0.1 µm away from a nerve terminal and 2 µm away from a myocyte.

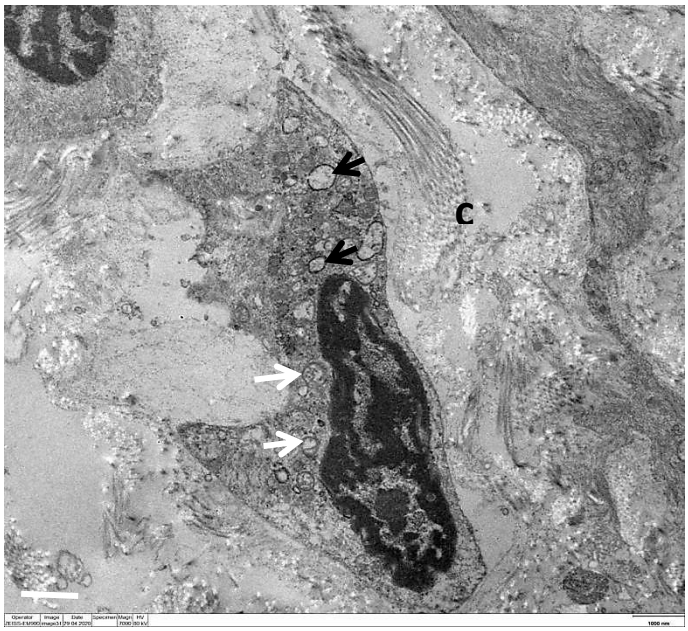

Figure 29. TEM of pig LA showing a fibroblast with the presence of dilated mitochondria (white arrows) and cytoplasmic vesicles of varied sizes (black arrow). In close proximity is the presence of collagen fibrils (C). Scale bar = 1 µm.

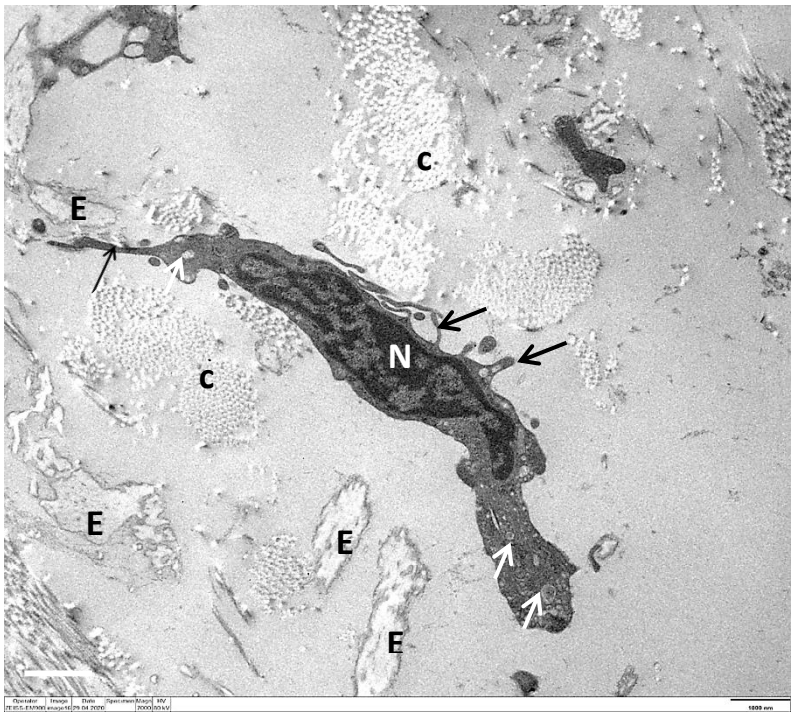

Figure 30. TEM of pig LA showing a fibroblast with the presence of mitochondria (white arrows), Nucleus (N), and cytoplasmic extensions of varied sizes (black arrows). In close proximity is the presence of collagen fibrils (C) and elastin (E). Scale bar = 1 µm.

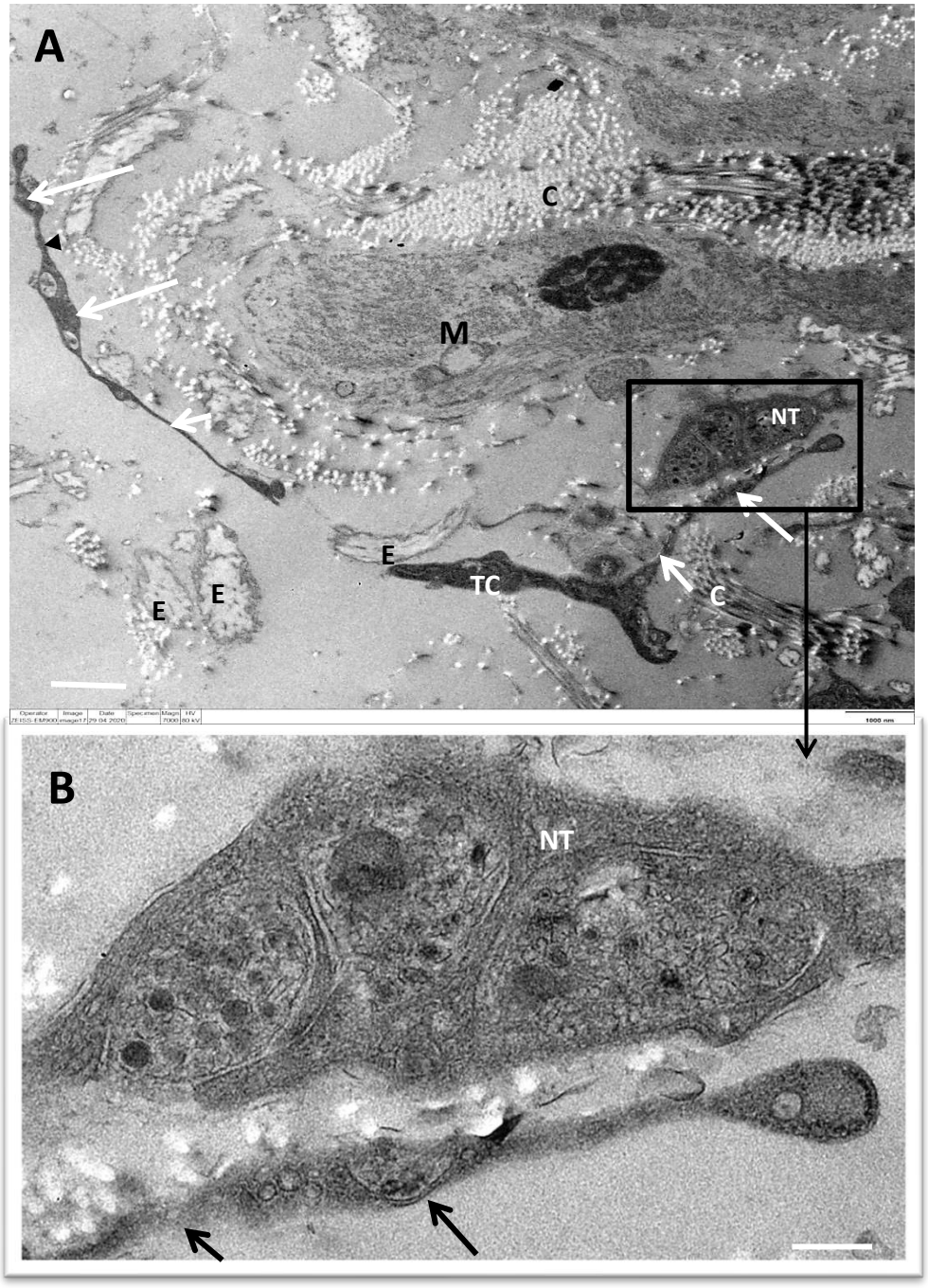

Figure 31. TEM of pig LA revealing a telopode (short white arrows) about 1.4 µm to myocyte (M). There is the presence of podoms (long white arrows) as well as podomer (black arrow head). Additionally, another telocyte (TC) with podom (long white arrow) and a telopodes (short white arrow) was observed. TC is in very close proximity to elastin (E), collagen fibrils (C) and nerve terminals (NT). Magnification of black boxed area in TC shown in lower panel. Scale bar: A = 1 µm, B = 0.25 µm.

3.3.4 Collagen fibers of the LA

3.3.4.1 Mouse

I observed the presence of numerous collagen fibrils running in various orientations and forming collagen fibers (Figure 32). The collagen fibrils in longitudinal orientation reported the characteristic striated banding commonly referred to as the D-period. The fibrils measured 55-60 nm in width (Figure 33).

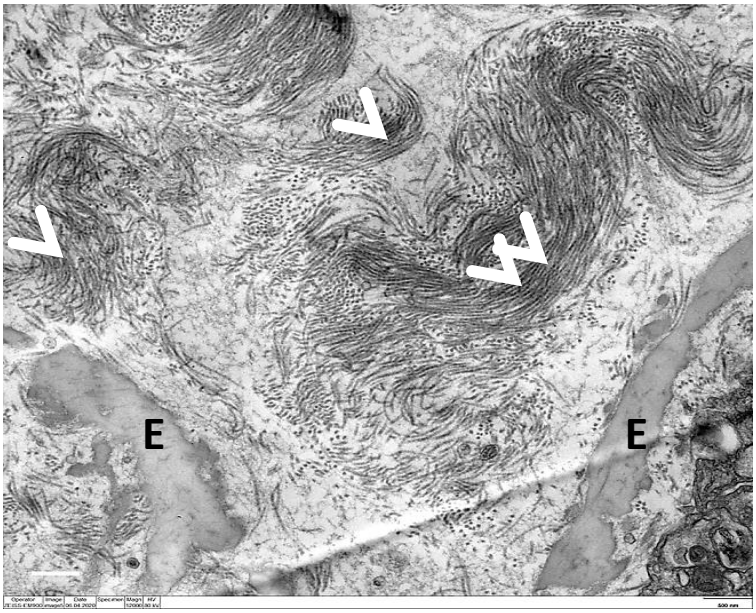

Figure 32. TEM of mice LA reporting the presence of numerous fibrils (white arrow head) running in different orientations. Additionally, there is the presence of elastin (E). Scale bar = 0.5 µm.

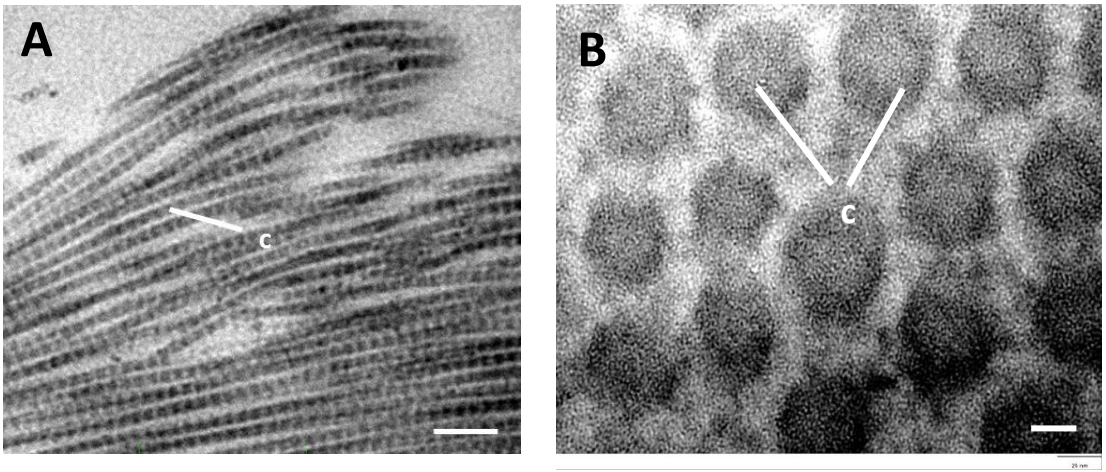

Figure 33. TEM of murine LA. A) Showing a collagen fibril in a longitudinal profiles and apparent striations (C). B) Showing a cross-sectional oriented collagen fibril measuring 55 nm. Scale bar = 0.025 µm.

3.3.4.2 Pig

I observed the presence of numerous collagen fibrils which represent the smaller unit of the fibres which is formed ultimately (Figure 34). The fibrils were running in different orientation and also had appearance of the D-period within the fibrils in longitudinal profile.

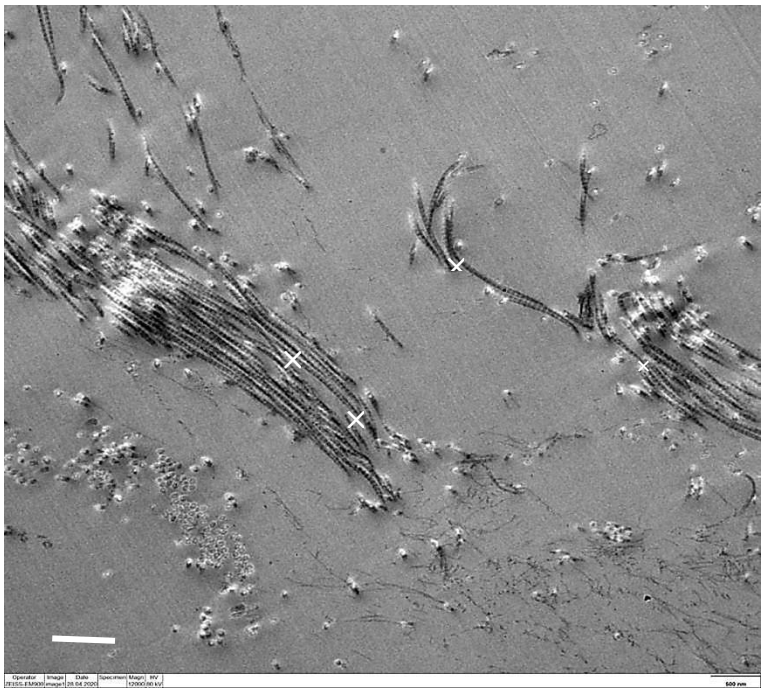

Figure 34. TEM of pig LA showing collagen fibrils mainly in longitudinal profile within the adventitia layer (white asterisk). Note the presence of dark striations. Scale bar = 0.5 µm.

3.3.5 Elastin fibers of the LA

3.3.5.1 Mouse

Mice LA revealed the presence of elastin fibers and sheets. The elastin observed within the fibers had a relatively amorphous appearance. There was fragmentation of the elastic sheets that make up the lamina especially in the region of the tunica media (Figure 35).

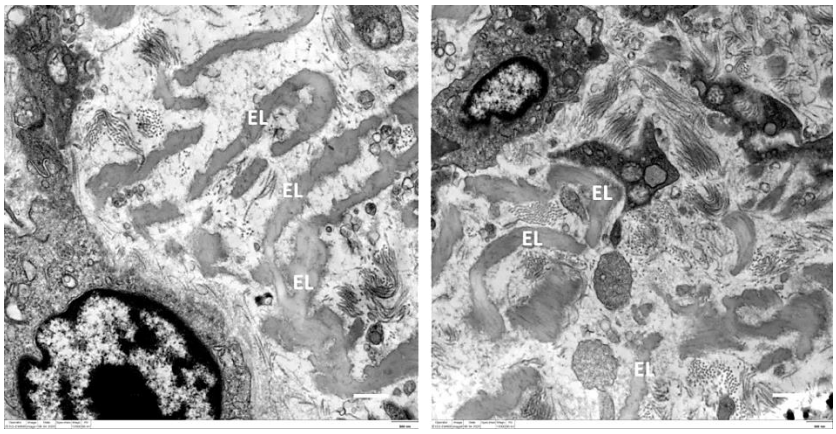

Figure 35. TEM of murine LA showing fragmentation of elastin lamina (EL) within tunica media. Scale bar = 0.5 µm.

3.3.5.2 Pig

Pig LA revealed the presence of elastic fibers. The elastic laminae observed in the region of the tunica media appeared as isolated pieces and not a continuous sheet (Figure 36).

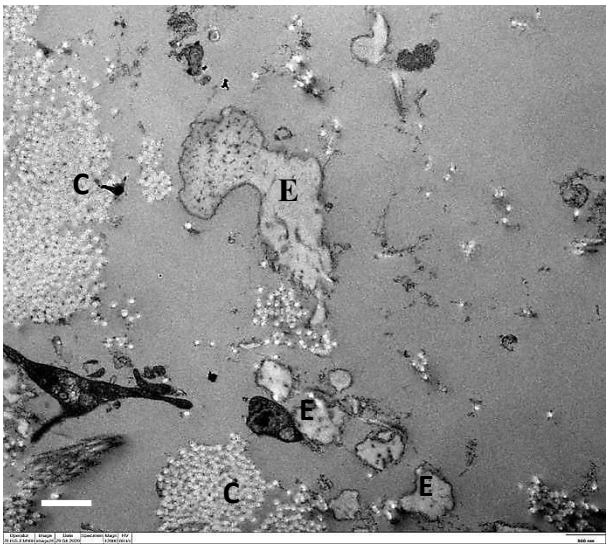

Figure 36. TEM of pig LA showing fragmented elastin fibers (E) and an aggregation of cross-sectionally oriented collagen fibrils (C). Scale bar = 0.5 µm.

3.3.6 Autofluorescence of elastin in mouse

Elastin was visualized in frozen sections of paraformaldehyde-fixed samples by its blue autofluorescenece when excited at 360-370 nm wavelength. This revealed the presence of an internal elastin lamina though there was pronounced fragmentation. Fragmented elastin lamellae were present in the musculature of the tunica media of the LA whereas

on the contrary, continuous elastin sheets were observed within the pulmonary trunk (Figure 37).

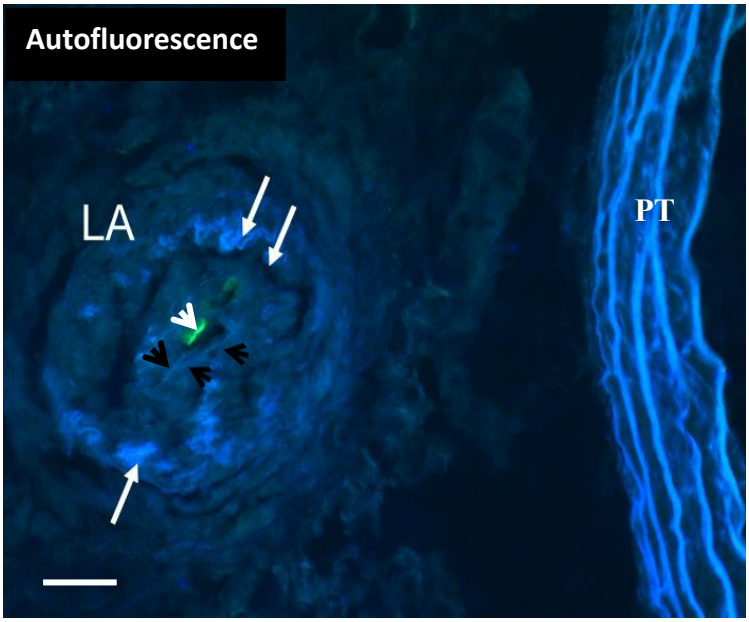

Figure 37. Elastin autofluorescence of murine LA showing the presence of fragmented internal elastic lamina (black arrows). Fragmented elastin lamellae (long white arrows) within the tunica media were observed. Note the continuous elastin lamellae within the pulmonary trunk (PT), devoid of fragmentation. Sample from *ChAT*-eGFP mouse with a positive cell in intimal region (short white arrow). Confer Figure 40. Scale bar = 50 µm.

3.4 TEM of the pulmonary trunk in mouse

TEM revealed the presence of a continuous sheet of elastin (internal elastic lamina) forming the basal layer of the intima which is made up by endothelial cells. The internal elastic lamina separated the first layer of smooth muscle from the endothelium. The elastic lamellae within the tunica media were concentric in nature, sometimes appearing angulated (Figures 38-39). Regardless of where they were located, the elastin sheets appeared in a continuous fashion without fragmentation. In comparism, LA and pulmonary trunk were similar in terms of the composition of vessel layers.

They both conformed to the typical vascular layers in vessels evident by the presence of tunica intima, media and adventitia from within outward.

However, some differences were observed. Firstly, in relation to their elastic lamina, there was fragmentation in the LA whereas that of the pulmonary trunk was devoid of fragmentation. Secondly, the myocytes within the LA, though present and numerous, lacked a consistent orientation. The myocyte within the pulmonary trunk were mostly in apposition with each other and arranged sequentially. They also had the typical spindle shape of smooth muscle cells. Finally, the internal elastic lamina was observed separating the endothelial from the tunica media in the pulmonary trunk and this was not seen in the LA due to fragmentation (Figure 38-39).

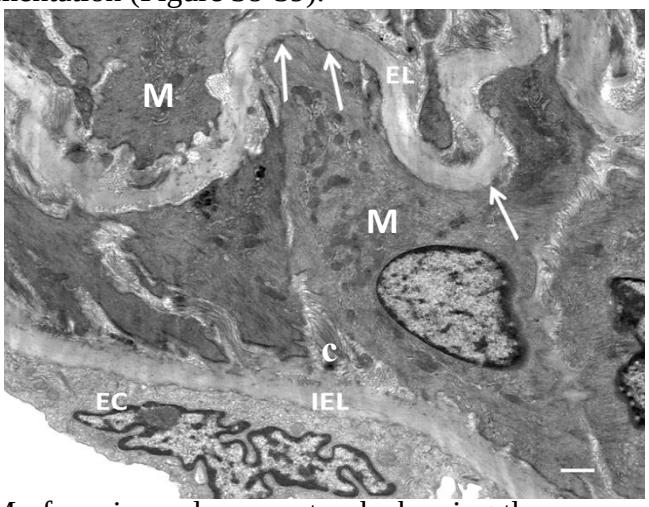

Figure 38. TEM of murine pulmonary trunk showing the presence of an endothelial cell (EC) separated from the myocytes (M) by a continuous sheet of internal elastic lamina (IEL). Elastin lamina (EL) separating first layer from the next layer of myocytes (M). Note angulation (white arrows) in some regions of the elastin lamina. Collagen fibrils (c) are observed between the myocytes as well as between the myocytes and the elastin sheets. Scale bar = 1 µm.

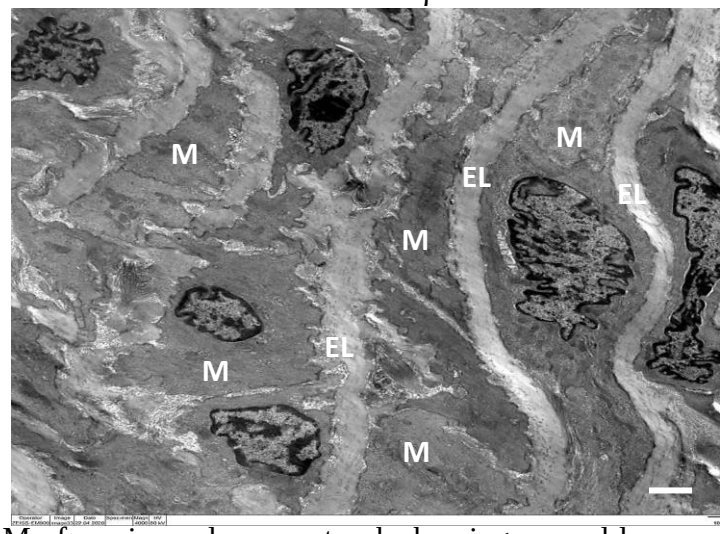

Figure 39. TEM of murine pulmonary trunk showing several layers of smooth muscle cells (M), each separated by an elastic lamina (EL). Scale bar = 1 µm.

3.5 General innervation and transmitter synthesising enzymes of LA

3.5.1 Single- and double-labelling immunofluorescence using antibodies against structural proteins and transmitter synthesizing enzymes in mouse

Immunohistochemistry was used to assess the general innervation of the LA. Cross-sectionally and longitudinally sectioned LA sections were subjected to double-immunolabeling directed against PGP9.5 and FITC-conjugated monoclonal antibodies directed against αSMA. PGP9.5-positive fibers were observed around the periphery, within the musculature and also at the point of attachment to the major vessels to which the LA was attached as well as within the recurrent nerve that was seen flanking the lateral side of the LA (Figure 40-42). Transgenic mice expressing eGFP driven by the *Chrna3* promoter were also used. nAChRα3-positive fibers were observed at the periphery of the LA and also at its point of attachment to the aorta.

Additionally, such fibres were found within the recurrent nerve. Transgenic mice expressing eGFP under the control of the promoter of the acetylcholine synthesizing enzyme, ChAT, were also used. *ChAT-eGFP*-positive fibers were neither present within the adventitia nor musculature or at points of attachment of the LA to the aorta nor pulmonary trunk. However, there were *ChAT-eGFP*-positive fibers within the recurrent nerve and a positive cell was present in the intimal region of the LA (Figure 40). Single-immunolabeling with primary antibody directed against TH revealed intense immunoreactive fibers (Figure 42) especially around the point of attachment of the LA to the pulmonary trunk. Additionally, there was co-localization between TH and *Chrna3*-eGFP (Figure 40). There was no reactivity in the LA when primary antibody was omitted. There were no immunoreactivities when samples were incubated with primary antibodies directed against nNOS (Figure 43). A histochemical marker of NOS activity, α-nicotinamide adenine dinucleotide phosphate (NADPH)-diaphorase reaction, was used to re-assess non-reactivity of nNOS in the LA (Figure 44-46). Results from NADPH-diaphorase showed no reactions in the LA, contrarily, within the endothelium of the pulmonary trunk, to which the LA attaches, cytoplasmic labelling (Golgi apparatus) were observed. In addition, reactions within the myenteric plexus were observed in murine gut samples which were used as positive controls (Figures 41-44).

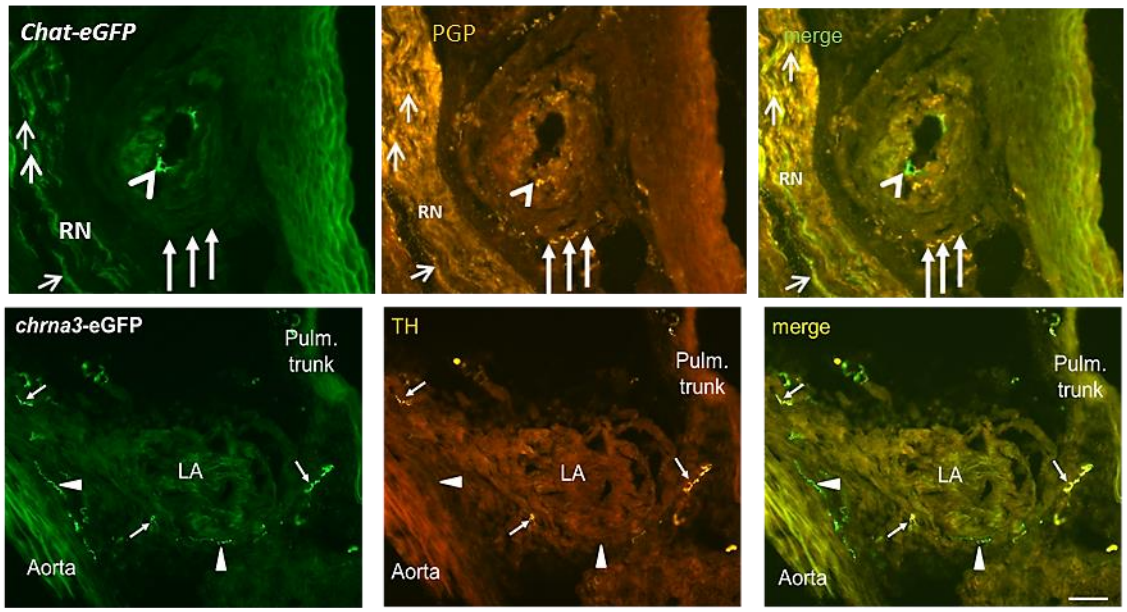

Figure 40. Endogenous GFP-fluorescence and single-immunolabeling of cross-sections of murine LA. The upper panel shows the LA attached to the aorta with the recurrent laryngeal nerve (RN) lateral to it. There are few cholinergic fibers (*Chat*-eGFP-positive) within the nerve (short white arrows). An intimal cell of the LA expresses GFP driven by the ChAT promoter (arrowhead). The upper middle panel reveals immunoreactivity in nerve fibers at the medio-adventitial border of the LA, which are negative for *ChAT*-eGFP. First picture in lower panel reveal *Chrna3*-eGFP^{+} fibers (white arrows). TH^{+} fibers (white arrows) are reported in the middle panel and the last panel shows co-localization between TH and *Chrna3*-eGFP (white arrows). However, solely *Chrna3*-eGFP^{+} fibers (white arrowheads) also occur. Scale bar = 50 µm.

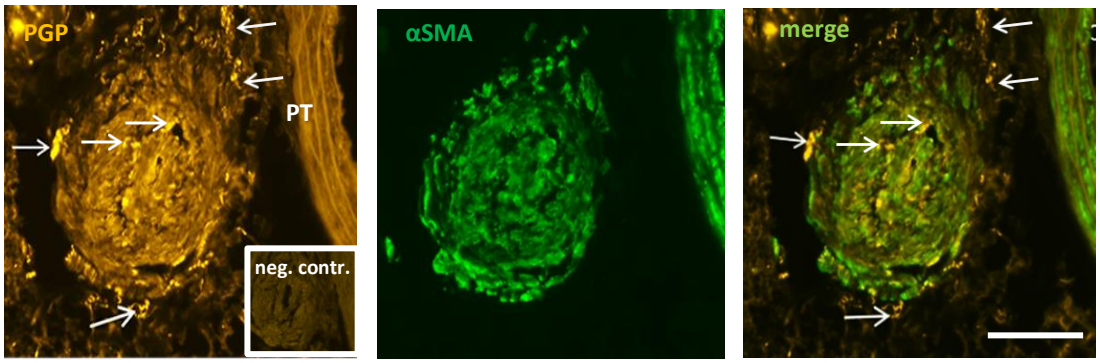

Figure 41. Double-immunolabeling of murine LA in cross section. First picture shows PGP-positive fibers (white arrows) present around the periphery, within the core and also at the point of attachment to the pulmonary trunk (PT). Middle picture shows presence of immunoreactivity to αSMA. Last picture is a merge of the first and middle picture. Control run without primary antibody directed against PGP (neg. contr.) shown in the insert. Scale bar = 50 µm.

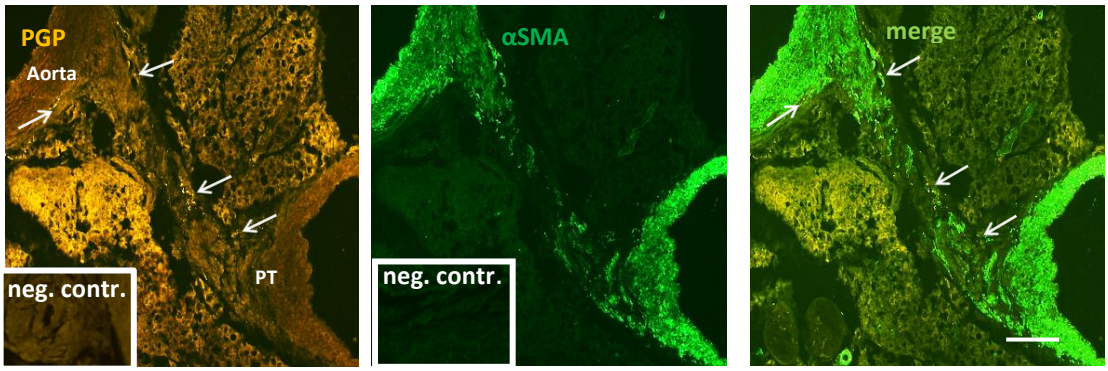

Figure 42. Double-immunolabeling of murine LA in longitudinal section. The first picture reveals the LA attached to the aorta and pulmonary trunk (PT) with PGP-positive fibers along the external borders, at the point of attachments to the aorta and pulmonary trunk (white arrows). Middle picture shows immunoreactivity against αSMA. The last picture is a merge showing PGP-positive fibers close to smooth muscle cells. Controls run without primary antibody (neg. contr.) shown in the inserts. Scale bar = 50 µm.

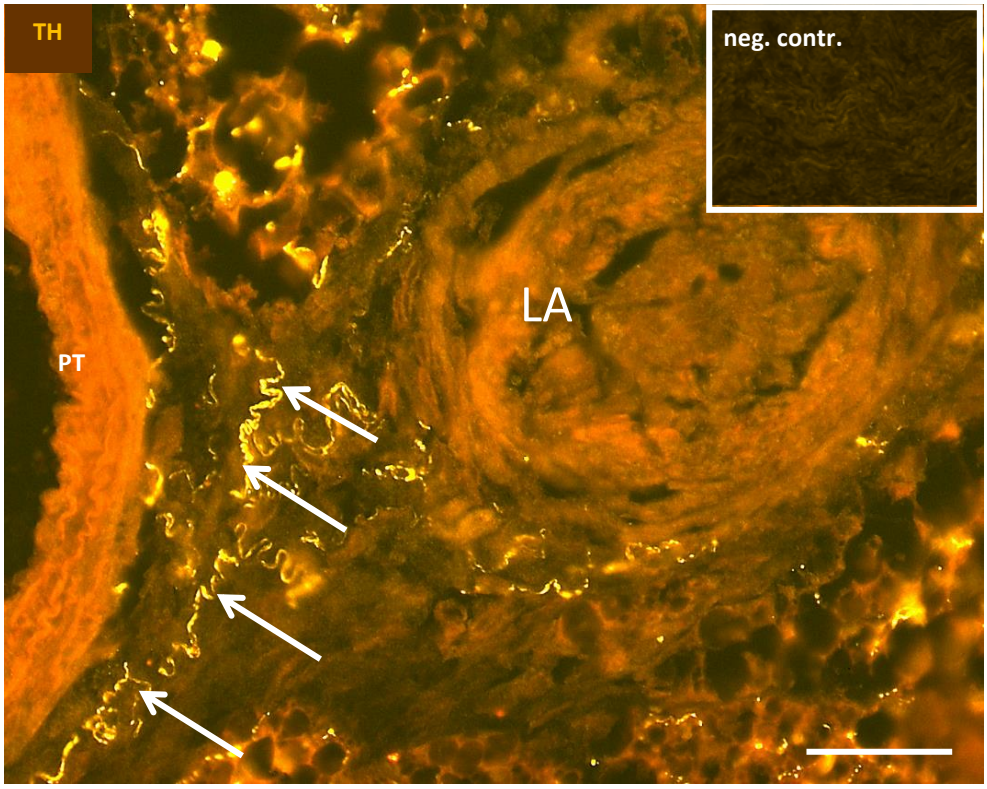

Figure 43. Single-immunolabeling of murine LA with TH^+ fibers (white arrows) abundant at its arterial attachments to the pulmonary trunk (PT). Controls run without antibody against TH (neg. contr.) shown in the insert. Scale bar = 50 µm.

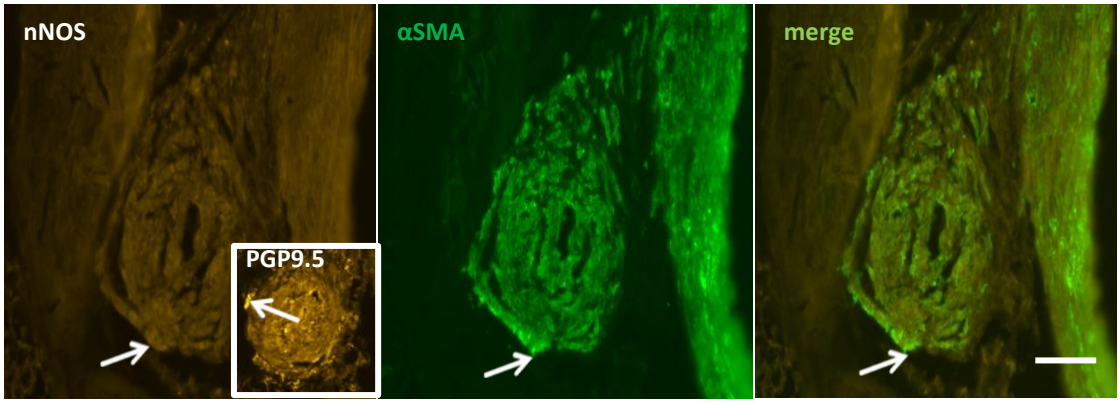

Figure 44. Double-immunolabeling of murine LA. In the first picture, there was no immunoreactivity using primary antibodies directed against nNOS. The middle picture shows immunoreactivity against αSMA. Control run with primary antibody directed against PGP (insert) shown in the insert. Scale bar = 50 µm

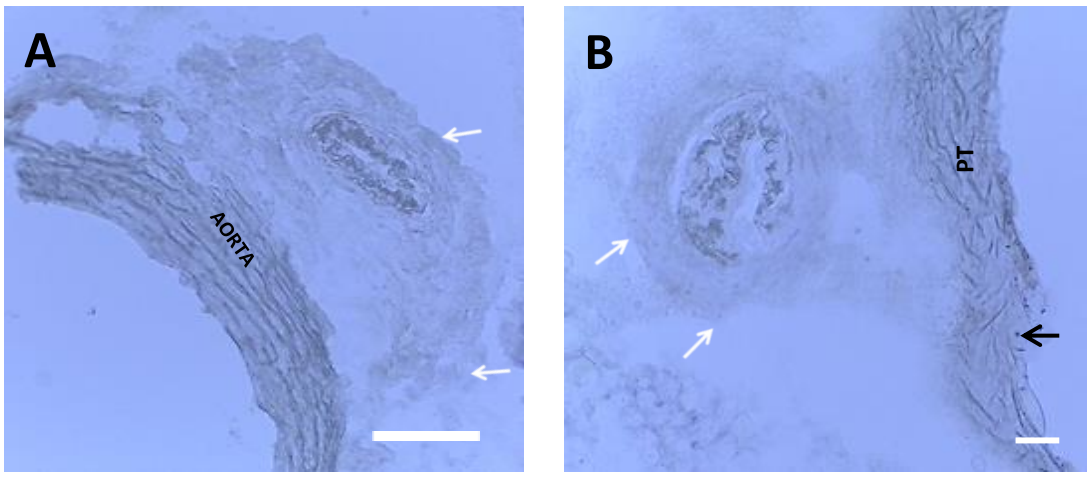

Figure 45. NADPH-diaphorase histochemical staining of mouse LA. A) Note no reaction in the LA (white arrows). B) White arrows indicating no reaction to the stain in LA and black arrow indicative of reaction (Golgi labelling) within the endothelium of the pulmonary trunk (PT). Note the non-reactivity of the LA to NADPH-diaphorase irrespective of its attachment to either the aorta or the pulmonary trunk. Scale bar = 50 µm.

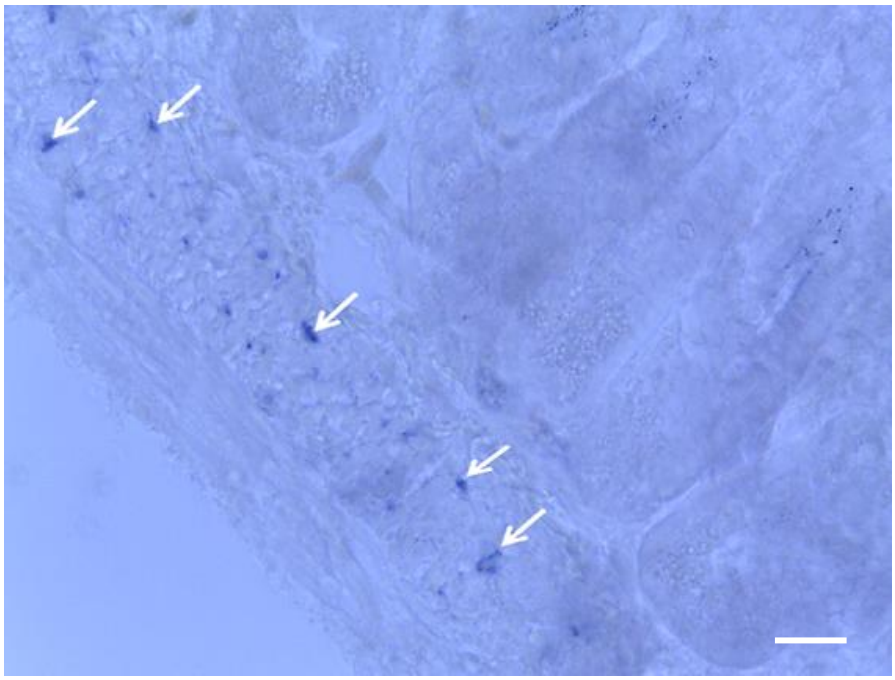

Figure 46. NADPH-diaphorase histochemical staining of murine small intestine. White arrows indicate positive reaction in the myenteric plexus. Scale bar = 50 µm.

3.5.2 Double-labelling immunofluorescence using antibodies against structural proteins and transmitter synthesizing enzymes in pig

Immunohistochemistry to assess the general innervation of the LA using antibodies against PGP reported immunoreactive nerve fibers. PGP-positive fibers were detected along bundles of smooth muscle cells (Figure 47). Double-immunolabeling with primary antibody directed against TH and FITC-conjugated monoclonal antibody against αSMA revealed TH-immunoreactive fibers present along bundles of smooth muscle cells (Figure 48). There were no nNOS-immunoreactive fibers even though fibers were seen in samples incubated with primary antibodies directed against PGP used as positive controls (Figure 49). To determine the specificity of the secondary antibody, primary antibodies were omitted and replaced by PBS (Figure 47-49 inserts).

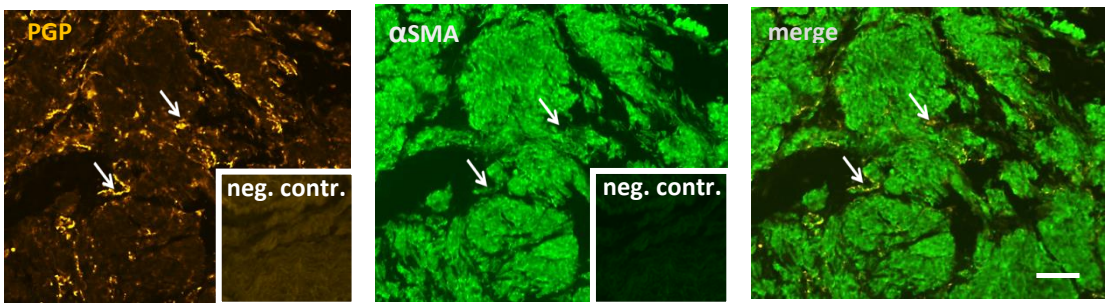

Figure 47. Double-immunolabeling of pig LA. First picture on the left showing numerous PGP-immunoreactive fibers (white arrows) present within the LA. Middle picture shows immunoreactivity against αSMA. The last picture is a merge showing PGP-positive fibers close to smooth muscle cells. Controls run without primary antibody (neg. contr.) shown in inserts. Scale bar = 50 µm.

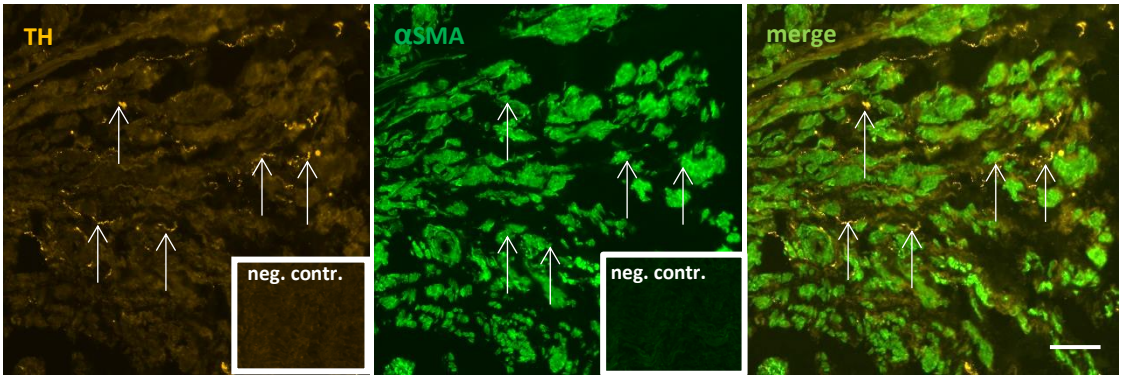

Figure 48. Double-immunolabeling of pig LA. First picture on the left showing TH-immunoreactive fibers (white arrows) present within the LA. Middle picture shows immunoreactivity against αSMA. The last picture is a merge showing TH-positive fibers close to smooth muscle cells. Controls run without primary antibodies (neg. contr.) shown in inserts. Scale bar = 50 µm.

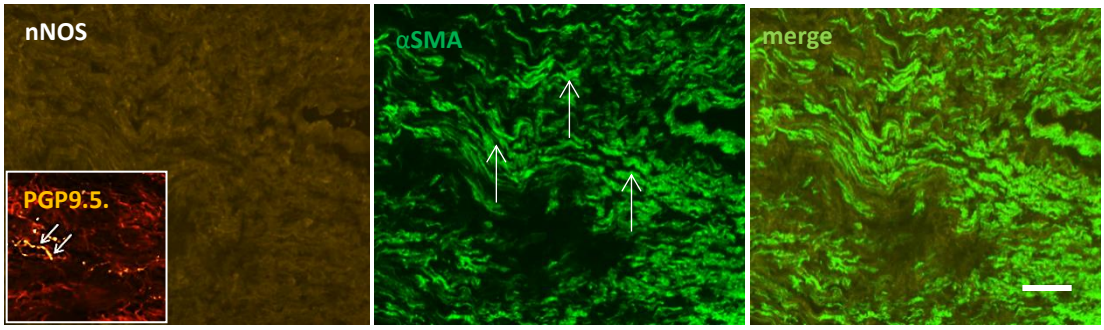

Figure 49 Double-immunolabeling of pig LA. In the first picture, there is no immunoreactivity to antibodies against nNOS. The middle picture shows immunoreactivity against αSMA (white arrows). The last picture is a merge. Controls run with antibody against PGP (insert) showing PGP-positive fibers in insert. Scale bar = 50 µm.

3.5.3 Double-labelling immunofluorescence using antibodies against structural proteins and transmitter synthesizing enzymes in human

To assess the general innervation of LA in human, double-labelling immunohistochemistry was performed using primary antibodies directed against PGP and a FITC-conjugated monoclonal antibody against αSMA. PGP-Positive fibers were detected along bundles of smooth muscle cells (Figure 50). Double-immunolabeling with primary antibody directed against TH and FITC-conjugated monoclonal antibody against αSMA also revealed TH

immunoreactive fibers and αSMA-positive cells (Figure 51). To determine the specificity of the secondary antibody, primary antibodies were omitted and replaced by PBS (Figures 50 & 51).

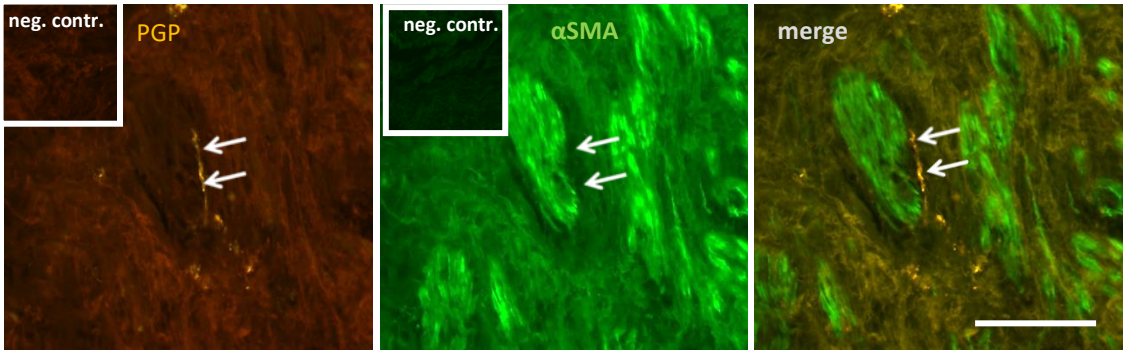

Figure 50 Double-immunolabeling of human LA. The first picture shows PGP-immunoreactive nerve fiber (white arrows). The middle picture shows immunoreactivity against αSMA. The last picture is a merge. Controls run without primary antibodies (neg. contr.) shown in the inserts. Scale bar = 50 µm.

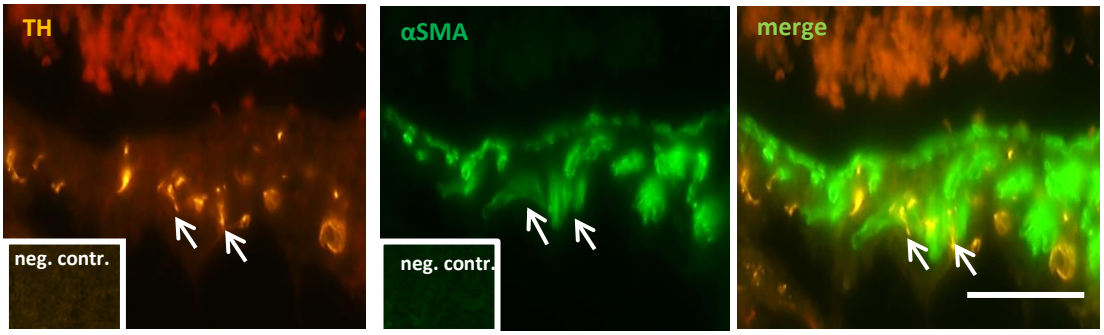

Figure 51. Double-immunolabeling of human LA. The first picture from the left showing TH^+ fibers (white arrows). The middle picture shows αSMA-positive cells (green). The last picture is a merge showing TH-positive fibers close to smooth muscle cells (white arrows). Controls run without primary antibodies (neg. contr.) shown in the inserts. Scale bar = 50 µm.

3.5.4 TEM of smooth muscle innervation in mice

TEM of mice LA revealed the presence of varicosities or nerve terminals confirming the earlier observed findings of immunohistochemistry. In total, all 81 nerve fibers observed were unmyelinated, had a Schwann cell present or not observed, and were predominately found within the media and adventitial layers. A higher number of these terminals (n = 47, 58%) were ≤ 2 µm away from the nearest myocyte, while 34 (42%) were ≥ 2.1 µm away from the nearest myocyte (Figure 52). Axonal nerve terminals were

primarily divided into two groups: the vesiculated and non-vesiculated. Fifty-seven (57) nerve terminals (71%) were vesiculated leading to a granulated appearance, whiles the remaining 24 (29%) had no granulation due to the absence of vesicles (Figure 53). Additionally, vesiculated nerve terminals contained large dense core and small clear vesicles with sizes measuring around 72 ± 3 nm and 40 ± 5 nm (mean ± SEM, n = 2,310, n = 3,026), respectively. A minimum of one axon and a maximum of 8 axons per Schwann cell were observed. It was not uncommon to see nerve terminals with the presence or absence of vesicles encapsulated within the same Schwann cell. Sixty-five (65) nerve terminal representing 80% had between 1-4 axons encapsulated within one Schwann cell (Figure 54). When present, Schwann cells partially or completely covered their respective nerve terminal. Partially covered nerve terminals had naked regions devoid of covering. Seventy (70) nerve terminals (86%) observed had partial Schwann cell covering with the remaining 11 (14%) entirely covered by Schwann cell (Figure 55).

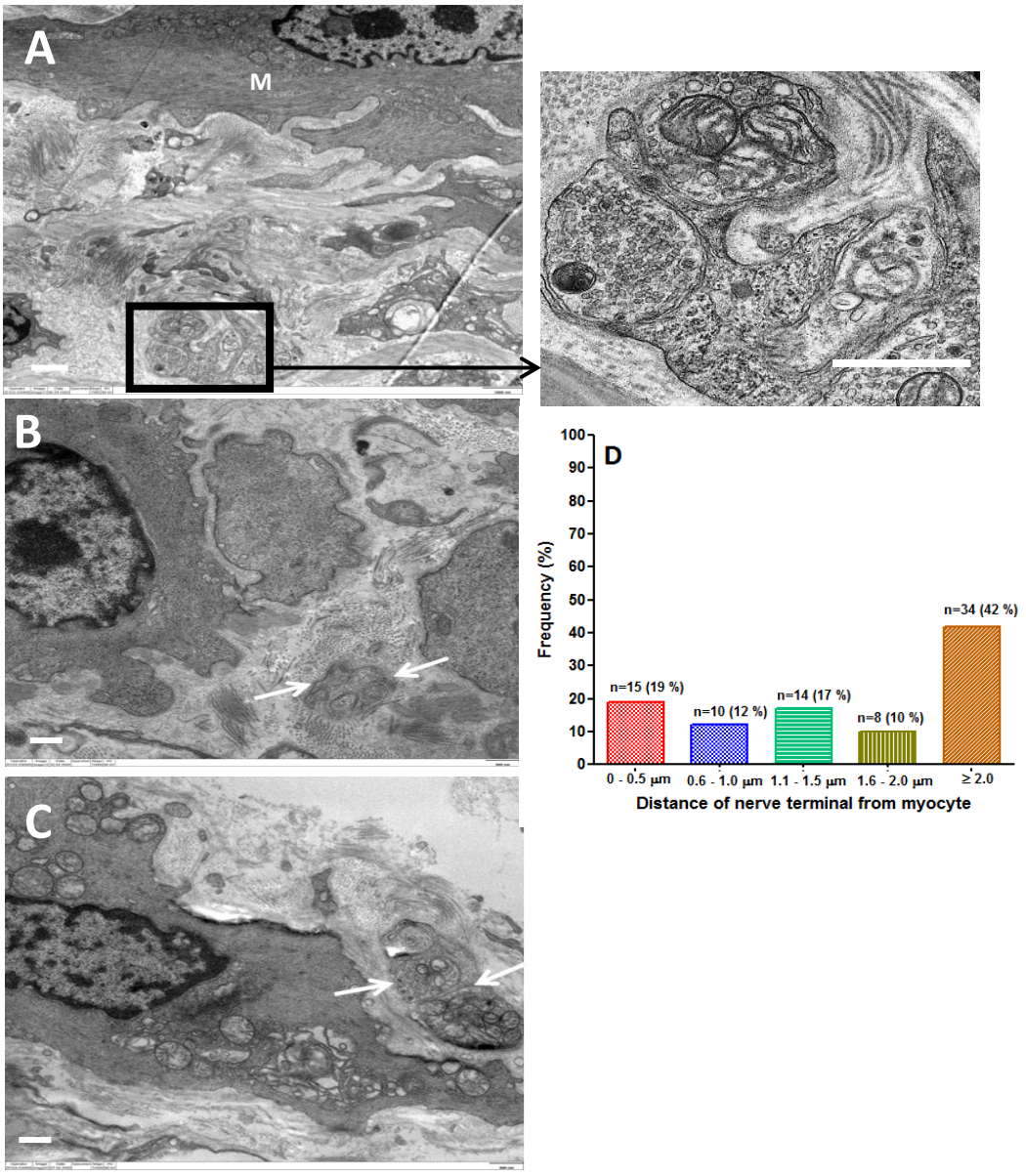

Figure 52. TEM of murine LA. A) Nerve terminal (boxed area) >2 µm away from a myocyte (M). B) Nerve terminal (white arrows) 0.8 µm away from a myocyte (M). C) Unmyelinated nerve terminal (white arrows) 0.4 µm from a myocyte (M). D) Histogram is a percentage representation of the number of nerve terminals with respect to their distance from the nearest myocyte. Scale bars: A = 1 µm, B, C = 0.5 µm.

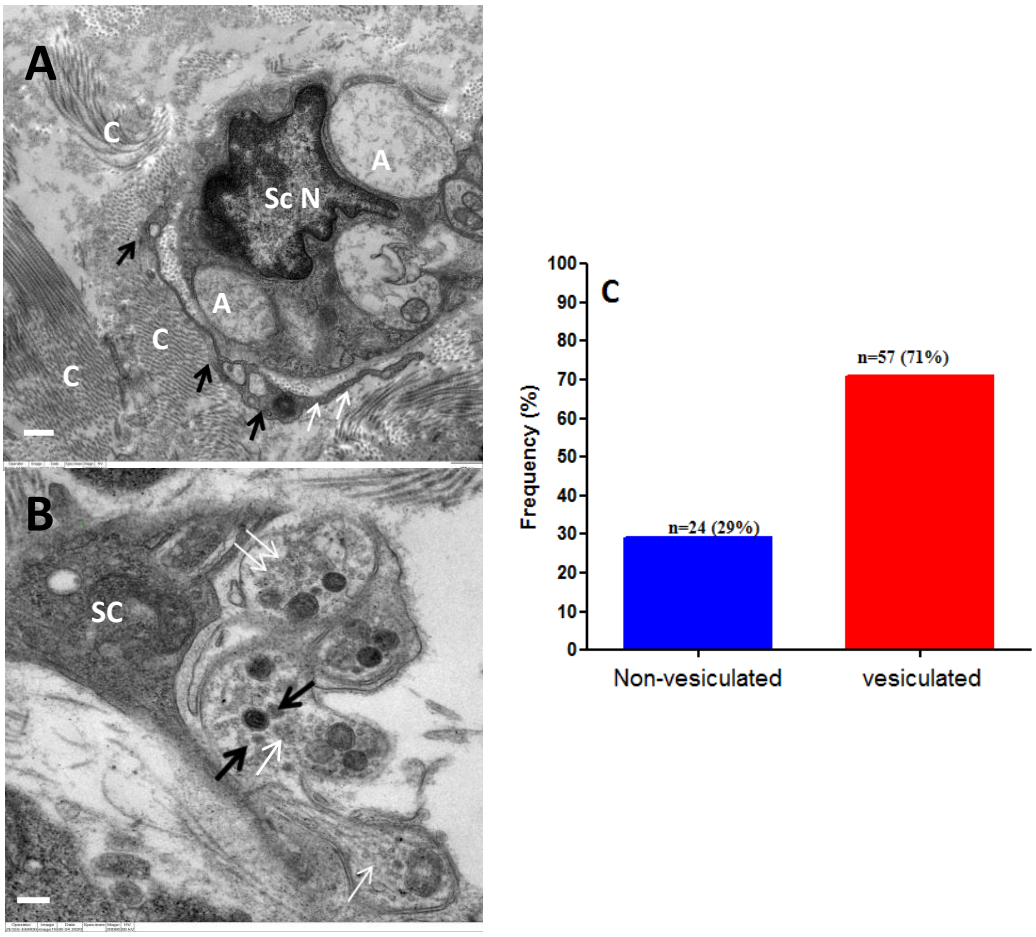

Figure 53. TEM of murine LA. A) Absence of vesicles within axon (A). Note the presence of a mononucleated (N) Schwann cell (SC) and collagen fibrils (C). There is also a telopode 0.1 µm away from the nerve fiber bundle with podoms (black arrows) and podomers (white arrows). B) Large dense core (black arrows) and small clear (white arrows) vesicles in nerve terminal. Schwann cell (SC) encapsulating axons also observed. C) Histogram demonstrating the relative frequencies of vesiculated and non-vesiculated nerve terminals. Scale bars: A = 0.5 µm, B = 0.25 µm.

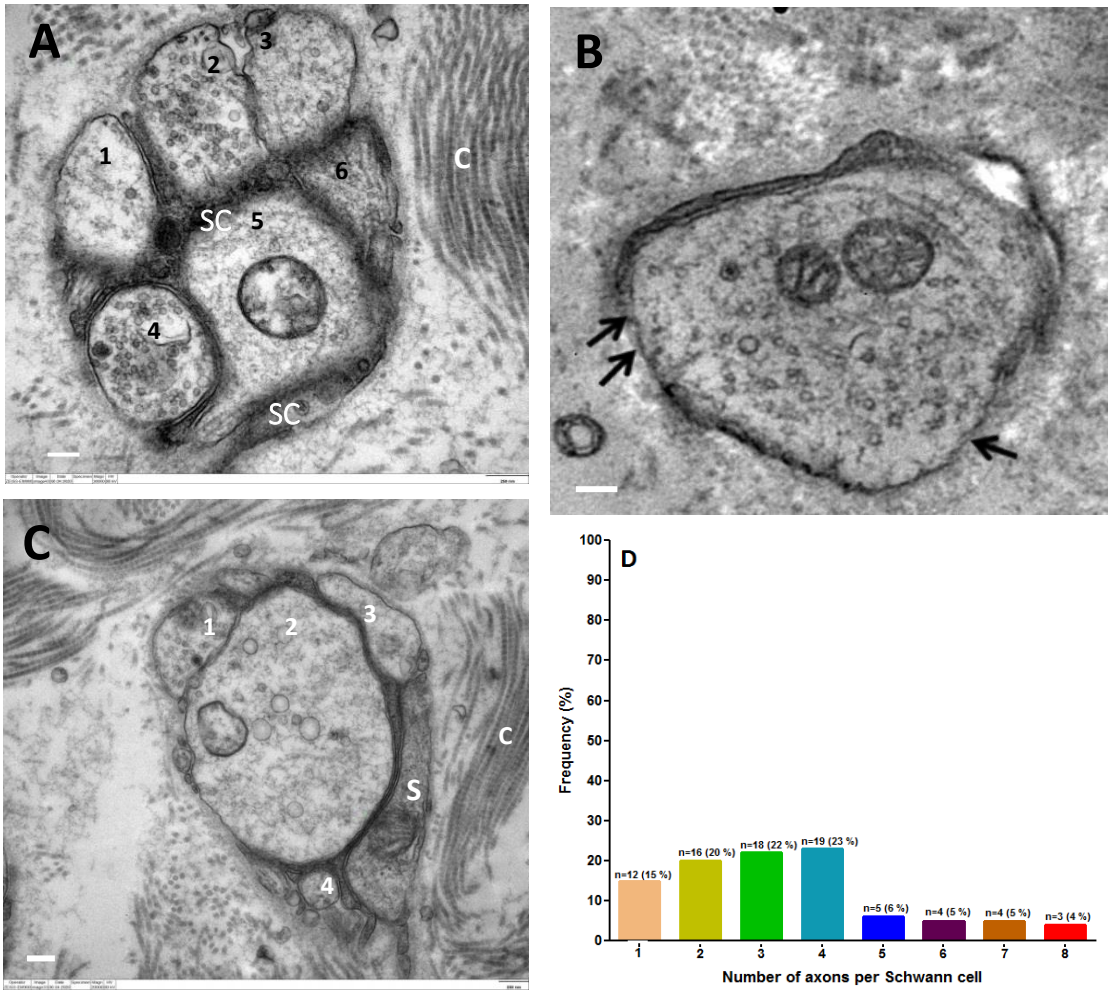

Figure 54. TEM of murine LA. A) Six axons (1-6) encapsulated within one Schwann cell (SC). Note the presence of vesicle accumulations in 2 & 4. B) A minimally vesiculated singular axon with partial Schwann cell covering. C) A Schwann cell encapsulating 4 axons (1-4) in close proximity to collagen fibrils (C). D). Histogram of percentage representation of the numerical data in terms axons per Schwann cell. Scale bars = 0.25 µm.

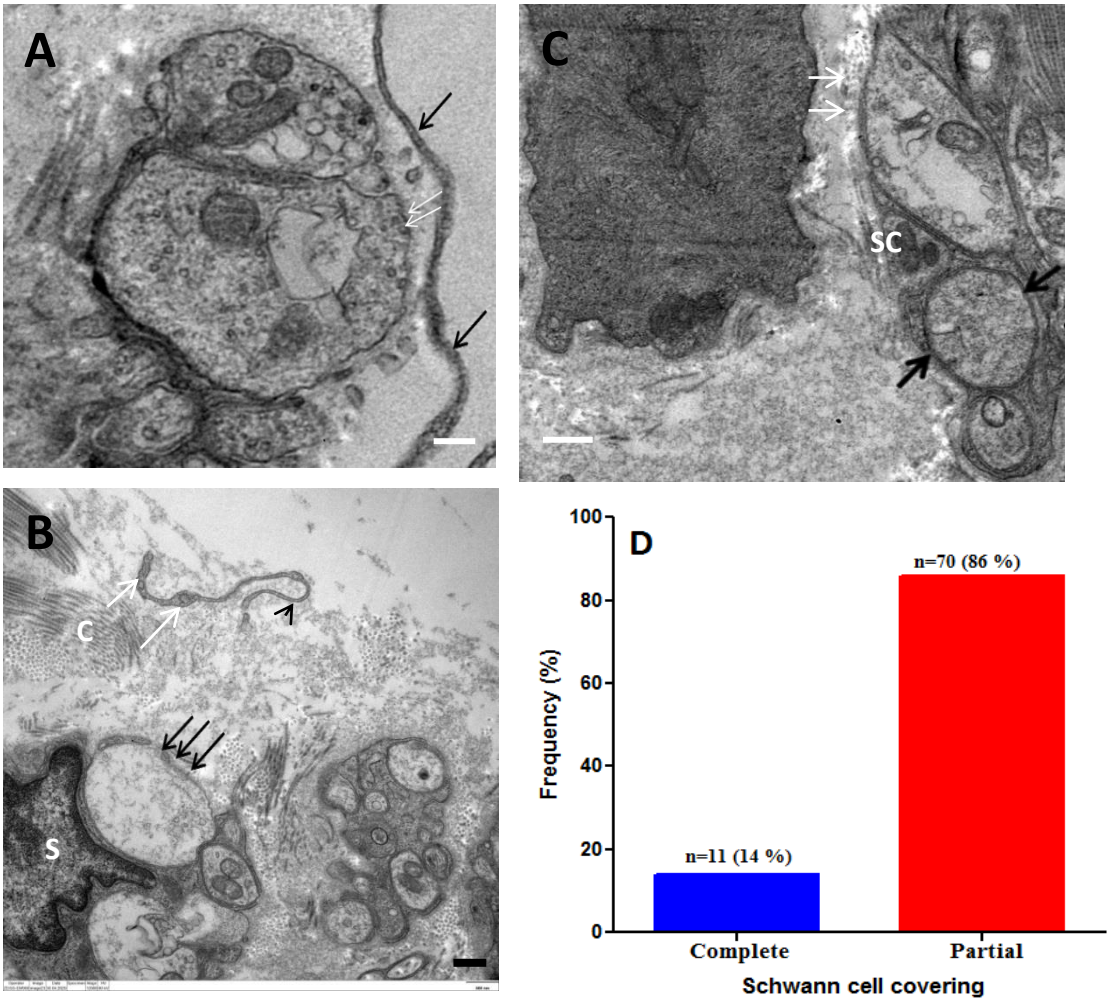

Figure 55. TEM of murine LA. A) Axons with partial Schwann cell covering (white arrows). Note the presence of podomers (black arrows) 0.10 µm from nerve fiber. B) Nerve terminal with Schwann cell (SC) and a naked region devoid of covering (black arrows). Note the presence of collagen fibrils (C) and a telopode with podoms (white arrows) and podomer (black arrow head). C) A nerve fiber bundle with partial (white arrows) and complete (black arrows) covering from Schwann cell (SC). D) Histogram of percentage representation of the numerical data in terms of nerve terminals with complete or partial Schwann cell covering. Scale bars = 0.5 µm.

3.6 Neuropeptides in LA innervation

3.6.1 Mouse

The LA was subjected to double-immunolabeling using antibodies against TH and NPY. In cross-sectional samples, TH- and NPY-immunoreactive nerve fibers were present in

the adventitial and surrounding connective tissue layer, at the medio-adventitial border as well as within the left recurrent nerve. There was co-localization of TH- and NPY-immunoreactivities (Figure 56) though some fibers were NPY- or TH-immunoreactive only. Antibodies directed against VIP paired with FITC-conjugated αSMA antibody revealed αSMA-immunoreactive cells only. There was no VIP-immunoreactive fiber (Figure 57). Incubation with antibodies against SP and CGRP revealed nerve fibers with immunoreactivity for both. Comparatively, SP-immunoreactivity in fibers was lesser than CGRP. There was co-localization of SP/CGRP immunoreactivities though some fibers were solely SP- or CGRP-positive (Figure 58). To determine the specificity of the secondary antibodies, the primary antibody was omitted and replaced with PBS.

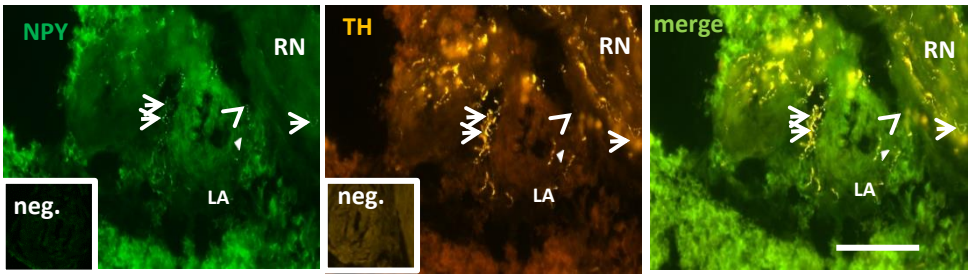

Figure 56 Double-immunolabeling of murine LA. In the first upper picture, the white arrows at the medio-adventitial border of the LA indicate NPY-positive fibers, white arrowheads indicates NPY-positive nerve fibers only. In the second picture, white arrows are indicative of TH immunoreactivity in same nerve fiber at same location of the medio-adventitial border shown in the first picture. Full white arrowhead indicative of TH-positive nerve fibers only. The third picture is a merge revealing co-localization of TH and NPY as well as TH and NPY only fibers (white arrows). Controls run without primary antibodies directed against TH/NPY (neg. contr.) shown in inserts. Scale bar = 50 µm.

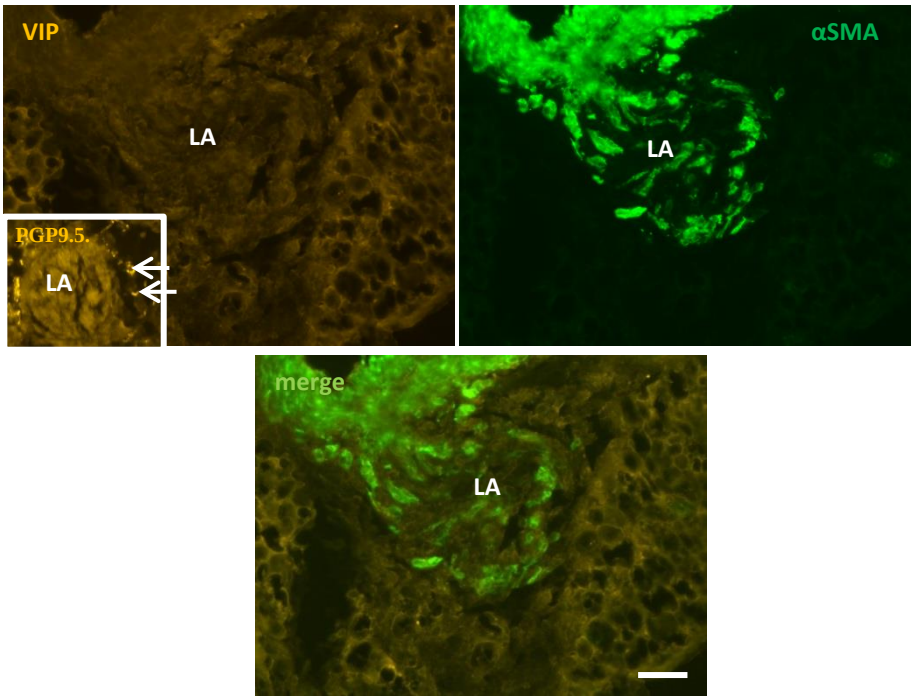

Figure 57. Double-immunolabeling of mouse LA. In left picture, there is no immunoreactivity to antibodies against VIP. The right picture shows immunoreactivity to antibodies against αSMA (white arrows). The picture below is a merge. Controls run with antibody against PGP9.5 showing PGP-positive fibers in insert. Scale bar = 50 µm.

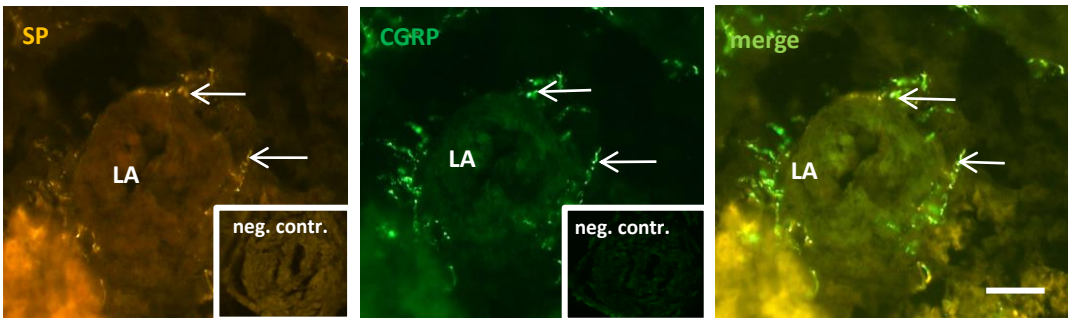

Figure 58 Double-immunolabeling of murine LA. In the first picture, the white arrows indicate SP-positive fibers. White arrows indicating CGRP-positive fibers are shown in the second picture. The third picture is a merge revealing co-localization of SP and CGRP in fibers. Controls run without SP/CGRP antibody (neg. contr.) shown in the inserts. Scale bar = 50 µm.

3.6.2 Pig

Immunohistochemistry using antibodies against NPY, CGRP, SP, and TH revealed the presence of immunoreactive nerve fibers. Double-immunolabeling using antibodies against TH and NPY revealed extensive co-localization, per contra, a smaller population were solely TH- or NYP-immunoreactive (Figure 59). Antibodies directed against VIP paired with FITC-conjugated αSMA antibodies revealed αSMA- immunoreactive smooth muscle cells of the LA, however, VIP-positive fibers were not observed (Figure 60). SP- and CGRP-immunoreactivities co-localized in nerve fibers and an additional population of nerve fibers was immunoreactive to CGRP only (Figure 61). To determine the specificity of the secondary antibody, the primary antibody was replaced with PBS.

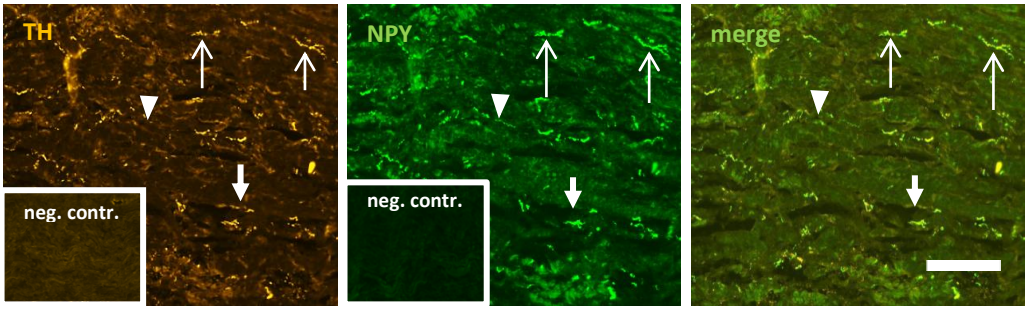

Figure 59. Double-immunolabeling of LA. First picture on the left showing immunoreactive TH-positive fibers (long white arrows) present within the LA. Note that solely TH^+ fibres (short white arrow) also occur. Middle picture shows immunoreactivity to antibody against NPY. Note that solely NPY^+ fibres (white arrowhead) also occur. The last picture on the right is a merge showing co-localization of TH and NPY immunoreactivities (white arrows). Controls run without TH/NPY antibodies (neg. contr.) shown in the inserts. Scale bar = 50 µm.

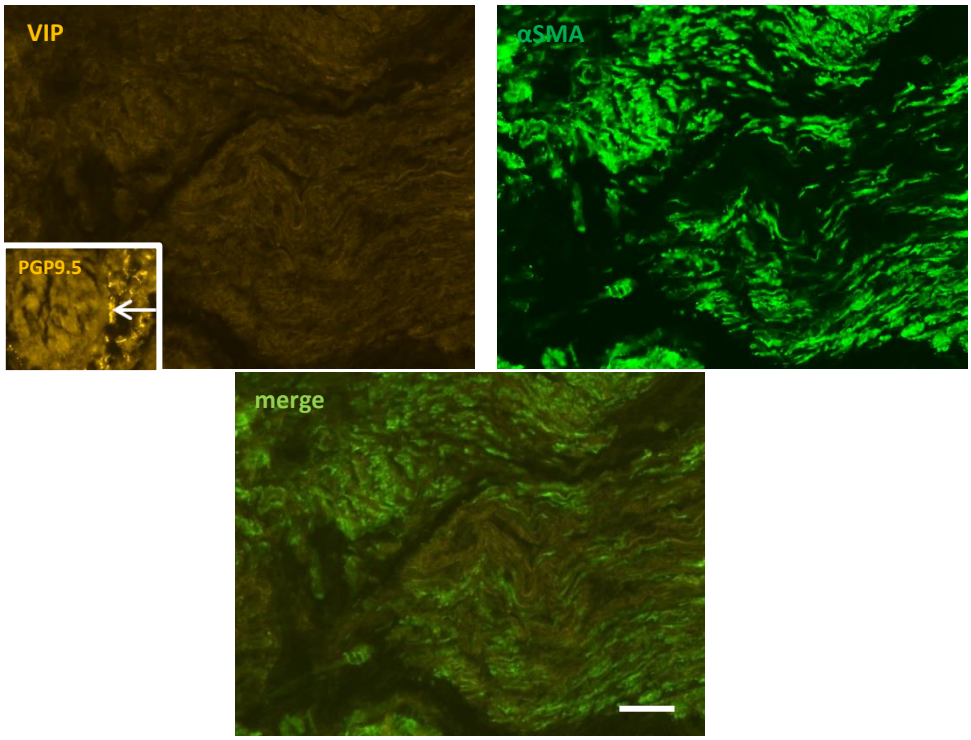

Figure 60. Double-immunolabeling of pig LA. In the left picture, there is no immunoreactivity to antibodies against VIP. The right picture shows immunoreactivity to antibodies against αSMA. The picture below is a merge. Controls run with primary antibody directed against PGP9.5 shown in insert. Scale bar = 50 µm.

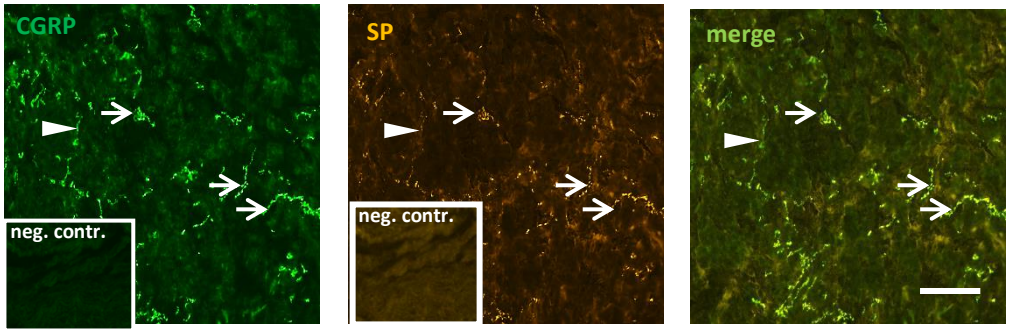

Figure 61. Double-immunolabeling of murine LA. In the first picture note the white arrows indicating CGRP-positive fibers. Note the occurrence of solely $CGRP^{+}$ fibres (white arrowhead). White arrows indicating SP-positive fibers are shown in the second picture. The third picture is a merge revealing co-localization of SP and CGRP in fibers. Controls run without SP/CGRP antibodies (neg. contr.) shown in the inserts. Scale bar = 50 µm.

3.6.3 Human

Sections were stained with antibodies against TH, NPY, CGRP, SP, and VIP. Double-immunolabeling with antibodies against TH and NPY revealed substantial immunoreactivity and co-localization (Figure 62). Antibodies directed against VIP paired with FITC-conjugated αSMA antibody revealed αSMA-positive smooth muscle cells but no positive signal with antibodies against VIP. Incubation with antibodies against SP and CGRP also showed the presence of co-localization of these neuropeptides in fibers and varicosities (Figure 63). To determine the specificity of the secondary antibody, the primary antibody was omitted and sections were only incubated with PBS.

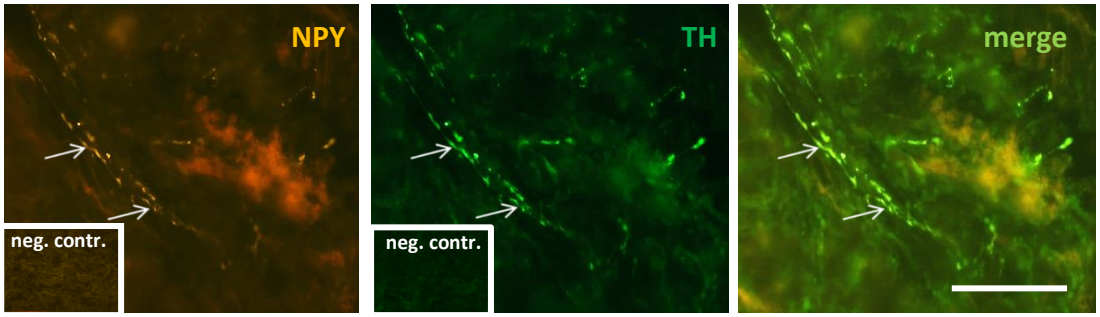

Figure 62. Double-immunolabeling of human LA. The first picture shows white arrows indicative of NPY-positive fibers. TH-positive fibers indicated with white arrows in middle picture. The last picture is a merge revealing Co-localization of TH and NPY in fibers (white arrows). Controls run without primary antibodies (neg. contr.) shown in the inserts. Scale bar = 50 µm.

Figure 63. Double-immunolabeling of human LA. The first picture shows white arrows indicative of CGRP-positive fibers. SP-positive fibers indicated with white arrows in middle picture. The last picture is a merge revealing co-localization of CGRP and SP in nerve fiber (white arrow). Controls run without primary antibodies (neg. contr.) shown in the inserts. Scale bar = 50 µm.

3.7 Functional role and contractility of pig LA in organ bath experiments

3.7.1 EFS and pharmacological administration of noradrenalin in pig LA

Pigs LA used as both control and treatment were subjected to three different increasing frequencies of electrical field stimulation (EFS) at 8, 16, and 32 Hz, 2 ms, 150 mA, 10 V. The first frequency, 8 Hz, 2 ms, 150 mA, 10 V, was continuous for 60 s. From a baseline of 0.6 g, the LA contracted to a maximum tension of 1 g. Stimulation was turned off after 60 s. During this time, the LA relaxed and tension also returned to baseline (0.6 g). A second higher stimulation of 16 Hz, 2 ms, 150 mA, 10 V, also produced a contraction from baseline, which in comparison to the prior was bigger. The maximum contraction for the second stimulation was 1.1 g. The LA was again given 5 min resting period and though a relaxation was observed, tension stalled at 0.7 g and did not return to baseline. The third stimulation, 32 Hz, 2 ms, 150 mA, 10 V, produced a maximum contraction of 1.5 g, and after stimulation was extenuated, the LA relaxed though tension did not return to baseline (Figure 64). The difference in maximum contraction of the LA upon exposure to the three frequencies was significant between 8 Hz and 32 Hz (Figure 65). After the last EFS stimulation, the LA was given 5 min of resting period and this was followed by administration of increasing but cumulative concentration of NA (0.1 µM, 1 µM, 10 µM, 100 µM, 500 µM, 1 mM, 1.5 mM). All these doses administered produced a concentration-dependent contraction with the only exception being the first dose (0.1 µM), which produced no contractile effect on the LA. The contraction evoked by 10^{-3} M of NA was not enhanced further at higher concentrations in all experiments. In the control sample, the NA was replaced with vehicle. Though contraction from EFS was present in the control group, no contraction from vehicle administration was observed further on (Figure 64). Half maximal effective concentration (EC_{50}) of NA was 4.195 x 10^{-6} M (Figure 66).

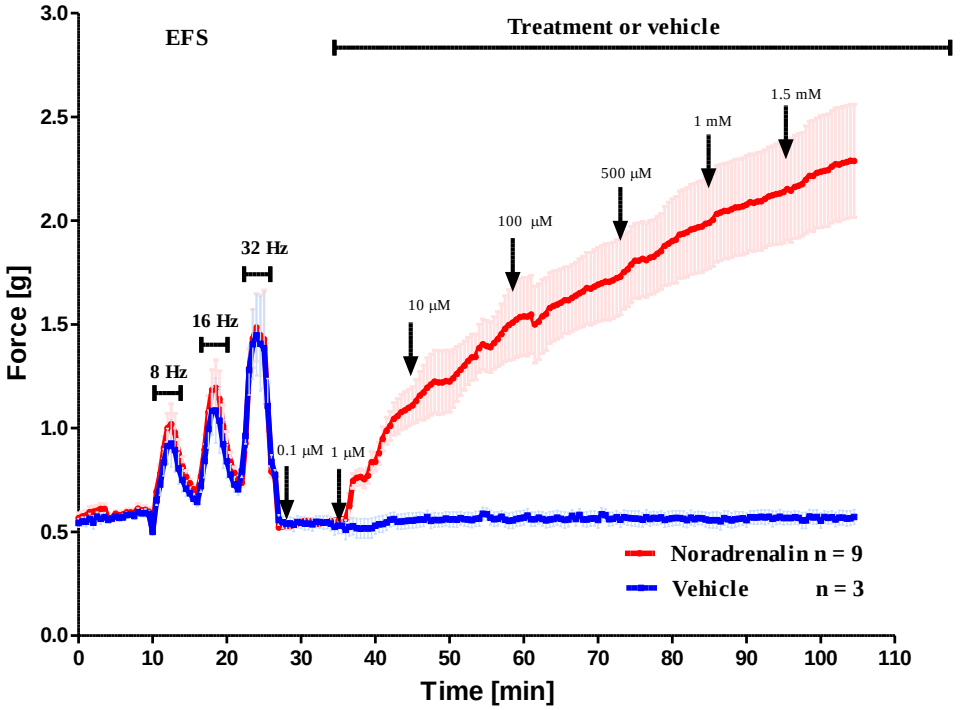

Figure 64 **EFS- and NA-induced contraction of pig LA in organ bath experiments.** LA subjected to a minute long EFS with 5 min resting time between each stimulation for both control (vehicle) and experimental samples (noradrenaline). There was a steady increase in contraction intensity in experimental sample with NA administration, whereas the vehicle did not evoke contraction Arrows indicate point of NA or vehicle administration. Mean ± SEM are shown.

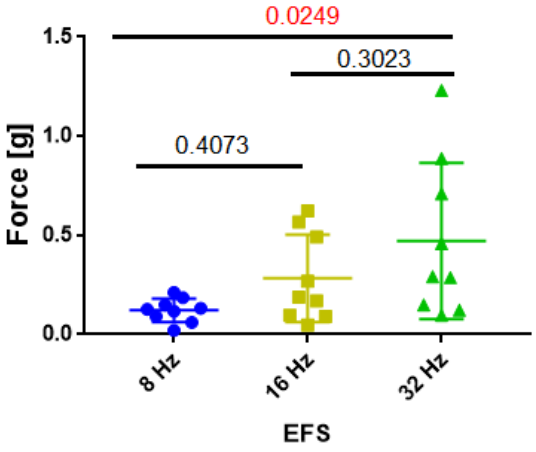

Figure 65**.** Testing for statistical significance of differences in means of maximal contraction value of EFS using one way ANOVA with $P \leq 0.05$. Significant value indicated in red (8 and 32 Hz).

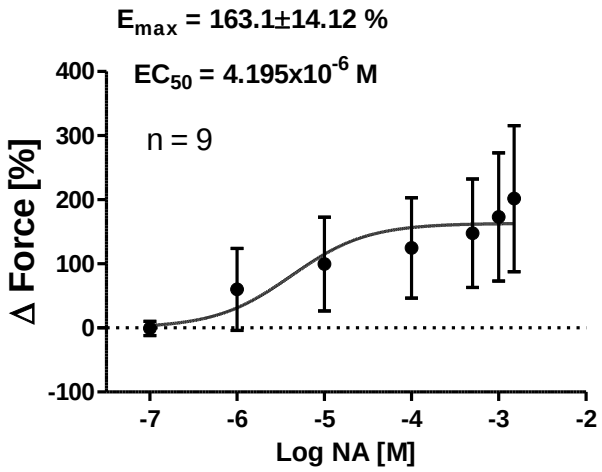

Figure 66**. Concentration response curve of contractility effect of NA on pig LA.** Concentration-dependent responses are shown as maximum reaction in force (E_{max}) and reactivity related to NA-induced contraction. Data are presented as mean ± SEM.

3.7.2 Adrenergic agonist and antagonist administration on pig LA

Pigs LA used as treatment and control were subjected to two increasing cumulative doses of NA (100 µm, 500 µm) with 10 min between each dose. There was no prior exposure to EFS. A concentration-dependent contraction was observed. The precontracted LA was further subjected to increasing but cumulative concentrations of prazosin (0.1 µM, 0.5 µM, 1 µM, 5 µM, 10 µM, 50 µM) or tamsulosin (1 µM, 5 µM, 10 µM, 50 µM, 100 µM, 500 µM). All doses, with the exception of 0.1 µM, 0.5 µM in prazosin and 1 µM, 5 µM in tamsulosin, showed antagonist effect on the precontracted LA. The subsequent doses produced a consistent relaxation of the LA until it was back to baseline (0.5 g). The control samples also contracted when they were subjected to two different doses of NA administration, however, no relaxation was observed upon administration of aqua or DMSO (vehicle) in place of prazosin and tamsulosin (Figures 67-68), respectively. The half maximal inhibitory concentration (IC_{50}) for prazosin and tamsulosin was 4.632 µM and 49.44 µM respectively (Figures 69-70).

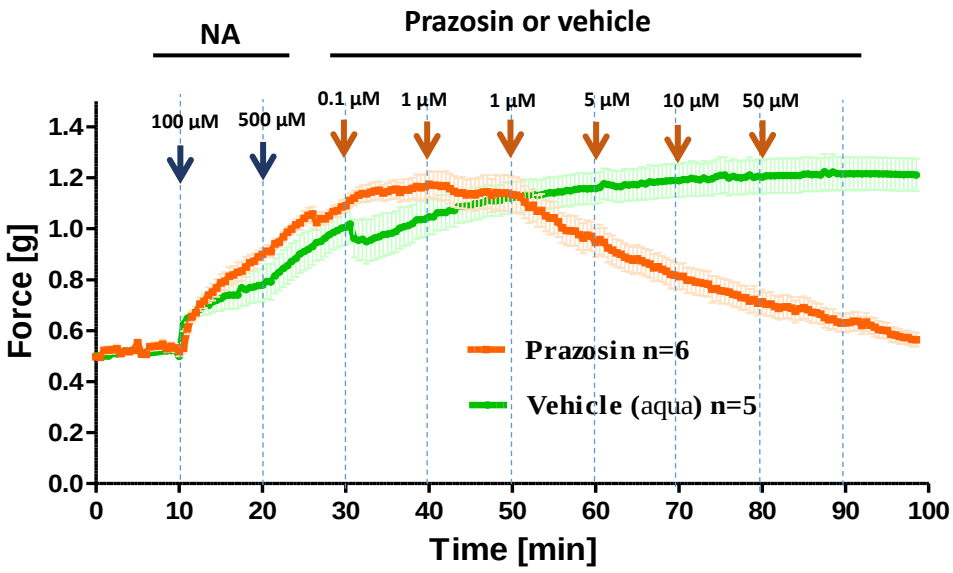

Figure 67. **Relaxant effect of prazosin on pig LA precontracted with NA**. There were contraction in both experimental and control samples with NA administration. The LA reported a stepwise relaxation from the precontraction induced by NA after being subjected to increasing cumulative concentrations of prazosin. In control samples, there was no relaxation observed upon administration of aqua in cumulative doses in place of prazosin. Arrows indicate point of substance or vehicle administration.

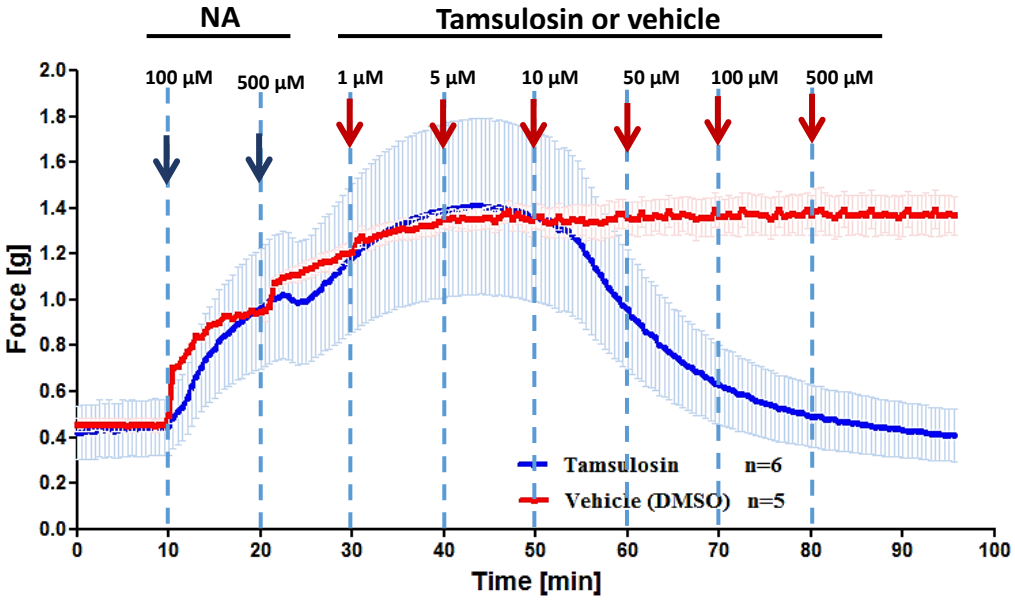

Figure 68. **Relaxant effect of tamsulosin on pig LA precontracted with NA**. There was cumulative contraction when samples were subjected to NA administration. The LA reported stepwise relaxation from the precontraction induced by NA administration after exposure to increasing cumulative concentrations of tamsulosin. There was no reaction upon administration of DMSO in cumulative doses in the control samples. Arrows indicate point of NA, tamsulosin or DMSO administration.

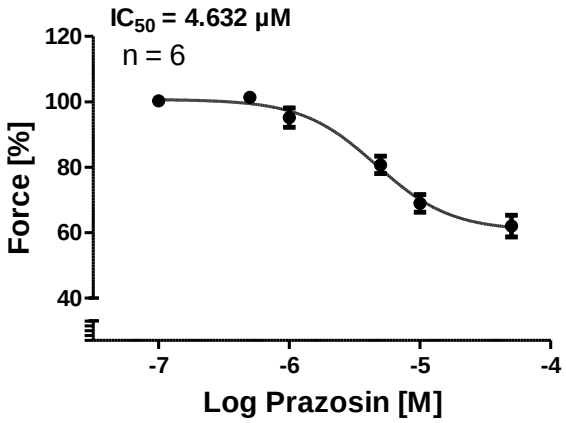

Figure 69**. IC_{50} of prazosin response in Pig LA.** The inhibitory curves for prazosin reporting an IC_{50} of 4.632 µM for NA-induced contraction (100 µM, 500 µM).

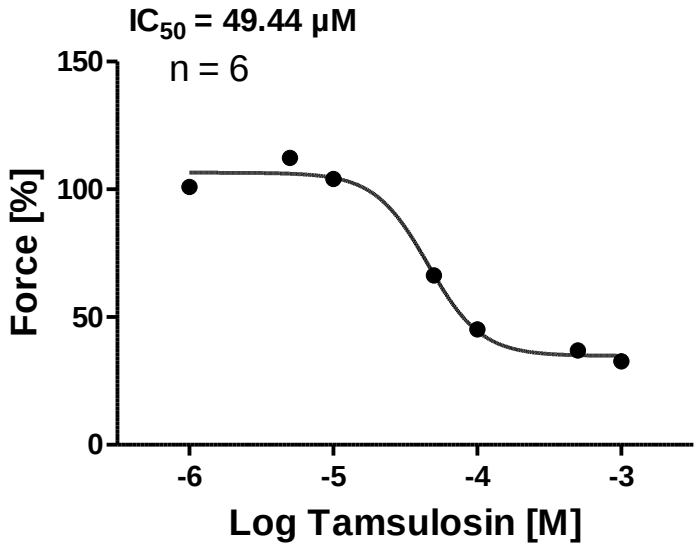

Figure 70. **IC_{50} of tamsulosin response of Pig LA.** Inhibitory curves for tamsulosin reporting an IC_{50} of 49.44 µM for NA-induced contraction (100 µM, 500 µM).

4 Discussion

4.1 Hypothesis and summary of major findings or results

Though the LA has generally been considered as a fibrosed remnant of the ductus arteriosus, rupture of the aortic arch in certain blunt trauma conditions indicates that it may still has mechanical impact on both the pulmonary bifurcation and the aortic arch. Significant evidence reports autonomic nerve fibers and baroceptive apparatus within the ductus arteriosus in-utero whereas for the LA, reports are anecdotal and contradictory. Based on this premise, we hypothesized that:

1. LA, the remnant of the foetal muscular artery (ductus arteriosus) which connects the main lung (pulmonary trunk) and main body (aorta) arteries during embryological circulation, is not a mere fibrotic remnant resulting from the complete metamorphosis of the ductus arteriosus but may retain some of its contractile muscular elements.

2. In post-uterine life, this foetal shunt still receives innervation.

3. This innervation controls contractility of the muscular elements.

The results from my study indicate that the LA, described as the fibrotic remnant of the foetal ductus arteriosus, still retains most of its characteristic as a muscular artery and has extensive amount of smooth muscle cells in its tunica media even until senescence. The muscle cells are contractile, mainly innervated by the adrenergic component of the autonomic nervous system and to a lesser extent by afferent fibers long after childbirth. The innervated myocytes found within the LA contracted in response to electrical field stimulation and exogenous NA. NA-inducted precontracted LA relaxed in response to the administration of the α-adrenergic blockers tamsulosin and prazosin.

4.2 General morphology and connective tissue component of the LA

The LA has generally been described as a fibrosed remnant of the ductus arteriosus (Chiruvolu and Jaleel 2009), though no known textbook, descriptive anatomy or publication brings to bear the gap in knowledge regarding a standard description in terms of the ultrastructural arrangement or layers of cells found in this structure or its reactivity to immunostaining. Contrary to reports of the LA being a small fibrous remnant of the fetal ductus arteriosus (Chiruvolu and Jaleel 2009), but in line with the hypothesis, the results

from the study show that the structure is mainly muscular. This agrees with the findings by Garcia (1975), who after studying the LA in eight healthy human adults using stereomicroscope dissected Zemper treated (50%), Celloidin embedded (25%), and paraffin embedded (25%) hearts, stained with Axan and ”resorcin-fuchsin”, described the structure as a small smooth muscle. Dohr et al. (1986) also studied the morphology of the LA using routine and special histological stainings in 15 bodies of both sexes aged between 60 – 80 years. The report from the study divided the LA into an outer and inner zone only. To the contrary, my study of human LA subjected to routine and special histological staining's to assess the general morphology of the structure revealed that the LA could be distinctively divided into three regions. This corresponded with publications and report with regard to the general histological anatomy of arteries (Pearce and Thomsen 2000). From outward within, a tunica adventitia, consisting of intertwining collagen fibers, nerve bundles, blood vessels, and elastin fibers embedded in numerous adipocytes were observed. The second region, tunica media, sharply contrasted from the first, was mainly made up of VSMC, collagen and elastin fibers. The presence of an extensive amount of vascular smooth muscle arranged in circular and longitudinal orientations within the tunica media authenticated the fact that, majority of the myocytes which make up this layer does not migrate to the intima during closure of the ductus arteriosus. This was contrary to the report by De Reeder et al. (1989) and Yoder et al. (1980) who reported the complete obliteration of the luminal part of the ductus arteriosus by migrated smooth muscle cells from the tunica media into the tunica intima after birth. Additionally, not only do the results from my study contradict their report on smooth muscle migration, but also on the complete obliteration of the ductus arteriosus. The lumen of the “ligament” was not always completely obliterated. Partial obliteration showing luminal remnants at the aortic end of the LA was observed, though it does not serve as a passage way for blood, because it does not open into the pulmonary trunk. Regardless of whether completely obliterated or otherwise, the core of the LA was sometimes made up of myocytes, although scanty, and cell debris. In some population, the core was fibrosed, whereas in others, it was calcified or both. A study by Bisceglia and Donaldson (1991) using 53 children aged between 5 months to 14 years, 7 (13%) made up of 4 boys and 3 girls, reported calcification of the entire LA during a routine CT examination. Wimpfheimer et al. (1996) also studied the same phenomena in 402 adults comprising of 214 women (53%) and 188 men (47%) aged between 18-97 years and reported calcification of LA as a common finding, and its frequency increased with age. Results from my study showed calcification and fibrosis at the core of human LA

obtained from 3 cadaveric females aged between 90 to 97 years old. This agrees with the findings by Wimpfheimer et al. (1996).

Knowledge of juvenile calcification/fibrosis in the LA is essential to avoid wrongful diagnosis of patients or children with mediastinal pathology. Further analysis of whether bodies used had other underlining cardiovascular disease such as atherosclerosis leading to calcification in the LA was not the focus of the present study, therefore, this was not addressed by further investigation.

This general morphology of the LA held true for all species used in the study. No difference was seen in morphology in term of gender or age. In the human samples for example, the tunica media in the oldest bodies aged 97 years still had the presence of VSMC and this confirms that the VSMC found in the LA is present until senescence. In line with the hypothesis, this confirms that there is the retainment of some of the muscular elements in the ductus arteriosus after it becomes the LA.

The ability to expand within an acceptable range and recoil are important mechanical properties of vessels in the performance of their basic role within the body (Fratzl 2008). Based on the premise of it being a structure that serves as a passage way for blood in vivo, the mechanical function of the LA was studied by authors such as Durst-Zivkovic 1972, Garcia 1975, Hayek 1935 and they all reported its ability to exhibit the mechanical properties of vessels reported by Fratzl in 2008. In 1986, Dohr et al. also studied the mechanical properties of LA by subjecting cadaveric human samples to a tensile test. He described the LA as a structure with viscoelastic properties. Dobrin in 1978 also alluded on the vital role played by the amount and orientation of collagen and elastin fibers on the passive mechanical properties of arteries. These two fiber systems, collagen and elastin, have direct effect on vessel stiffness and distension or elasticity respectively (Kielty et al. 2002, 2005, 2007). Using TEM, Elastica van Gieson and Masson Goldner special histological stainings, I studied the localization of these two proteins. The study reported the presence of collagen and elastin fibers in varied amounts and running in different orientations, which were in agreement with report from Dobrin (1978).

To a large extent, the biological physiology of collagen within vessels lies in its ability to have a viscoelastic response by providing a certain degree of stiffness and resistance while allowing for some degree of elasticity to withstand tensile forces (Fratzl 2008). Secreted by fibroblasts as procollagen, collagen is the most common fibrous protein in the ECM.

Fibrils usually come together to form the collagen fibers. There are numerous collagen types found within the human body, however within muscular and small arteries mainly types I and III and to a lesser extent IV, V and VIII are usually found with unique differences in their distribution and orientation (Barnes and Farndale 1999, Holzapfel 2008). Ultrastructural results from our study indicated that the collagen found within the LA was mainly the type I. This finding though new, agrees with previous literature reporting the presence of type I collagen in vasculature in other body regions (Keene et al. 1987, Miller et al. 1991). The structural arrangement of collagen fibrils in longitudinal and circumferential orientation within arteries gives collagen the ability to respond to stress or strain both in the circumferential and axial directions and accounts for its resilient nature (Piez and Miller 1974). This is crucial for the provision of tensile strength and ultimate determination of its mechanical properties. For the first time, results from the TEM revealed cross-sectional profiles of longitudinal collagen bundles scattered within the LA. Another population of circumferential collagen bundles was also visible in the vicinity of the longitudinal sectional profiles. Though physiologically they are a significant part of basic vessel structure, their role in pathological conditions such as hypertension, atherosclerosis etc. or remodelling of vessel wall cannot be overemphasized (Wang and Chesler 2012). Collagen I has also been implicated in luminal thickening and plaque formation (Koyama and Reidy 1998).

Elastin, another key protein of the ECM, often works in conjunction with collagen. The co-existence of collagen and elastin fibers gives rise to the nonlinear mechanical properties that are central to their mechanical function typically in vessels (Pearce and Thomsen 2000). Results from the TEM of LA showed elastin fibers often in close proximity to collagen fibrils or in the vicinity of collagen fibrils and this agrees with report from Pearce and Thomsen (2000). Elastin's elastic property allows for a considerable amount of tolerance for stress and strain.

Generally, elastin fibers are found in all three layers of blood vessel, though with distinct roles and in varying amounts. For example, the elastin found separating the endothelium and the tunica media, referred to as the internal elastic lamina (IEL), plays a role in elasticity and recoil to the vessel wall. It also functions as a barrier to prevent the entry of macromolecules and cells into the intima as this has been implicated in intimal thickening (Gonzalez et al. 2005, Sims et al. 1993). The results from my study reported an intact IEL in the pulmonary trunk.

This was contrary to what was observed in the LA. The IEL in the LA, though present was fragmented. In the pulmonary trunk, the tunica intima was easily distinguished from the tunica media due to the presence of the IEL and endothelial cells, whereas in the LA, the two layers were distinguished based on the cell types observed.

Generally, in the tunica media, elastin is concentrically arranged as lamellar or layered unit alternating with successive layers of VSMC (Glasgov and Wolinsky 1964, Pease and Paule 1960). This is significant in adaption of wall tension and the number of the lamellae is dependent on lumen size and type of vessel. Comparatively, there is usually less elastic lamellae in the tunica media of muscular arteries than in elastic arteries (Glasgov and Wolinsky 1964). In the pulmonary trunk results from my study agreed with the report by Glasgov and Wolinsky (1964) and Pease and Paule (1960). On the contrary, the lamellae found within the tunica media of the LA had the same fragmented appearance as had been observed for the IEL. Additionally, they were usually found anchored to the plasma membrane of VSMC. Briones et al. (2003) and Wong and Langille 1996) both reported that elastin is autofluorescent in the range of 488 nm and it can be detected in arteries of rats and rabbits after other fluorescent components have been eliminated. The present study agrees with the above assertion as blue autofluorescence was observed in frozen mouse sections of paraformaldehyde-fixed LA samples when it was excited at 360-370 nm wavelength. The autofluorescence revealed fragmentation of both the IEL and elastin lamellae. Fragmentation could be due to ageing or pathologies like atherosclerosis. The results from this study did not provide information on the effect of IEL or lamellae fragmentation observed in the LA. Further studies into the implication of the fragmentation could be explored. Comparatively, this is contrary to the intact IEL and elastic lamellae found in the pulmonary artery.

The tunica adventitia provides a limiting barrier, protecting the vessel from overexpansion as well as providing an area of transition between vessels and surrounding tissue (Pearce and Thomsen 2000). Additionally, scientific reports have associated the regulation of vessel morphology and physiology through autocrine and paracrine signaling mechanisms with the adventitia (Di Wang et al. 2010).

In the tunica adventitia, a collection of lose collagen–rich connective tissue, fibroblasts, nerves and elastin fibers are usually present (Pearce and Thomsen 2000). This anchors the vessel to nearby organs providing stability. The result from the study agrees with this report

as the presence of elastin, nerves and fibroblasts embedded in adipocytes were observed in the adventitia of the LA. This gives further data to the conclusive evidence by our study that the LA indeed retains some embryonic originality of the ductus arteriosus.

Located along the aortic arch is also the presence of peripheral chemoreceptors referred to as aortic bodies. Most are located above the aortic arch (Ahluwalia et al. 2013), whereas a much lesser population are located on the posterior side of the aortic arch between it and the pulmonary artery below (Kazemi et al. 2002). Aortic bodies measure changes in oxygen, carbon dioxide, and pH (Balcombe et al. 2007, Prabhakar et al. 2016). For the first time, in 4 out of 10 human samples from my study, aortic bodies were observed in the tunica adventitia layer of the LA. It is recommended that the implications for this finding may be explored in future experiments.

The mechanical properties of the LA are also determined by both cellular elements and ECM. Structurally, the ECM provides support to cells and the complexity and variance in composition is generally dependent on the cell type or state (Brown and Badylak 2014). There are numerous cells responsible for the production of ECM and the maintenance of its composition and structure. However, our project focused on fibroblasts and myofibroblasts cells. Fibroblast, myofibroblasts and telocytes were reported by the results of the study. No known publication has reported this in the LA. Fibroblasts are one of the most abundant ECM maintaining cells (Kishimoto et al. 2016). Though present in multiple systems with varying roles, the morphology is unvaried except under stress, injury or pathology which triggers an adaptation response through dispatch of specific signals, excessive production of fibers (collagen) and cell modification or dysregulation (Stenmark et al. 2006). One of the well-described fibroblasts modifications is its transformation into myofibroblasts, which has a trait of both fibroblast and smooth muscle cell (Schmidt et al. 2003). In certain cases, myofibroblasts may be present in healthy tissues (Darby and Hewitson 2007).

Our study revealed fibroblasts as well as myofibroblasts mainly within the tunica adventitia, though they were not as numerous as the myocytes found within the tunica media. It is difficult to conclude that the presence of myofibroblasts in the LA is indicative of mechanical stress, since myofibroblasts may be present in healthy tissues (Darby and Hewitson 2007).

Fibroblasts were always surrounded by bundles of collagen running in varied directions. From literature, it could be postulated that the collagen produced by fibroblasts plays a role in reasonable stiffness of the LA (Yeung et al. 2005).

In the 1900s, peculiar cells within the intestitium considered relevant to heart beat regulation and implicated in gut motility and neurotransmission were discovered by the Spanish neuroscientist and pathologist Santiago Ramón y Cajal (Cajal 1911). These cells were named the interstitial cells of Cajal (ICC) or interstitial neurons and were generally found sandwiched between gut smooth muscle cells and their nerve endings. Further on, peculiar cells with similar features to ICC were identified within and outside the gastrointestinal musculature and were named interstitial Cajal-like cells (ICLC) (Faussone-Pellegrini 1977, Thuneberg et al. 1982). Numerous researches in this area revealed a distinction in features between ICC and ICLC and in 2010, Popescu renamed ICLC as telocytes based on their extremely long prolongations (Popescu and Faussone-Pellegrini 2010). Generally, telocytes are ultrastructurally characterized by a small cell body and very long processes that are called telopodes with alternating regions of thin segments (podomers) and thick bead-like portions (podoms, Faussone-Pellegrini and Popescu 2011, Popescu and Faussone-Pellegrini 2010). These cells can range from several tens to hundreds of micrometres in length and form junctions with a number of cells (Popescu and Faussone-Pellegrini 2010, Popescu and Nicolescu 2013, Xiao et al. 2013). Since their discovery, numerous roles such as ensuring that connective tissues within organs are properly organized through mechanical support, enhancement of cell to cell communication between smooth muscle cells, microvessels, immune cells and nerve bundles, through either direct cell to cell contacts or paracrine signaling pathway, have been attributed to them (Faussone-Pellegrini and Popescu 2011, Pieri 2008, Kondo and Kaestner 2019).

Numerous studies have revealed the presence of telocytes with similar ultrastructural and phenotypic characteristics in many organs (Chen et al. 2013, Yang et al. 2014, Zheng et al. 2011) and this led to the assumption that telocytes may exist in all organs. However, to the best of our knowledge, the existence of telocytes in the LA has not yet been reported and this study provides the first demonstration that telocytes exist in mouse and pig LA. The present ultrastructural study revealed the existence of telocytes and their long thin telopodes with alternating regions of podomers and podoms in mouse and pig LA.

Spindle and irregularly shaped cell bodies were observed with small amounts of cytoplasm around them. Our data confirmed the existence of telocytes in the LA of mice and pigs and agreed with the diagnostic criteria for telocytes suggested by Popescu and Faussone-Pellegrini (2010). The present study observed telocytes in close proximity to elastin and collagen fibers and may be postulated to be involved in the remodeling, regeneration and repair of the interstitial tissue of the LA. These findings are in line with previous studies that reported the presence of telocytes in close proximity to collagen and elastic fibers and its involvment in remodeling, regeneration and repair (Ceafalan et al. 2012, Rusu et al. 2012). Additionally, results from the study revealed telocytes in close proximity to nerve terminal bundles and micro-vessels. Its role in smooth muscle contraction or modulation of neurotransmission within the LA may only be postulated based on data published by Cretoiu et al 2015), proving the presence of T-type calcium channels in telocytes which was implicated in myometrium contractions regulation. Though the current data may offer new insights for understanding the function of the LA, further research into the role of the telocytes within the LA is recommended.

4.3 Myocyte of the LA

VSMC makes up the majority of cells making up the tunica media layer of blood vessels. This layer makes up the bulk of vessel wall in arteries and is usually made up of mono-nucleated spindle shaped cells. Its role in determining vessel wall thickness, regulating vessel diameter, differentiating arteries from veins and maintenance of vessel tone cannot be overemphasized (Tucker et al. 2021). Alpha smooth muscle actin is expressed in VSMC (Abberton et al. 1999). Immunofluorescence staining using antibodies against αSMA showed reactivity throughout the whole LA. No known publication has reported immunostaining of LA with antibodies against αSMA. The reactivity was intense and supported my results from earlier H&E, Masson Goldner and Elastica Van Gieson stainings.

Ultrastructural studies of the ductus arteriosus by Kim et al. (1993) in foetal and neonatal rabbits reported the presence of smooth muscle in the ductus arteriosus. In comparism with the myocytes found in the aorta, they appeared more differentiated the study concluded. For the first time in the LA, results from TEM of wild-type mice and pigs confirmed and supported the presence of myocyte in the LA. About 80% of the myocytes found within the tunica media of the LA in both mice and pigs had the typical morphology of contractile

smooth muscle cells. A lesser population were more of synthetic smooth muscle cell-type than contractile in nature, which agrees with the report by Kim et al. (1993). There was the presence of a single nucleus with a prominent nucleolus. I also observed caveoli, the membrane indentations which supply calcium ions by sequestration from the extra-cellular fluid. The caveoli in pigs were more pronounced than that in mice. Again, the presence of myofilaments, with role integral for muscle contraction was found within the cytoplasm. Furthermore, cellular organelles such as mitochondria and rough endoplasmic reticulum were observed. Myocytes observed had the presence of dense bodies within the cytoplasm and dense bands, providing anchorage to contractile proteins, present at the cell margins of the plasma membrane. There was the formation of coupling cell junctions between adjacent myocytes and their closely aligned dense bands. Statistically, the difference in length and width of dense bands within the pulmonary trunk in comparism to the ones within the LA was significant. There were areas with extracellular elastin abutting the dense bands and these regions usually appeared more pronounce. The relevance of dense bands in enhancing the mechanical properties of VSMC through force transference from the contractile apparatus to the stroma of tissue has been extensively studied (Gabella 1983, Pease and Mol-Inari 1960). The contractile role of vascular smooth muscle has also been extensively studied. A study by Bond and Somlyo 1982 described the contractile unit in VSMC to consist of dense bodies, the thick and thin myofilaments. These features constituting the contractile unit were all present in the smooth muscle cell observed in this study. Furthermore, the presence of dense bands which are believed to enhance mechanical and contractile ability of VSMC was also observed in this study. As described by Galen in his *De usu partium*, the two elastic vessels (aorta and pulmonary trunk) are held together by the LA. It is fact that the LA no longer serves in its original capacity as a foetal shunt connecting the two great vessels. Results from this study reports the presence of contractile smooth muscle long after its obliteration and it may be postulated that the contractile abilities of the LA may act on the two great vessels to which it is attached thereby causing a change in their distensibility. It remains to be determined in future studies whether LA might influence impedance/compliance of the vascular segments to which it is attached, which are the best prognostic parameters for patient survival in pulmonary hypertension (Hunter et al. 2008).

4.4 General innervation and neurochemistry of LA

4.4.1 The LA is innervated

Innervation of the fetal ductus arteriosus has been described early. On a macroscopic level, such fibers reach the ductus via the vagus nerve and branches originating from the thoracic sympathetic chain (Boyd 1941). Either of these pathways may carry sensory (vagal or spinal) or autonomic efferent (parasympathetic or sympathetic) fibers. Although contractile properties and their potential control by sympathetic fibers have been mentioned (Aronson et al. 1970), presumed sensory functions have received more attention. Their role has been speculated as being concerned in reflexes which aid in fetal blood pressure control, in particular serving a depressor function (Boyd 1941, Gavrilov 1958). In line with this assumption, the nerve fibers still found in that region in the early postnatal period were considered as continuing this depressor function until the baroreceptors of the aortic arch have taken over (Gavrilov 1958).

The present study, however, demonstrates an extensive innervation of the LA in adult animals (mice and pigs) and in senescent humans, which cannot be explained alone by maintaining a sensory function in early postnatal life. This finding was validated by three independent methods, i.e. immunolabeling with an antibody directed against a general neuronal marker protein (PGP9.5), fluorescence microscopical evaluation of a reporter mouse strain genetically modified to express a fluorescent protein in all autonomic and some additional sensory neurons (*Chnra3*-GFP), and, finally, TEM. All these techniques validated that the LA itself receives nerve terminals rather than just representing a guide rail for nerve fibers passing by to reach the heart. Such preterminal fibers are grouped in bundles and separated from the surrounding tissue by, at minimum, a perineurial sheath. Clearly, such nerve fiber bundles were also seen in the outer adventitia of the LA and in the nearby surrounding, but they will not be considered further here.

Axons controlling vascular smooth muscle are incompletely covered by Schwann cell cytoplasm and exhibit local enlargements (“varicosities”) packed with synaptic vesicles (Luff 1996).

Nerve fibers found at the medio-adventitial border of the LA fully shared these characteristics at the ultrastructural level, and a beaded, varicose appearance of fibers was also clearly visible in fluorescence microscopy both in the reported mouse strain and in

PGP-immunolabeling. TEM revealed that about 30% of all terminals were less than 1 µm away from smooth muscle cells in the LA, which clearly differs from elastic arteries, where the distance between autonomic terminals and smooth muscle cells is rarely less than 1 µm (Cowen 1984, Luff and McLachlan 1988). In small arteries, vesiculated axonal swelling can establish distinct neuromuscular junctions with smooth muscle cells. Defining criteria of such neuromuscular junctions are: 1. The two membranes (axonal and muscular) are separated by only 50-100 nm. 2. The basal laminae of the axon and the smooth muscle cell are fused and form a single lamina between the axon and the muscle cell. 3. Synaptic vesicles are aggregated towards the prejunctional membrane (Luff 1996). Not all axons establish such neuromuscular junctions, and varicose swellings at some distance also release transmitters which reach the target cells by diffusion. The proportion of varicosities that form junctions has been investigated by ultrastructural serial sectioning in a number of different blood vessels, and, as a rule of thumb, a high proportion (>70%) of neuromuscular junctions is seen in small arterioles, whereas only <50% of varicosities of that type were found in the middle-sized rat tail artery (Luff et al. 1987, Luff et al. 1991, Luff et al. 1995, Luff and MacLachlan 1988). Albeit nearly 20% (15/81) of axon terminals were found closer than 0.5 µm away from myocytes in the murine LA in the present study, they did not show this direct type of contact with fused basal laminae. Thus, neuromuscular units in the LA do neither fully match those of small arterioles, nor those of elastic arteries, but a rather similar to muscular arteries. The results of these experiments suggested that the LA is clearly not a passive structure. It is an active structure with the dense innervation.

4.4.2 Neurochemistry of LA innervation

To get some clues as to the potential function of LA innervation, its equipment with transmitter synthesizing enzymes and neuropeptides was investigated by various means. Small-sized, fast acting and short-lived transmitters, such as NA, ACh and NO, cannot be detected directly by antibodies in tissue sections. Instead, nerve fibers utilizing such transmitters are identified by labelling of their synthesizing enzymes.

In this study, three strategies were used to demonstrate the respective enzymes: 1) Immunohistochemistry served to localize the NA and NO synthesizing enzymes TH and NOS, respectively. 2) Enzyme histochemistry (NADPH-diaphorase reaction) was used as an additional tool to demonstrate NOS activity. 3) A reporter mouse strain expressing GFP under the control of the ChAT promotor (ACh synthesizing enzyme) was used to visualize

cholinergic fibers. These techniques revealed a dense innervation by TH-immunoreactive axons which are considered as sympathetic noradrenergic fibers. In contrast, neither cholinergic nor nitrergic nerve fibers were observed in the LA. Although some postganglionic sympathetic neurons do utilize ACh and/or NO rather than NA as transmitter, such non-noradrenergic sympathetic neurons supply other targets e.g. sweat glands, airways, periosteum (Bataille et al. 2012, Francis et al. 1997, Kummer et al. 1992) than blood vessels. Parasympathetic perivascular neurons are cholinergic and/or nitrergic (Dey et al. 1993, Hoyle et al. 1996, Kummer et al. 1992, Van Geldre and Lefebvre 2004), and if neither of these enzymes can be observed, it may be assumed that parasympathetic fibers are not present. Thus, it is reasonable to assume that the LA receives a well-developed sympathetic, but no parasympathetic innervation. In this aspect, it is principally comparable to the thoracic aorta (Morris and Gibbins 1990), although the innervation density of the LA was much higher than in the adjacent aortic arch. With respect to a parasympathetic innervation of the adjacent bifurcation region of the pulmonary trunk and the proximal pulmonary arteries, marked species differences have been reported (Kummer 2011). For the first time, the present study revealed much higher general sympathetic innervation density of the LA at this location but not cholinergic and/or nitrergic fibers.

Sympathetic perivascular axons often utilize the neuropeptide NPY as a co-transmitter (Morris and Murphy 1988). Usually, neuropeptides are packed within and released from large dense core vesicles that are structurally and functionally different from the small vesicles containing catecholamines (Marx et al. 1999, Paquet et al. 1996). TEM showed large dense core vesicles together with small synaptic vesicles in axon terminals in the LA. NPY is a vasoconstrictor co-released with NA from sympathetic nerve endings (Fabi et al 1998, Lacroix et al. 1997, Morris and Murphy 1988). Studies on the independent effect of NPY on VSMC reported enhancement of smooth muscle proliferation and mild vasoconstriction (Crnkovic et al. 2014, Edvinsson 1987, Kuo et al 2007).

Other studies reported the potentiation of the constrictive effect of NA when co-localized with NPY in arteries (Edvinsson 1987, Ekblad et al. 1984). For the first time, data from double-immunolabeling with primary antibodies directed against TH and NPY of human, pig and mouse LA from our study revealed independent TH- and NPY-immunoreactivities at the periphery and musculature within nerve fibers present. Mostly, however, there was co-localization of TH- and NPY-immunoreactivities within nerve fibers. This finding agrees with reports from Fabi et al. (1998) and Lacroix et al. (1997) who studied the co-

localization and (or) co-release of NPY and NA in rats, humans and pigs. It can be extrapolated that the LA is innervated by the adrenergic division of the autonomic nervous system and may contract when its α1 adrenoceptors are targeted by pharmacological application.

Further neuropeptides investigated in this study included SP, CGRP and VIP. In general, none of them is specifically expressed in one distinct functional subset of neurons. In vascular innervation, VIP can occur as co-transmitters of cholinergic and/or nitrergic vasodilator axons (Dey et al. 1993, Hoyle et al. 1996, Kummer et al. 1992, Van Geldre and Lefebvre 2004) which are usually of parasympathetic origin. Such innervation is particularly found around cranial and pelvic vessels (Morris 1990). Consistent with the lack of cholinergic and nitrergic fibers in the LA, there was no immunoreactivity when the LA in all the species understudied were incubated with primary antibodies directed against VIP or nNOS.

Generally, CGRP, a neuropeptide with active roles in nociception, also possesses vasoactive properties, and often co-exists with the tachykinin SP in a subclass of sensory neurons that targets blood vessels (Kusakabe et al. 1995, Lundberg et al. 1985). Such fibers have the peculiar property that, upon stimulation, they not only convey this information to the CNS, but they also release these neuropeptides into their surrounding (local effector function of sensory neurons: Holzer and Maggi 1998). In arterial vasculature, CGRP released from nociceptive C-fibers, decrease blood pressure through VSMC relaxation leading to vasodilatation (McEwan et al. 1988, Schlereth et al. 2016). SP has been reported to increase vascular permeability ultimately leading to extravasation (Leis et al. 2003). For the first time, my study reported immunoreactivities when the LA of human, pig and mouse were incubated with primary antibodies directed against SP and CGRP. Some fibers were solely SP- or CGRP-positive. Comparatively, SP-immunoreactive fibers were lesser than CGRP fibers. Additionally, there was co-localization of SP- and CGRP-immunoreactivities within fibers. Results from TEM also were also consistent with the presence of sensory terminals containing neuropeptides within the LA illustrated by observation of large dense core vesicles in the nerve terminals. Vesiculated nerve terminals were either made up of only dense core vesicles or a mixture of both dense and clear core vesicles. As described in detail above, occurrence of both types of vesicles is a characteristic feature of autonomic efferent terminals.

On the other hand, peptidergic sensory terminals contain nearly exclusively large dense core vesicles, with SP and CGRP co-stored within the same vesicle (Kummer et al. 1989). Hence, axon profiles with mainly large dense core vesicles may represent the SP/CGRP-positive fibers identified by immunolabeling. Collectively, our data indicates that the perivascular fibers found in the LA are not only adrenergic but some are peptidergic sensory fibers which may have a dual role as local regulators of muscle tone and carriers of sensory information.

Conceivably, these results imply that the LA is innervated and this is not only by the adrenergic division of the autonomic nervous system but receives further innervation from some sensory fibers with peptides operating as NANC neurotransmitters. The dense sympathetic and presumably sensory innervation could influence impedance/compliance of the vascular segments to which it is attached. Notably, this has been reported to be the best prognostic parameter for patient survival in pulmonary hypertension (Hunter et al. 2008).

4.5. LA response to electrical field stimulation and adrenergic drugs

4.5.1 Force generated on LA by EFS

Electrical field stimulations are applied to stimulate nerve terminals to evoke local release of transmitters (Angus et al. 1988). Stimulation may also induce a nerve-independent vasoconstriction through direct activation of smooth muscle (Jongejan et al. 1989). To avoid this, it is essential to use a short pulse width (0.7–5 ms), which has been reported to selectively stimulate nerves but not smooth muscle (Tomita 1970). Smooth muscle requires a much longer pulse width (60–133 ms) for direct excitation (Tomita 1970). For the first time, and also in agreement with our hypothesis 3, our study reported reproducible EFS-induced contractions and spontaneous relaxation afterwards of the pig LA. The LA was stimulated with a pulse width of 2 ms, which makes nerves the focus of our stimulation. This is in agreement with Tomita's report during his investigation into electrical responses in guinea-pig taenia coli (Tomita 1970). In both treatment and control samples, EFS-induced contractions were frequency-dependent. A greater tension was produced at 32 Hz and the difference between the maximal forces generated was statistically significant in comparison with the maximal force generated at 8 Hz.

The results of these experiments suggested that the direct stimulation of LA by EFS induces isometric tension resulting from the stimulation of the nerves to release their vesicular products and this ultimately results in contraction of the muscular elements within the LA of pigs even in the absence of pharmacological agent administration. It also confirms that the muscular elements found within the LA are controlled by this innervation, which is in agreement with hypothesis 3. Preliminary data revealed a decrease in subsequent isometric tension generated by EFS on the LA upon the administration of α1 adrenoceptor antagonist. Further investigation into this, as well as the effect of the neurotoxin tetrodotoxin (TTX) on isometric force generated by EFS on the LA and their implications in LA functionality is highly recommended.

4.5.2 Force generated on LA by noradrenergic agonist and antagonist

In vasculature, force-producing smooth muscle cells sensitive to pharmacological agents lie within the media and the response of the vessels to drug actions depends on various factors such as muscle layer thickness, densities of different receptors and activities of second messenger systems. Furthermore, isometric tensions developed within VSMC are organ and region specific (Mulvany 1984, Murphy et al. 1974). VSMC are mainly innervated by noradrenergic fibers. TH-immunoreactivity was identified in the nerve terminals of humans, pig and mice LA by immunofluorescence labeling, indicating an involvement of the noradrenergic division of the autonomic nervous system in LA innervation. Based on this analogy, the question is whether or not the LA will contract when its α1 adrenoceptors are targeted by pharmacological application. For the first time, and also in agreement with hypothesis 3, our study reported dose dependent contraction of pig LA upon subjection to cumulative doses of exogenous noradrenalin.

This agrees with a report by Hennenberg et al. (2017), who reported the vital role played by α1-adrenoceptors in vasoconstriction. Vasodilatory effects were observed upon the administration of cumulative doses of α1 antagonists prazosin and tamsulosin on NA-induced precontracted LA. Precontracted LA was relaxed to baseline. Selective alpha antagonists have been reported to block type 1 alpha-adrenergic receptors and thus inhibit smooth muscle contraction. Prazosin and tamsulosin are classical examples of such selective alpha antagonists (Ko et al. 1994).

Generally, pulmonary hypertension may have various pathophysiologies. Its etiology may originate from a dysfunction within the heart, lungs, high blood pressure or loss in

compliance (windkessel effect) within the elastic vessels associated with pulmonary circulation (Hoeper et al. 2017). Impedance/compliance of the pulmonary trunk and arteries has been reported to be the best prognostic parameter for patient survival in pulmonary hypertension (Hunter et al. 2008). Parameters that determine this compliance are muscle contraction and the mechanical properties of the vessel wall. Both are under the control of the sympathetic nervous system. The present findings point to a further mechanism that might control distensibility of the pulmonary bifurcation region, i.e. tension produced by the contracting LA. Notably, the present findings demonstrate that this is also under sympathetic control. Further, Mckenzie and Klein reported a substantial influence of the sympathetic nervous system on collagen increase within the pulmonary trunk and arteries in chronic hypoxia (Mckenzie and Klein 1984). Collagen accumulation and (or) increase has been implicated in pulmonary trunk remodeling and pulmonary artery stiffening, which are classical features of pulmonary hypertension (Wang et al. 2013). Remodelling of the LA itself might also have impact on the pulmonary trunk to which it is attached, thereby also having an impact on impedance. It remains to be determined whether such trophic effects are also operative in the LA. A "first-in-man" clinical study demonstrated that acute denervation at the level of pulmonary trunk bifurcation, not more distally, significantly improved clinical parameters of patients, whose pulmonary hypertension may not be sufficiently controlled with pharmacotherapy (Chen et al. 2013), highlighting the clinical relevance of the innervation of this region. My present experiments showed that α1-adrenoreceptors are involved in the sympathetic regulation of tension in the pig LA. This was evident by the selective blockade by antagonistic agents such as prazosin and tamsulosin. Based on this premise, it may be hypothecated that this could provide a relevant approach to potential future treatments of pulmonary hypertension.

4.6 Conclusion

Taken together, the results of the present study demonstrate that LA is not a mere band of fibrosed tissue but an innervated, contractile muscular structure. It may be speculated that the contractile abilities of LA myocytes may act on the two great vessels to which it is attached causing a change in their distensibility and the dense innervation could influence impedance/compliance (reported to be the best prognostic parameter for patient survival in pulmonary hypertension, Hunter et al. 2008) of the vascular segments to which it is attached. However, the intricate functional consequence of the presence of contractile smooth muscle and substantive innervation remains to be demonstrated.

5 Summary

Ductus arteriosus is a muscular artery in foetal circulation, which spans from the bifurcation of the pulmonary trunk to the aortic arch, shunting blood from pulmonary circulation directly into systemic circulation thus by-passing the fluid-filled lungs. Postnatally, it becomes the ligamentum arteriosum (LA) upon physiological closure within hours which precedes later anatomical closure. Though the LA has generally been considered as a fibrosed remnant, rupture of the aortic arch in certain blunt trauma conditions indicates that it still has mechanical impact on both the pulmonary bifurcation and the aortic arch. Significant evidence reports autonomic nerve fibers and baroceptive apparatus within the ductus arteriosus in-utero, whereas for the LA, reports are anecdotal and contradictory. We hypothesized the likelihood of the retainment of contractile muscular elements functioning under nervous control in this so-called ligament. To investigate this, mediastinum of wild-type mouse, two transgenic reporter mice strains, pig and human LA were subjected to routine and special histological staining, single- and double-immunolabeling, enzyme histochemistry (mouse), electron microscopy (mouse and pig only), and tension recording of explanted pig LA in organ bath. Contrary to a canonical ligament, the LA was mainly made up by α-smooth muscle actin-positive cells in all three species, this was confirmed by electron microscopy. The presence of collagen, elastin and telocytes were also observed. In reporter mice, a noticeable amount of *chrna3*-eGFP-positive fibers concentrated at its points of attachment to the great vessels were observed. Cholinergic innervation was absent. In all experimental species, PGP 9.5- (neuronal marker), TH-, NPY-, SP-, and CGRP-positive fibers were observed in close proximity to smooth muscle cells, however there were no vasoactive intestinal peptide- and neuronal NO synthase (nNOS)-positive fibers. Absence of nNOS-immunoreactivity was confirmed by NADPH-diaphorase reaction. Myocytes found within the LA contracted in response to electrical field stimulation and exogenous noradrenalin (NA). NA-induced precontracted LA relaxed upon administration of α1-adrenergic blockers. Though the LA does not function in its original capacity as a fetal shunt, it is clearly not a passive structure. It may be described as a densely innervated contractile smooth muscle structure. The contractile abilities of LA myocytes may act on the two great vessels to which it is attached causing a change in their distensibility. Also, the dense innervation could influence impedance/compliance of the pulmonary trunk, which has been reported to be the best prognostic parameter for patient survival in pulmonary hypertension.

6 Zusamenfassung

Der Ductus arteriosus leitet im fetalen Kreislauf das Blut vom Truncus pulmonalis an der Lunge vorbei zum Aortenbogen direkt in die systemische Zirkulation. Postnatal schließt er sich zunächst funktionell innerhalb von Stunden, später auch strukturell, und wird so zum Ligamentum arteriosum (LA). Obwohl das LA generell als fibröse Reststruktur gesehen wird, zeigen Risse des Aortenbogens bei bestimmten Traumata, dass es weiterhin mechanische Auswirkungen auf Pulmonalarterie und Aortenbogen hat. Der Ductus arteriosus ist in-utero durch autonome und barorezeptive Nervenfasern innerviert, wohingegen für das LA nur anekdotische und gegensätzliche Beschreibungen zur Innervation vorliegen. Wir stellten die Hypothese auf, dass in diesem sogenannten Ligament weiterhin kontraktile muskuläre Elemente vorliegen und durch Nerven kontrolliert werden. Untersucht wurden das Mediastinum von Wildtypmäusen und zwei transgenen Reportermausstämme sowie das LA vom Schwein und Menschen mit histologischen Färbungen, Einfach- und Doppel-Immunfluoreszenzmarkierungen, Enzymhistochemie (Maus), Transmissionselektronenmikroskopie (Maus und Schwein) und die Kontraktionsfähigkeit des explantierten Schweine-LA im Organbad. Im Gegensatz zu einem kanonischen Ligament bestand das LA in allen Spezies weitgehend auf glattmuskelaktin-positiven Zellen; Elektronenmikroskopie bestätigte das Vorliegen glatter Muskelzellen. Das LA enthielt auch Collagen, Elastin und Telozyten. In den Reportermausstämmen zeigten sich *chrna3*-eGFP-positive Fasern mit Konzentration an den Ansatzstellen des LA an den großen Gefäßen, aber keine cholinergen Fasern. In allen Spezies zeigten sich an den glatten Muskelzellen PGP 9.5- (neuronaler Marker), Tyrosinhydroxylase-, NPY-, SP- und CGRP-positive Fasern, jedoch keine mit VIP- und NO-Synthase-Immunreaktivität; letzteres wurde durch NADPH-Diaphorase-Reaktion bestätigt. Das LA kontrahierte auf elektrische Feldstimulation und exogen gegebenes Noradrenalin (NA). Durch NA präkontrahiertes LA relaxierte auf Gabe von α1-adrenergen Blockern. Obwohl das LA nicht mehr als Shunt fungiert, ist es dennoch eindeutig keine passive Struktur, sondern ein dicht innervierter kontraktiler Muskel. Diese Kontraktion könnte sich auf die großen Gefäße, zwischen denen es ausgespannt ist, auswirken und deren Dehnbarkeit beeinflussen, dies unter nervaler Kontrolle. Bemerkenswerterweise ist diese Dehnbarkeit/Compliance des Truncus pulmonalis der beste prognostische Parameter für das Überleben von Patienten mit pulmonaler Hypertension.

7 List of abbreviations

Acetylcholine	ACh
Acetylcholinesterase	AChE
Adenosine triphosphate	ATP
Alpha smooth muscle actin	αSMA
Aromatic L-amino acid decarboxylase	AADC
Bacterial artificial chromosome	BAC
Calcitonin gene-related peptide	CGRP
Choline acetyltransferase	ChAT
Computed tomography	CT
Cyanine 3	Cy3
Cyclic adenosine monophosphate	cAMP
4-Dihydroxyphenylalanin	L-DOPA
Dimethyl sulfoxide	DMSO
Distyrene plasticizer xylene	DPX
Dopamine-beta-hydroxylase	DβH
Enhanced green fluorescent protein	eGFP
Enteric nervous system	ENS
Extracellular matrix	ECM
Fluorescein isothiocyanate	FITC
G protein-coupled receptors	GPCRs
Green fluorescence protein	GFP
Haematoxylin and eosin	H&E

List of abbreviations cont'd

Internal elastic lamina	IEL
Interstitial Cajal-like cells	ICLCs
Interstitial cells of Cajal	ICC
L-Amino acid decarboxylase	AADC
Ligamentum arteriosum	LA
Minimum essential medium	MEM
Muscarinic acetylcholine receptor	mAChR
Neuronal nitric oxide synthase	nNOS
Neuropeptide Y	NPY
Nicotinamide adenine dinucleotide phosphate	NADPH
Nicotinic acetylcholine receptor subunit alpha-3	nAChRα3
Nicotinic acetylcholine receptor	nAChR
Nitric oxide	NO
Non-adrenergic and non-cholinergic	NANC
Noradrenalin	NA
Optimal cutting temperature	OCT
Paraformaldehyde	PFA
Peptide histidine isoleucine	PHI
Peptide histidine methionine	PHM
Peripheral nervous system	PNS
Phenylalanine Hydroxylase	PH
Phenylethanolamine-N-methyltransferase	PNMT

List of abbreviations cont'd

Phenylethanolamine-n-methyltransferase	PNMT
Phosphate buffered saline	PBS
Protein gene product 9.5	PGP 9.5
Platelet-derived growth factor receptor	PDGFR
Standard error of mean	SEM
Substance P	SP
Tetrodotoxin	TTX
Transmission electron microscopy	TEM
Tyrosine hydroxylase	TH
Vascular smooth muscle cell	VSMC
Vasoactive intestinal peptide	VIP

8 References

Abberton K, Healy D, Rogers P: **Smooth muscle alpha actin and myosin heavy chain expression in the vascular smooth muscle cells surrounding human endometrial arterioles.** *Hum Reprod* 1999, **14(12):** 3095-3100.

Ahlquist RP: **A study of the adrenotropic receptors**. *Am J Physiol* 1948, **153(3)**:586-600.

Ahluwalia N, Owens RL, Badr S, Malhotra A: **Sleep and the Control of Breathing**. *Ency of Sleep* 2013, Kushida, Clete A. (ed.), Waltham: Academic Press, pp. 525–532.

Altman JD, Trendelenburg AU, MacMillan L, Bernstein D, Limbird L, Starke K, Kobilka BK, Hein L: **Abnormal Regulation of the Sympathetic Nervous System in α2A-Adrenergic Receptor Knockout Mice**. *Mol Pharmacol* 1999, **56 (1)**:154-161.

Andersson PO.Scand: Vascular control in the colon and rectum. J Gastroenterol 1984, **93**:65-78.

Angus JA, Broughton A, Mulvany MJ: **Role of alpha-adrenoceptors in constrictor responses of rat, guinea-pig and rabbit small arteries to neural activation**. *J Physiol* 1988, **403**:495–510.

Aronson S, Gennser G, Owman C & Sjöberg NO**: Innervation and contractile response of the human ductus arteriosus**. *Eur J Pharmacol* 1970, **11(2)**:178-186.

Balcombe J, Torigian DA, Kim W, Miller WT: **Cross-Sectional Imaging of Paragangliomas of the Aortic Body and Other Thoracic Branchiomeric Paraganglia**. *Am J Roentgenol* 2007, **188 (4):**1054–1058.

Baraniuk JN.J Allergy: **Sensory, parasympathetic, and sympathetic neural influences in the nasal mucosa.** *Clin Immunol* 1992, **90(6):**1045-1050.

Barcroft J, Kennedy JA, Mason MF: **The relation of the vagus nerve to the ductus arteriosus in the guinea-pig.** *J Physiol* 1938, **92**:1.

Barnes MJ, Farndale RW: **Collagens and atherosclerosis**. *Exp Gerontol* 1999, **34(4):**513-525.

Bataille C, Mauprivez C, Haÿ E, Baroukh B, Brun A, Chaussain C, Marie PJ, Saffar JL, Cherruau M: **Different sympathetic pathways control the metabolism of distinct50(5)**:1162-72.

Beluffi G, Rotoli P, Calò L, Tinelli C, Fiori P: **Botallo's duct calcification in children: radiologic findings**. *Radiol Med* 1998, **96(3):**204–208.

Benirschke K, Kaufmann P, Baergen R: **Anatomy and pathology of the umbilical cord. Pathology of the human placenta.** 5th Ed: 2006:380–451. Chap 12.

Bisceglia M, Donaldson JS: **Calcification of the ligamentum arteriosum in children: a normal finding on CT**. *Am J Roentgenol* 1991, **156(2):**351-352.

Blanco-Rivero J, Couto GK, Paula SM, Fontes MT, Rossoni LV: **Enhanced sympathetic neurotransduction in the superior mesenteric artery in a rat model of heart failure: role of noradrenaline and ATP**. *Am J Physiol Heart Circ Physiol* 2021, **320(2)**:H563-H574.

Bond M, Somlyo AV: Dense bodies and actin polarity in vertebrate smooth muscle. *J Cell Biol* 1982, **95(2 Pt 1):**403-413.

Boreus LO, Malmfors T, McMurphy DM, Olson L: **Demonstration of adrenergic receptor function and innervation in the ductus arteriosus of the human foetus**. *Acta Physiol* 1969, **77:**316

Borow KM, Hessel SJ, Sloss LJ: **Fistulous aneurysm of ductus arteriosus**. *Br Heart J* 1981, **45:**467-470.

Boudreau N, Rabinovitch M: **Developmentally regulated changes in extracellular matrix in endothelial and smooth muscle cells in the ductus arteriosus may be related to intima proliferation.** *Lab Invest* 1991, **64**:187–199.

Boudreau N, Turlay E, Rabinovitch M: **Fibronectin,hyaluronan binding protein contribute to increased ductus arteriosus smooth muscles cell migration**. *Dev Biol* 1991, **143**:235–247.

Boyd JD & Mocullagh GP: **Experimental hypertension following carotico-aortic denervation in the rabbit**. *J Exp Physiol* 1938, **27**:293–306.

Boyd JD: **Absence of the Right Common Carotid Artery**. *J Anat* 1934, **68(4):**551-557.

Boyd JD: **The nerve supply of the mammalian ductus arteriosus**. *J Anat* 1941, **75:**457–468.

Brain SD, Williams TJ, Tippins JR, Morris HR, MacIntyre I: **Calcitonin gene-related peptide is a potent vasodilator.** *Nature* 1985, **313(5997)**:54-56.

Bredt DS, Hwang PM, Snyder SH: **Localization of nitric oxide synthase indicating a neural role for nitric oxide.** *Nature* 1990, **347(6295)**:768-770.

Briones AM, González JM, Somoza B, Giraldo J, Daly CJ, Vila E, et al: **Role of elastin in spontaneously hypertensive rat small mesenteric artery remodeling.** *J Physiol* 2003, **552**:185–195.

Brodde OE, Michel MC: **Adrenergic and muscarinic receptors in the human heart**. *Pharmacol Rev* 1999, **51**:651–690.

Brown BN, Badylak SF: **Extracellular matrix as an inductive scaffold for functional tissue reconstruction.** *Transl Res* 2014, **163(4):**268-285.

Cajal SR: **Histologie du système nerveux de l'homme et des vertébrés**. *Par Mal* 1911, **2**:891-942.

Carlson AB, Kraus GP. **Physiology, Cholinergic Receptors**. In: StatPearls. StatPearls Publishing, Treasure Island (FL); 2019.

Cassels DE &. Moore RY: **Sympathetic Innervation of the Ductus Arteriosus in Relation to Patency.** *Chest* 1973, **63(5):**727-731.

Ceafalan L, Gherghiceanu M, Popescu LM, Simionescu O: **Telocytes in human skin–are they involved in skin regeneration**. *Cell Mol Med* 2012, **16**:1405– 1420.

Chen SL, Zhang FF, Xu J, Xie DJ, Zhou L, Nguyen T, Stone GW: **Pulmonary artery denervation to treat pulmonary arterial hypertension: the single-center, prospective, first-in-man PADN-1 study (first-in-man pulmonary artery denervation for treatment of pulmonary artery hypertension).** *J Am Coll Cardiol* 2013, **62(12):**1092-1100.

Chen X, Zheng Y, Manole CG, Wang X, Wang Q: **Telocytes in human oesophagus**. *J Cell Mol Med* 2013, **17**:1506– 1512.

Chiruvolu A & Jaleel MA: **Pathophysiology of patent ductus arteriosus in premature neonates**. *Early Hum Dev* 2009, **85(3):**143–146.

Chuaqui B, Piwonka G, Farru O: "**Uber den Wandbau des persistierenden Ductus arteriosus".** *Arch A Pathol Anat Histol* 1977, **372:**315–324.

Clyman RI, Chan CY, Mauray F, Chen YQ, Cox W, Seidner SR,et al: **Permanent anatomic closure of the ductus arteriosus in newborn baboons: the roles of postnatal constriction, hypoxia, and gestation**. *Pediatr Res* 1999, **45(1):**19-29.

Clyman RI: **Mechanisms regulating the ductus arteriosus**. *Biol Neonate* 2006, **89(4):**330–335.

Coceani F, Baragatti B: Mechanisms for ductus arteriosus closure. *Semin Perinatol*. 2012, **36(2)**:92-97.

Cowen, T: **An ultrastructural comparison of neuromuscular relationships in blood vessels with functional and non-functional neuromuscular transmission.** *J Neurocytol* 1984, **13**:369–392.

Cretoiu SM, Radu BM, Popescu LM: **Isolated human uterine telocytes: immunocytochemistry and electrophysiology of T-type calcium channels**. *Histochem Cell Biol* 2015, **143(1):**83-94.

Crnkovic S, Egemnazarov B, Jain P, Seay U, Gattinger N, Marsh LM, Bálint Z, Kovacs G, Ghanim B, Klepetko W, Schermuly RT, Weissmann N, Olschewski A, Kwapiszewska G: **NPY/Y_1 receptor-mediated vasoconstrictory and proliferative effects in pulmonary hypertension**. *Br J Pharmacol* 2014, **171(16):**3895-3907.

Currarino G, Jackson JH: **Calcification of the ductus arteriosus and ligamentum botalli.** *Radiology* 1970, **94(1):**139–142.

Darby IA, Hewitson TD, **Fibroblast differentiation in wound healing and fibrosis**. *Int Rev Cytol* 2007, **257**:143-179.

de Jonge WJ, van der Zanden EP, The FO, Bijlsma MF, van Westerloo DJ, Bennink RJ, Berthoud HR, Uematsu S, Akira S, van den Wijngaard RM, Boeckxstaens GE. **Stimulation of the vagus nerve attenuates macrophage activation by activating the Jak2-STAT3 signaling pathway**. *Nat Immunol* 2005, **6(8):**844-851.

De Reeder EG, Poelmann RE, Munsteren JC, Patterson DF, Gittenberger-de-Groot AC: **Ultrastructural and immunohistochemical changes of the extracellular matrix during intimal cushion formation in the ductus arteriosus of the dog**. *Atherosclerosis* 1989, **79:**29–40.

Dey RD, Mayer B, Said SI: **Colocalization of vasoactive intestinal peptide and nitric oxide synthase in neurons of the ferret trachea**. *Neuroscience* 1993, **54:**839– 843.

Di Wang H, Rätsep MT, Chapman A, Boyd R. **Adventitial fibroblasts in vascular structure and function: the role of oxidative stress and beyond**. *Can J Physiol Pharmacol* 2010, **88(3):**177-186.

Ditting T, Hilgers KF, Scrogin KE, Stetter A, Linz P, Veelken R: **Mechanosensitive cardiac C-fiber response to changes in left ventricular filling, coronary perfusion pressure, hemorrhage, and volume expansion in rats**. *Am J Physiol Heart Circ Physiol* 2005. **288(2)**:H541–H552.

Dobrin PB: **Mechanical properties of arteries**. *Physiol Rev* 1978, **58:**397–460.

Dohr G, Ebner I, Gallasch E: **Morphological and biomechanical studies of the ligamentum arteriosum**. *Acta Anat* 1986, **126(2):**97-102.

Dorland WAN: **Dorland"s Illustrated Medical Dictionary**. 25th Edition. Philadephia: W.B. Saunders 1974.

Durst-Zivkovic B: **Einige an das Lig. arteriosum gebundene morphologische Beobachtungen [Various morphological observations of the ligamentum arteriosum].** *Anat Anz* 1972, **132(3):**310-314.

Edvinsson L, Håkanson R, Wahlestedt C, Uddman R: **Effects of neuropeptide Y on the cardiovascular system.** *Trends Pharmacol Sci*. 1987, **8(6):**231–235.

Ekblad E, Edvinsson L, Wahlestedt C, Uddman R, Håkanson R, Sundler F: **Neuropeptide Y co-exists and co-operates with noradrenalin in perivascular nerve fibers.** *Regul Pept* 1984, **8:**225–235.

Everitt BJ, Hokfelt T, Terenius L, Tatemoto K, Mutt V, Goldstein M: **Differential co-existence of neuropeptide Y (NPY)-like immunoreactivity with catecholamines in the central nervous system of the rat.** *Neuroscience* 1984, **11:**443–462.

Fabi F, Argiolas L, Ruvolo G, & Basso P: **Neuropeptide Y-induced potentiation of noradrenergic vasoconstriction in the human saphenous vein: involvement of endothelium generated thromboxane.** *Br. J. Pharmacol* 1998, **124(1):**101–110.

Fagerholm V, Haaparanta M, Scheinin M: **α2-adrenoceptor regulation of blood glucose homeostasis.** *Basic Clin Pharmacol Toxicol 2*011, **108(6)**:365-370.

Faussone-Pellegrini MS, Popescu LM: **Telocytes**. *BioMol Concepts* 2011, **2**:481–489.

Faussone-Pellegrini, M. S., Cortesini, C. and Romagnoli, P: **Ultrastructure of the tunica muscularis of the cardial portion of the human esophagus and stomach, with special reference to the so-called Cajal's interstitial cells**. *Arch Ital Anat Embriol* 1977, **82:**157-177.

Feneis H: **Pocket Atlas of Human Anatomy**. Stuttgart: GeorgThieme Publishers, 1976.

Ferrer-Lorente R, Cabot C, Fernández-López JA, Alemany M: **Combined effects of oleoyl-estrone and a β3-adrenergic agonist (CL316, 243) on lipid stores of diet-induced overweight male Wistar rats.** *Life Sci* 2005, **77(16)**:2051–2058.

Fischer A, Canning BJ, Kummer W: **Correlation of vasoactive intestinal peptide and nitric oxide synthase with choline acetyltransferase in the airway innervation**. *Ann N Y Acad Sci* 1996, **805**:717-722.

Fisher LA, Kikkawa DO, Rivier JE, Amara SG, Evans RM, Rosenfeld MG, Vale WW, Brown MR: **Stimulation of noradrenergic sympathetic outflow by calcitonin gene-related peptide**. *Nature* 1983, **305(5934)**:534-536.

Forsey JT, Elmasry OA, Martin RP: **Patent arterial duct**. *Orphanet J of Rare Dis* 2009, **10(4)**:17.

Frahm S, Slimak MA, Ferrarese L, Santos-Torres J, Antolin-Fontes B, Auer S, Filkin S, et al: **Aversion to nicotine is regulated by the balanced activity of beta4 and alpha5 nicotinic receptor subunits in the medial habenula**. *Neuron* 2011, **70:**522–535.

Francis NJ, Asmus SE, Landis SC: **CNTF and LIF are not required for the target-directed acquisition of cholinergic and peptidergic properties by sympathetic neurons in vivo**. *Dev Biol* 199, **182(1)**:76-87.

Franklin KJ: **Ductus venosus (Arantii) and ductus arteriosus (Botalli).** *Bull Hist Med* 1941, **9:**580-584.

Fransson SG: **The Botallo mystery.** *Clin Cardiol* 1999, **22(6):**434-436.

Fratzl P: **Collagen: Structure and Mechanics, An Introduction**. In: Fratzl P. (eds) Collagen. Boston, MA: Springer 2008. httelopodes://doi.org/10.1007/978-0-387-73906-9_1.

Friedman AH1, Fahey JT: **The transition from fetal to neonatal circulation: normal responses and implications for infants with heart disease**. *Semin Perinatol* 1993, **(2):**106-121.

Furness JB, Papke RE, Della NG, Costa M, Eskay RL: **Substance P-like immunoreactivity in nerves associated with the cardiovascular system of guinea pigs**. *Neuroscience* 1982, **7:**447–459.

Gabella G: **Asymmetric distribution of dense bands in muscle cells of mammalian arterioles**. *J Ultrastruct Res* 1983, **84(1):**24-33.

Garcia OS: **Functional architecture of the ligamentum arteriosum in adults**. *Acta Anat* 1975, **91(2):**313-320.

Gatzsche H: **Congenital Heart Disease**. Copenhagen: Published by the author, 1952

Gavrilov LF: **The nerve supply of the ductus arteriosus in dogs.** *Bull Exp Biol Med* 1958, **46:**862–865.

Gibbins IL, Furness JB, Costa M, MacIntyre I, Hillyard CJ, Girgis S: **Co-localization of calcitonin gene-related peptide-like immunoreactivity with substance P in cutaneous, vascular and visceral sensory neurons of guinea-pigs.** *Neurosci Lett* 1985, **57:**125-130.

Gillispie CC: **Dictionary of Scientific Biography**. *ACLS* 1970, **7**:15.

Gittenberger-de Groot Ac, Strengers JLM, Mentink MPoelmann RE, Paterson DF: **Histological studies on normal and persistent ductus arteriosus in the dog**. *J Am Coll Cardiol* 1985, **6:**394–404.

Gittenberger-de Groot AC, Van Ertbruggen I, Moulaert AJMG, Harinck E: **The ductus arteriosus in the preterm infant: histological and clinical observations.** *J Pediatr* 1980, **96:**88–93.

Glasgov S and Wolinsky H: **Structural basis for the static mechanical properties of the aortic media.** *Circ Res* 1964, **24**:400-413.

González JM, Briones AM, Starcher B, Conde MV, Somoza B, Daly C, Vila E, McGrath I, González MC, Arribas SM: **Influence of elastin on rat small artery mechanical properties.** *Exp Physiol* 2005, **90(4):**463-468.

Greiss FC Jr, Gobble FL Jr, Anderson SG, McGuirt WF: **Effect of parasympathetic nerve stimulation on the uterine vascular bed**. *Am J Obstet Gynecol* 1967, **99(8):**1067-1072.

Groneberg DA, Rabe KF, Fischer A: **Novel concepts of neuropeptide-based drug therapy: vasoactive intestinal polypeptide and its receptors**. *Eur J Pharmacol* 2006, **533(1-3)**:182-194.

Guimarães S, Moura D: **Vascular adrenoceptors: an update**. *Pharmacol Rev* 2001, **53**:319–356.

Hayek HV: **Das Verhalten der Arterien bei Beugung der Gelenke.** *Z Anat Entwickl Gesch* 1935, **105:**25–36.

Hennenberg M, Acevedo A, Wiemer N, Kan A, Tamalunas A, Wang Y, Yu Q, Rutz B, Ciotkowska A, Herlemann A, Strittmatter F, Stief CG, Gratzke C: **Non-adrenergic, tamsulosin-insensitive smooth muscle contraction is sufficient to replace alpha1-adrenergic tension in the human**. *Prostate* 2017, **77**:697-707.

Heymann MA, Rudolph AM: **Control of the ductus arteriosus**. *Physiol Rev* 1975, **55(1):**62–78.

Ho SY, Anderson RH**: Anatomical closure of the ductus arteriosus: a study in 35 specimens.** *J Anat* 1979, **128(4):**829–836.

Hoeper MM, Ghofrani HA, Grünig E, Klose H, Olschewski H, Rosenkranz S: **Pulmonary Hypertension**. *Dtsch Arztebl Int* 2017, **3114(5)**:73-84.

Hokfelt T, Lundberg JM, Lagercrantz H, Tatemoto K, Mutt V, Lindberg J, et al: **Occurrence of neuropeptide Y (NPY)-like immunoreactivity in catecholamine neurons in the human medulla oblongata**. *Neurosci Lett* 1983, **36:**217–222.

Holzapfel G: **Collagen in Arterial Walls: Biomechanical Aspects**. In: Fratzl P. (eds) Collagen. Springer, Boston, MA, 2008.

Holzer P, Maggi CA: **Dissociation of dorsal root ganglion neurons into afferent and efferent-like neurons.** *Neuroscience* 1998, **86(2)**:389-398.

Holzer P, Maggi CA: **Dissociation of dorsal root ganglion neurons into afferent and efferent-like neurons**. *Neuroscience* 1998, **86(2**):389-398.

Holzer P: **Neurogenic vasodilatation and plasma leakage in the skin**. *Gen Pharmacol*. 1998, **30(1)**:5-11.

Hoyle CH, Stones RW, Robson T, Whitley K, Burnstock G: **Innervation of vasculature and microvasculature of the human vagina by NOS and neuropeptide-containing nerves**. *J Anat* 1996, **188(3):**633-644.

Huang X, Yang N, Fiore VF, Barker TH, Sun Y, Morris SW, Ding Q, Thannickal VJ, Zhou Y: **Matrix stiffness-induced myofibroblast differentiation is mediated by intrinsic mechanotransduction**. *Am J Respir Cell Mol Biol* 2012, **47(3):**340-348.

Hunt SP, Emson PC, Gilbert R, Goldstein M, Kimmell JR: **Presence of avian pancreatic polypeptide-like immunoreactivity in catecholamine and methionine-enkephalin-containing neurones within the central nervous system**. *Neurosci Lett* 1981, **21**:125–30.

Hunter KS, Lee PF, Lanning CJ, Ivy DD, Kirby KS, Claussen LR, Chan KC, Shandas R: **Pulmonary vascular input impedance is a combined measure of pulmonary vascular resistance and stiffness and predicts clinical outcomes better than pulmonary vascular resistance alone in pediatric patients with pulmonary hypertension**. *Am Heart J* 2008, **155(1):**166-174.

Ikeda M: **Adrenergic innervation of the ductus arteriosus of the fetal lamb**. *Experientia* 1970, **15:26(5):**525-526.

Insel PA: **Adrenergic receptors, G proteins, and cell regulation: implications for aging research**. *Exp Gerontol* 1993, **28(4-5)**:341-348

Jin RC, Loscalzo J: **Vascular Nitric Oxide: Formation and Function**. *J Blood Med* 2010, **1**:147–162.

Jongejan RC, de Jongste JC, Raatgeep RC, Bonta IL, Kerrebijn KF: **Electrically stimulated Krebs-Henseleit buffer does not relax precontracted human bronchi in vitro.** *Agents Actions* 1989, **26**:75–76.

Kalamida D, et al: **Muscle and neuronal nicotinic acetylcholine receptors. Structure, function and pathogenicity**. *FEBS J* 2007, **274(3799)**:845-847.

Kawashima M, Yajima T, Tachiya D, Kokubun S, Ichikawa H, Sato T: **Parasympathetic neurons in the human submandibular ganglion**.*Tissue Cell* 2021, **70**:101496.

Kazemi H, Johnson DC, Ramachandran VS: Respiration, Encyclopedia of the Human Brain. New York: Academic Press 2002, pp. 209–216.

Keene DR, Sakai LY, Bächinger HP, Burgeson RE: **Type III collagen can be present on banded collagen fibrils regardless of fibril diameter**. *J Cell Biol* 1987, **105(5):**2393–2402.

Kielty CM, Sherratt MJ, Marson A, Baldock C: **Fibrillin microfibrils**. *Adv Protein Chem* 2005, **70**:405–436.

Kielty CM, Sherratt MJ, Shuttleworth CA: **Elastic fibres**. *J Cell Sci* 2002, **115**:2817–2828.

Kielty CM, Stephan S, Sherratt MJ, Williamson M, Shuttleworth CA: **Applying elastic fibre biology in vascular tissue engineering.** *Philos Trans R Soc B Biol Sci* 2007, **362**:1293–1312.

Kim HS, Aikawa M, Kimura K, Kuroo M, Nakahara KI, Suzuki T, Katoh H, Okamoto, EI, Yazaki Y, Nagai R: **Ductus arteriosus: Advanced differentiation of smooth muscle cells demonstrated by myosin heavy chain isoform expression in rabbits**. *Circulation* 1993, **88(4):**1804-1810.

Kishimoto Y, Kishimoto AO, Ye S, Kendziorski C, Welham NV: **Modeling fibrosis using fibroblasts isolated from scarred rat vocal folds.** *Lab Invest* 2016**, 96:**807–816.

Ko FN, Guh JH, Yu SM, Hou YS, Wu YC, Teng CM: **Discretamine, a selective alpha 1D-adrenoceptor antagonist, isolated from Fissistigma glaucescens**. *Br J Pharmacol* 1994, **112(4):**1174-1180.

Kondo A, Kaestner KH: **Emerging diverse roles of telocytes**. *Dev* 2019, **146(14)**: 175018.

Koyama H & Reidy M A: **Expression of extracellular matrix proteins accompanies lesion growth in a model of intimal reinjury**. *Circ Res* 1998, **82:**988–995.

Kummer W, Fischer A, Heym C: **Ultrastructure of calcitonin gene-related peptide- and substance P-like immunoreactive nerve fibres in the carotid body and carotid sinus of the guinea pig.** *Histochemistry* 1989, **92(5)**:433-439.

Kummer W, Fischer A, Mundel P, Mayer B, Hoba B, Philippin B, Preissler U: **Nitric oxide synthase in VIP-containing vasodilator nerve fibres in the guinea-pig** *Neuroreport* 1992, **3(7)**:653-655.

Kummer W, Heym C: **Different types of calcitonin gene-related peptide-immunoreactive neurons in the guinea-pig stellate ganglion as revealed by triple-labelling immunofluorescence** *Neurosci Let*t 1991, **128(2)**:187-190.

Kummer W: **Pulmonary vascular innervation and its role in responses to hypoxia: size matters.** *Proc Am Thorac Soc* 2011, **8(6):**471-476.

Kuo LE, Abe K, Zukowska Z: **Stress, NPY and vascular remodeling: Implications for stress-related diseases.** *Peptides* 2007, **28(2):**435-440.

Kusakabe T, Kawakami T, Takenaka T. **Calcitonin gene-related peptide and substance P in the pharynx and lung of the bullfrog**. *Cell Tissue Res* 1995, **279(1)**:115-121.

Lacroix JS, Correia F, Fathi M, Grouzmann E: **Post-exercise nasal vasoconstriction and hyporeactivity: possible involvement of neuropeptide Y**. *Acta Otolaryngol* 1997, **117(4):**609-613.

Laflamme MA, Sebastian MM, Buetow SB: **Comparative Anatomy and Histology: A Mouse and Human Atlas.** 1st Ed. Montine Publishers: Academic Press 2012. pp 135-153.

Leblanc GG, Trimmer BA, Landis SC: **Neuropeptide Y-like immunoreactivity in rat cranial parasympathetic neurons: coexistence with vasoactive intestinal peptide and choline acetyltransferase**. *Proc Natl Acad Sci* 1987, **84(10)**:3511-3515.

Leis S, Weber M, Isselmann A, Schmelz M, Birklein F: **Substance-P-induced protein extravasation is bilaterally increased in complex regional pain syndrome**. *Exp Neurol* 2003, **183(1):**197-204.

Longhurst JC. **Cardiac receptors: their function in health and disease**. *Prog Cardiovasc Dis* 1984, **27(3)**:201-22.

Luff SE, Hengstberger SG, McLachlan EM, Anderson WP: **Two types of sympathetic axon innervating the juxtaglomerular arterioles of the rabbit and rat kidney differ structurally from those supplying other arteries.** *J Neurocytol* 1991, **20**:781–795.

Luff SE, McLachlan EM, Hirst GDS: **An ultrastructural analysis of the sympathetic neuromuscular junctions on arterioles of the submucosa of the guinea pig ileum**. *J Comp Neurol* 1987, **257**:578–594.

Luff SE, McLachlan EM: **The form of sympathetic postganglionic axons at clustered neuromuscular junctions near branch points of arterioles in the submucosa of the guniea pig ileum.** *J Neurocytol* 1988, **17:**451–463.

Luff SE, McLachlan EM: **The form of sympathetic postganglionic axons at clustered neuromuscular junctions near branch points of arterioles in the submucosa of the guniea pig ileum.** *J Neurocytol* 1988, **17**:451–463.

Luff SE, Young SB, McLachlan EM (1995): **The proportions and structure of contacting and non-contacting varicosities in the perivascular plexus of the rat tail artery.** *J Comp Neurol* 1995, **361:**699–709.

Luff SE: **Ultrastructure of sympathetic axons and their structural relationship with vascular smooth muscle.** *Anat Embryol* 1996, **193(6):**515-531.

Lundberg JM, Franco-Cereceda A, Hua X, Hökfelt T, Fischer JA: **Co-existence of substance P and calcitonin gene-related peptide-like immunoreactivities in sensory**

nerves in relation to cardiovascular and bronchoconstrictor effects of capsaicin. *Eur J Pharmacol* 1985, **108(3):**315-319.

Lundberg JM, Terenius L, Hökfelt T, Martling CR, Tatemoto K, Mutt V, Polak J, Bloom S Goldstein M: **Neuropeptide Y (NPY)-like immunoreactivity in peripheral noradrenergic neurons and effects of NPY on sympathetic function**. *Acta Physiol Scand* 1982, **116:**477–480.

Marty M, Lui F: **Embryology, Fetal Circulation**. Treasure Island (FL): StatPearls Publishing 2019.

Marx R, Meskini RE, Johns DC, Mains RE: **Differences in the Ways Sympathetic Neurons and Endocrine Cells Process, Store, and Secrete Exogenous Neuropeptides and Peptide-Processing Enzymes.** *J Neurosci* 1999, **19(19)**:8300–8311.

Mato M, Aikawa E: **Observations on the obliteration of ductus arteriosus Botalli using the electron microscope**. *Z Anat Entwickl-Gesch* 1968, **127:**327–345.

Mazurek R, Dave JM, Chandran RR, Misra A, Sheikh AQ, Greif DM: **Vascular Cells in Blood Vessel Wall Development and Disease**. *Adv Pharmacol* 2016, **78:**323-350.

McEwan JR, Benjamin N, Larkin S, Fuller RW, Dollery CT, MacIntyre I: **Vasodilatation by calcitonin gene-related peptide and by substance P: a comparison of their effects on resistance and capacitance vessels of human forearms**. *Circulation* 1988, **77(5):**1072-1080.

McKenzie JC, Klein RM: **The effect of neonatal guanethidine administration on hemodynamic and physical alterations in the adult rat pulmonary artery during the development of hypoxia-induced pulmonary hypertension**. *J Auton Nerv Syst* 1984, **10(2):**199-203.

Miller EJ, Furuto DK, Narkates AJ: **Quantitation of type I, III, and V collagens in human tissue samples by high-performance liquid chromatography of selected cyanogen bromide peptides.** *Anal Biochem* 1991, **196(1):**54-60.

Morris JL, Gibbins IL, Campbell G, Murphy R, Furness JB, Costa M: **Innervation of the large arteries and veins of the toad (Bufo marinus) by adrenergic and peptide-containing neurons.** *Cell Tissue Res* 1986, **243:**171–184.

Morris JL, Gibbins IL, Campbell G, Murphy R, Furness JB, Costa M: **Innervation of the large arteries and veins of the toad (Bufo marinus) by adrenergic and peptide-containing neurons**. *Cell Tissue Res* 1986a, **243**:171–184

Morris JL, Gibbins IL, Kadowitz PJ, Herzog H, Kreulen DL, Toda N, Claing A. **Roles of peptides and other substances in cotransmission from vascular autonomic and sensory neurons**. *J Physiol Pharmacol* 1995, **73(5)**:521-532

Morris JL, Gibbins IL: **Structure-function relationships of the autonomic nervous system in the thoracic circulations**. *Proc Austr Physiol Pharmacol Soc* 1990, **21(1)**: 29-39.

Morris JL, Murphy R: **Evidence that neuropeptide Y released from noradrenergic axons causes prolonged contraction of the guinea-pig uterine artery.** *J Auton Nerv Syst* **1988, 24(3):**241-249**.**

Morris JL. **Peptides as neurotransmitters in vascular autonomic neurons**. *Clin Exp Pharmacol Physiol* 1995, **22(11)**:792-802.

Morton SU, Brodsky D: **Fetal Physiology and the Transition to Extrauterine Life**. *Clin Perinatol* 2016, **43(3):**395–407.

Mulvany MJ: **Determinants of vascular hemodynamic characteristics**. *Hypertension* 1984, **6(6)**:13–18.

Muratori, G: **Contributi morfologici allo studio deirecettori aortico-arteriosi dei reflessi cardiopressoregolatore**. *Arch Ital Anat Embriol* 1937, **38:**387-427.

Murphy RA, Herlihy JT, Megerman J: **Force-generating capacity and contractile protein content of arterial smooth muscle.** *J Gen Physiol* 1974, **64(6):**691-705.

Nonidez JF: **The aortic (depressor) nerve and its associated epithelioid body, the glomus aorticum.** *Am J Anat* 1935, **57:**259–301.

Nagatsu T, Levitt M, Udenfriend S: **Tyrosine Hydroxylase. The Initial Step in Norepinephrine Biosynthesis**. *J Biol Chem* 1964, **239**:2910–2917.

Nagatsu T: **Tyrosine hydroxylase: human isoforms, structure and regulation in physiology and pathology**. *Essays Biochem* 1995, **30**:15–35.

O'Rahilly R, Müller F: **Human embryology and teratology.** 3rd Edition. Willey-Liss:New York 2001.

Olsson, C: **Tyrosine hydroxylase immunoreactivity is common in the enteric nervous system in teleosts**. *Cell Tissue Res* 2016, 364**(2):**231–243.

Papka RE, Furness JB, Della NG, Murphy R, Costa M: **Time course of effect of capsaicin on ultrastructure and histochemistry of substance P immunoreactive nerves associated with the cardiovascular system of the guinea-pig.** *Neuroscience* 1984, **12**:1277–1292.

Paquet L, Massie B, Mains RE: **Proneuropeptide Y Processing in Large Dense-Core Vesicles.** *J Neurosci* 1996, **76(3)**:964-973.

Park KS, Kim Y, Lee YH, Earm YE, Ho WK: **Mechanosensitive cation channels in arterial smooth muscle cells are activated by diacylglycerol and inhibited by phospholipase C inhibitor**. *Circ Res* 2003, **93(6)**:557-564.

Pearce JA, Thomsen SL: **Blood vessel architectural features and their effects on thermal phenomena: Matching the Energy Source to the Clinical Need: A Critical Review**. *Proc SPIE* 2000, 10297.

Pease Dc, Mol-Inari S: **Electron microscopy of muscular arteries, pial vessels of the cat and monkey.** *J Ultrastruct Res*. 1960, **3**:447-468.

Pease DC, Paule WJ: **Electron microscopy of elastic arteries; the thoracic aorta of the rat.** *J Ultrastruct Res*. 1960, **3:**469-483.

Pieri L, Vannucchi MG, Faussone-Pellegrini MS: **Histochemical and ultrastructural characteristics of an interstitial cell type different from ICC and resident in the muscle coat of human gut**. *J Cell Mol Med* 2008, **12**:1944–1955.

Piez KA, Miller A: **The structure of collagen fibrils**. *J Supramol Struct* 1974, **2(2-4):**121–137.

Poeppelman RS, Tobias JD**: Patent Ductus Venosus and Congenital Heart Disease: A Case Report and Review.** *Cardiol Res* 2018, **9(5):**330-333.

Popescu LM, Faussone-Pellegrini MS: **Telocytes—A Case of Serendipity: The Winding Way from Interstitial Cells of Cajal (ICC), via Interstitial Cajal-Like Cells (ICLC) to Telocytes.** *J Cell Mol Med* 2010, **4**:729–740.

Popescu LM, Nicolescu MI: **Telocytes and stem cells**. Oxford: Academic Press, 2013. pp. 205–231.

Prabhakar NR, Zufall FM, Steven D: **O2 and CO2 Detection by the Carotid and Aortic Bodies, Chemosensory Transduction**. (eds.) Chapter 18 2016, Academic Press, pp. 321–338.

Purves, Dale, George J. Augustine, David Fitzpatrick, William C. Hall, Anthony-Samuel LaMantia, James O. McNamara, and Leonard E. White (2008). **Neuroscience** (4th Ed.). Sinauer Associates. pp. 122–6.

Ralevic V: **P2 receptors in the central and peripheral nervous systems modulating sympathetic vasomotor tone**. *J Auton Nerv Syst*. 2000, **81(1-3):**205-211.

Rang HP, Dale MM, Ritter JM, Flower RJ: **In Rang and Dale's Pharmacology**. Churchill. 2007.

Rang HP: **Pharmacology.** Edinburgh: Churchill Livingstone. p. 270. ISBN 978-0-443-07145. 2003.

Reese J: **Towards a greater understanding of the ductus arteriosus**. *Semin Perinatol* 2018, **42(4):**199–202.

Rusu MC, Mirancea N, Mănoiu VS, Vâlcu M, Nicolescu MI, Păduraru D: **Skin telocytes.** *Ann Anat.* 2012, **194(4**):359-367.

Schlereth T, Schukraft J, Krämer-Best HH, Geber C, Ackermann T, Birklein F: **Interaction of calcitonin gene related peptide (CGRP) and substance P (SP) in human skin.** *Neuropeptides* 2016, **59:**57-62.

Schmidt M, Sun G, Stacey MA, Mori L, Mattoli: **Identification of circulating fibrocytes as precursors of bronchial myofibroblasts in asthma**. *J Immunol* 2003, **171(1):**380-389.

Schneider CA, Rasband WS, Eliceiri KW: **NIH Image to ImageJ: 25 Years of Image Analysis.** *Nat Methods* (2012), **9(7):**671-675.

Schümann HJ: **What role do alpha- and beta-adrenoceptors play in the regulation of the heart?** *Eur Heart J* 1983, **4 (Suppl A):**55-56.

Schwartz DD: **Activation of alpha-2 adrenergic receptors inhibits norepinephrine release by a pertussis toxin-insensitive pathway independent of changes in cytosolic calcium in cultured rat sympathetic neurons**. *J Pharmacol Exp Ther* 1997, **282(1)**:248-255

Sheng Y & Zhu L: **The crosstalk between autonomic nervous system and blood vessels.** *Int J physiol pathophysiol pharmacol* 2018, **10(1):**17–28.

Silver MM, Freedom RM, Silver MD, Olley PM: **The morphology of the human newborn ductus arteriosus.** *Human Pathol* 1981, **12:**1123–1136.

Sims FH, Chen X, Gavin JB: **The importance of a substantial elastic lamina subjacent to the endothelium in limiting the progression of atherosclerotic changes**. *Histopathology* 1993, **23(4):**307-317.

Stenmark KR, Davie N, Frid M, Gerasimovskaya E, Das M: **Role of the adventitia in pulmonary vascular remodeling**. *Physiology* 2006, **21:**134-145.

Strosberg AD: **Structure, function, and regulation of adrenergic receptors.** *Protein Sci* 1993, **2(8)**:1198–1209.

Sundler F, Brodin E, Ekblad E, Hakanson R, Uddman R: **Sensory nerve fibers: distribution of substance P, neurokinin A and calcitonin gene-related peptide. In: Tachykinin Antagonists** (Fernstrom Symp 6) (Hakanson R, Sundler F, eds), Amsterdam, Elsevier, pp 3-14. 1985.

Szyszka-Mróz J1, Woźniak W: **A histological study of human ductus arteriosus during the last embryonic week.** *Folia Morphol* 2003, **62(4):**365-367.

Takino M, Watanabe S: **Über die Bedeutung des Ligamentum arteriosum bzw. des Ductus Botalli und der Ansatzstelle desselben an der Pulmonalwand (A. pulm.) als Blutdruckzügler bei verschiedenen Tierarten**. *Arch Kreislaufforsch* 1937, **2**:1-5.

Tallini YN, Shui B, Greene KS, Deng KY, Doran R, Fisher PJ, Zipfel W, Kotlikoff MI: **BAC transgenic mice express enhanced green fluorescent protein in central and peripheral cholinergic neurons**. *Physiol Genomics* 2006, **27**:391–397.

Tan CMJ, Green P, Tapoulal N, Lewandowski AJ, Leeson P, Herring N: **The Role of Neuropeptide Y in Cardiovascular Health and Disease.** *Front Physiol.* 2018, 1**9(9)**:1281.

Thuneberg L, Rumessen JJ, Mikkelsen HB: **Interstitial cells of Cajal - an intestinal impulse generation and conduction system.** *Scand J Gastroenterol Suppl*. 1982, **71**:143-144.

Tucker WD, Arora Y, Mahajan K: **Anatomy, Blood Vessel**. Treasure Island (FL): StatPearls Publishing 2021.

Toda T, Tsuda N, Takagi T, Nishimori I, Leszczynski D, Kummerow F: **Ultrastructure of developing human ductus arteriosus.** *J Anat* 1980, **131(1):**25–37.

Tomita T: **Electrical properties of mammalian smooth muscle.** In: Bulbring E, Brading AF, Jones AW, Tomita T, eds. Smooth muscle. London: Edward Arnold, 1970, **197**:243.

Uddman R, Edvinsson L, Ekman R, Kingman T, McCulloch J: **Innervation of the feline cerebral vasculature by nerve fibers containing calcitonin gene-related peptide: trigeminal origin and co-existence with substance P.** *Neurosci Lett* 1985, **62:**131-136.

Van Andel CJ1, Pistecky PV, Borst C: **Mechanical properties of porcine and human arteries: implications for coronary anastomotic connectors**. *Ann Thorac Surg*. 2003, **76(1):**58-64.

Van Geldre LA, Lefebvre RA: **Interaction of NO and VIP in gastrointestinal smooth muscle relaxation.** *Curr Pharm Des* 2004, **10(20):**2483-2497.

Wahl M.J: **Local chemical, neural, and humoral regulation of cerebrovascular resistance vessels**. *Cardiovasc Pharmacol* 1985, **7(3)**:36-46.

Wang Y, Zhao S: **Vascular Biology of the Placenta.** San Rafael (CA): Morgan & Claypool Life Sciences 2010. Chapter 2, *Placental Blood Circulation.*

Wang Z, Chesler NC: **Role of collagen content and cross-linking in large pulmonary arterial stiffening after chronic hypoxia**. *Biomech Model Mechanobiol* 2012, **11(1-2):**279–289.

Wang Z, Lakes RS, Eickhoff JC, Chesler NC: **Effects of collagen deposition on passive and active mechanical properties of large pulmonary arteries in hypoxic pulmonary hypertension**. *Biomech Model Mechanobiol* 2013, **12(6)**:1115-1125.

Wassall RD, Teramoto N, Cunnane TC: **Noradrenalin**. *Ency Neurosci* 2009, 1221–1230.

Watanabe, M: **The Sensitive Innervation of Thoracic Aorta**. *Fol endocr Jap* 1938, **14:**39.

Weihe, E., Depboylu, C., Schütz, B., Schäfer, M. K., & Eiden, L. E: **Three types of tyrosine hydroxylase-positive CNS neurons distinguished by dopa decarboxylase and VMAT2 co-expression.** *Cell Mol Neurobiol* 2006, **26(4-6):**659–678.

Wess J. (1996): **Molecular biology of muscarinic acetylcholine receptors.** *Crit. Rev. Neurobiol* 1996, **10**:69–99.

Westfall TC, Westfall DP: **Adrenergic Agonists and Antagonists in Goodman and Gilman's The Pharmacological Basis of Therapeutics, eleventh editions**, (Brunton LL, Lazo JS and Parker KL, eds), McGraw-Hill Medical Publishing Division, New York, 237-295, 2006.

Wharton J, Polak JM, McGregor GP, Bishop AE, Bloom SR: **The distribution of substance P-like immunoreactive nerves in the guinea-pig heart.** Neuroscience 1981, **6:**2193–2204.

Wimpfheimer O, Haramati LB, Haramati N: **Calcification of the ligamentum arteriosum in adults: CT features.** *J Comput Assist Tomogr* 1996, **20(1):**34–37.

Wong LC, Langille BL: **Developmental remodeling of the internal elastic lamina of rabbit arteries: effect of blood flow**. *Circ Res* 1996, **78:**799– 805.

Xiao J, Wang F, Liu Z, Yang C: **Telocytes in liver: electron microscopic and immunofluorescent evidence.** *J Cell Mol Med* 2013, **17(12):**537–1542.

Yang Y, Sun W, Wu SM, Xiao J, Kong X: **Telocytes in human heart valves**. *J Cell Mol Med* 2014, **18**:759– 765.

Yoder MJ, Baumann FG, Grover-Johnson NM, Brick I, Imparato AM: **A morphological study of early cellular changes in the closure of the rabbit ductus arteriosus.** *Anat Rec* 1978, **192:**19–39.

Yeung T, Georges PC, Flanagan LA, Marg B, Ortiz M, Funaki M, Zahir N, Ming W, Weaver V, Janmey PA. **Effects of substrate stiffness on cell morphology, cytoskeletal structure, and adhesion.** *Cell Motil Cytoskel* 2005, **60(1)**:24-34.

Zhang K, Zhang J, Gao ZG, Zhang D, Zhu L, Han GW, Moss SM, Paoletta S, Kiselev E, Lu W, Fenalti G, Zhang W, Müller CE, Yang H, Jiang H, Cherezov V, Katritch V, Jacobson KA, Stevens RC, Wu B, Zhao Q: **Structure of the human P2Y12 receptor in complex with an antithrombotic drug.** *Nature.* 2014, **509(7498)**:115-118.

Zheng Y, Li H, Manole CG, Sun A, Ge J, Wang X: **Telocytes in trachea and lungs**. *J Cell Mol Med* 2011, **15**:2262– 2268.

9 List of publications

Published abstracts

1. Quaye B, Kummer W**: The ligamentum arteriosum is more than a ligament.** Book of abstract paper.38. 12th Annual GGL conference on life science, 2019. Justus Liebig University.

2. Quaye B, Kummer W: **The curious case of the ligamentum arteriosum: it's more than a ligament.** *Faseb J* 2020**, 34(s1):**02270. **http://doi.ord/10.1096/fasebj.2020.34.s1.02270**

3. Quaye B, Kummer W**: Idiosyncratic innervation of ligamentum arteriosum.** Book of abstract paper.38. 12th Annual GGL conference on life science, 2020. Justus Liebig University.

10 Declaration

Hiermit erkläre ich, dass ich die vorliegende Arbeit selbständig und ohne unzulässige Hilfe oder Benutzung anderer als der angegebenen Hilfsmittel angefertigt habe. Alle Textstellen,

die wörtlich oder sinngemäß aus veröffentlichten oder nichtveröffentlichten Schriften entnommen sind, und alle Angaben, die auf mündlichen Auskünften beruhen, sind als solche kenntlich gemacht. Bei den von mir durchgeführten und in der Dissertation erwähnten Untersuchungen habe ich die Grundsätze guter wissenschaftlicher Praxis, wie sie in der „Satzung der Justus-Liebig-Universität Gießen zur Sicherung guter wissenschaftlicher Praxis“ niedergelegt sind, eingehalten. Ich versichere, dass Dritte von mir weder unmittelbar noch mittelbar geldwerte Leistungen für Arbeiten erhalten haben, die im Zusammenhang mit dem Inhalt der vorgelegten Dissertation stehen, und dass die vorgelegte Arbeit weder im Inland noch im Ausland in gleicher oder ähnlicher Form einer anderen Prüfungsbehörde zum Zweck einer Promotion oder eines anderen Prüfungsverfahrens vorgelegt wurde. Alles aus anderen Quellen und von anderen Personen übernommene Material, das in der Arbeit verwendet wurde oder auf das direkt Bezug genommen wird, wurde als solches kenntlich gemacht. Insbesondere wurden alle Personen genannt, die direkt an der Entstehung der vorliegenden Arbeit beteiligt waren.

Mit der Überprüfung meiner Arbeit durch eine Plagiatserkennungssoftware bzw. ein internetbasiertes Softwareprogramm erkläre ich mich einverstanden.“

Giessen, 2021

_____

Benedicta Mensah

11 Acknowledgements

I would first like to thank my mentor and doctor father, Prof. Dr Wolfgang Kummer, whose in-depth expertise in autonomic innervation was invaluable. His insightful feedback, suggestion and constructive criticism pushed me to sharpen my thinking and brought my work to a higher level. I am also thankful to him for offering me the opportunity to be part of the anatomy preparation course for the medical and dental students of the institute in the year 2019/2020 academic year.

I will like to express gratitude to my second supervisor Prof. Martin Diener for his support and excellent encouragement throughout my dissertation.

I am also thankful to the government of Ghana, DAAD and the equal opportunity office of the Justus Liebig University for providing me with funding during my studies.

I would also like to thank Dr. Renate Paddenberg and Dr. Maryam Keshavarz, for their valuable guidance throughout my studies. They were always there to solve my day to day laboratory work problems.

I would like to acknowledge my section speakers Prof. Christoph Rummel and Prof. Gebhard Sammer for organising excellent, insightful seminars and neurokoloquim to improve my basic knowledge in neurosciences.

I would also like to thank Prof. Dr. Ralf Middendorf and Prof. Dr. Andreas Meinhardt for giving me the opportunity to do my laboratory rotations with them.

Many thanks to all of the members of staff in the department especially Dr. Uwe Pfeil, Martin, Claudia, Petra, Alex, Ulrich and Anika for their kind support during my study. Also, I extend my thanks to all my colleagues for their continuous encouragement and support.

Finally, I want to thank Michael Mensah, my partner and best friend for putting his dream on hold so that I can build mine. To Jaden and Noel, your priceless smiles were my daily motivation.

Der Lebenslauf wurde aus der elektronischen Version der Arbeit entfernt.

The curriculum vitae was removed from the electronic version of the paper.